UNIVERSITY OF GENOA

Polytechnic school

Department of Civil, Chemical and Environmental Engineering

Master's degree in Chemical and Process Engineering

Design and characterization of vascular scaffolds: A dual approach with iron oxide nanoparticles for diagnostics and layered gelatin-based coating for therapeutic applications

Supervisors
Prof. Pier Francesco Ferrari
Prof. Jan Oscar Pralits

Co-supervisor
Dr. Fatemeh Ahmadpoor

Candidate
Valentina Parodi

Academic year 2023-2024

General Index

Index of Figures

Index of Tables

Abstract

Cardiovascular diseases represent a leading cause of morbidity and mortality worldwide, necessitating innovative solutions to improve the diagnosis, treatment, and management of these conditions. This thesis focuses on the design, fabrication, and functionalization of vascular scaffolds to address critical challenges in cardiovascular applications.

The initial phase of this work focused on the production of vascular scaffolds through electrospinning technique, utilizing a polymeric blend of polycaprolactone (PCL) and poly(glycerol sebacate) (PGS) with the addition of quercetin to modulate inflammatory responses. The resulting prostheses were coated with gelatin using a conventional dip-coating method to reduce porosity and enhance biocompatibility. Chemical, thermal, and morphological characterizations of the scaffolds were performed to highlight their intrinsic properties. To validate the produced prostheses, cell compatibility and hemocompatibility tests were conducted.

In the subsequent phase, the focus shifted to developing a coating method that ensures uniformity and standardization of the process. An innovative layer-by-layer (LbL) coating technique was implemented, employing alternating layers of gelatin and tannic acid, a polyphenol with antioxidant properties. This method allowed for precise control over the amount of coating deposited on the scaffolds, thereby standardizing the process. In addition to chemical, thermal, and morphological characterizations, release studies were conducted on the LbL-coated scaffolds. These studies were carried out under both static and dynamic conditions using a bioreactor that simulates the flow and pressure conditions of the cardiovascular system.

The final phase of this thesis focused on diagnostic applications. Specifically, Iron Oxide nanoparticles (IONPs) were successfully incorporated into the electrospun scaffolds. The addition of IONPs enabled the visualization of the scaffolds using Magnetic Resonance Imaging (MRI). This represents a promising methodology for verifying the correct positioning of the graft after *in vivo* implantation.

Abstract

Le malattie cardiovascolari rappresentano una delle principali cause di morbilità e mortalità a livello mondiale, rendendo necessarie soluzioni innovative per migliorare la diagnosi, il trattamento e la gestione di tali condizioni. Il presente lavoro di tesi è incentrato sulla produzione e funzionalizzazione di scaffold vascolari per il trattamento delle suddette patologie.

La fase iniziale del corrente lavoro ha avuto come obiettivo la produzione tramite elettrofilatura di scaffolds vascolari costituiti da una miscela polimerica di PCL e PGS, con aggiunta di quercetina al fine di modulare la risposta infiammatoria. Le protesi così prodotte sono state rivestite con un coating di gelatina, tramite un convenzionale metodo ad immersione, al fine di diminuire la porosità e migliorare la biocompatibilità. Sono state condotte caratterizzazioni chimiche, termiche e morfologiche degli scaffolds al fine di evidenziarne le caratteristiche intrinseche. Per validare le protesi prodotte, sono state condotte analisi di compatibilità cellulare e emocompatibilità.

Come fase successiva dello studio, l'attenzione è stata posta sull' ottenimento di un metodo di coating degli scaffolds che garantisse uniformità e standardizzazione del processo. È stato quindi implementato sugli scaffolds un innovativo coating layer-by-layer con strati alternati di gelatina e acido tannico, un polifenolo con proprietà antiossidanti. Il metodo implementato ha permesso di ottenere un controllo preciso sulla quantità di gelatina depositata come coating sugli scaffolds, permettendo di standardizzare il processo. Oltre alle caratterizzazioni chimiche, termiche e morfologiche, sono state condotte analisi di rilascio dei componenti dagli scaffolds rivestiti con il coating layer-by-layer. I rilasci sono stati condotti sia in condizioni statiche sia in condizioni dinamiche, grazie all'impiego di un bioreattore che simula le condizioni di flusso e di pressione dell'apparato cardiovascolare.

Come fase finale del presente lavoro di tesi, si è focalizzata l'attenzione sull' ambito diagnostico. Specificatamente, sono state aggiunte con successo nanoparticelle di ossido di ferro (IONPs) all'interno degli scaffolds elettrofilati. Grazie all'aggiunta delle IONPs, è stato possibile visualizzare lo scaffold tramite risonanza magnetica. Tale risultato rappresenta una metodica promettente per poter verificare il corretto posizionamento del graft e la sua degradazione nel tempo dopo l'impianto *in vivo*.

1 Introduction

1.1 Regenerative Medicine

Regenerative medicine is a new frontier of medicine, extremely innovative and that keeps up with scientific progress. It makes use of the contribution of multiple disciplines such as biology, chemistry, medicine, computer science and engineering for the resolution of many acute and chronic diseases in which conventional medicine has proven inadequate. [1].
This growing field aims to repair, regenerate or replace tissues or organs damaged by disease, trauma, aging or due to congenital defects [2]. While this research scope has gained significant traction in recent decades, its roots stretch back to the early days of organ transplantation and tissue grafting. In fact, the term "Regenerative Medicine" was first popularized in the late 1990s, but the concept of regeneration has fascinated scientists for centuries. Ancient cultures, such as the Greeks and Egyptians, recognized the body's inherent ability to heal. However, it wasn't until the 20th century that the field began to take shape, with advancements in cell biology, tissue culture, and surgical techniques.

Regenerative Medicine encompasses a broad range of techniques and technologies designed to regenerate damaged tissues or organs. It employs biological processes such as cell therapy, gene therapy, and tissue engineering to promote healing and regeneration.
There are 3 main approaches that can be exploited in this sector:

1) **In Situ Regeneration:** this approach aims to stimulate the body's natural regenerative processes, often through the use of growth factors, biomaterials, or signaling molecules;
2) **Cell-Based Therapies:** this category includes the transplantation of cells to repair or replace damaged tissues;
3) **Tissue Engineering:** this approach involves creating tissues or organs outside the body, which can then be implanted into the patient. It encompasses the use of scaffolds, bioreactors, and other advanced techniques.

A. Cell Therapy

Cell therapy involves the transplantation of living cells into a patient to restore function or repair damaged tissues. The cells used in these therapies can be autologous (from the patient), allogeneic

(from a donor), or even xenogeneic (from another species). Stem cells, known for their ability to differentiate into multiple cell types, are a critical component of cell therapy.

In the context of this type of therapy, stem cells can work in two distinct ways: they can be physically integrated into damaged tissue and differentiate into specialized cells of that tissue, helping to restore or maintain its functionality, or they can release molecules that trigger molecular and cellular processes, leading to a therapeutic effect on the damaged tissue.

CAR-T therapy is one of the most successful examples of cell therapy. The term CAR-T, which stands for Chimeric Antigen Receptor T cells, describes a treatment where T cells are taken from a patient, genetically engineered in a lab, and then reintroduced into the patient's body to make them more effective against tumors. T cells are crucial components of the immune system and play a key role in fighting a wide range of diseases, including cancer. To create CAR-T cells, scientists insert a gene into the T cells' DNA using a deactivated viral vector. This protein is responsible of transforming the T cells into a kind of killer of tumor cells that bear a specific target on their surface, which is recognized by the CAR. The name "chimeric" reflects the fact that CAR is a combination of segments from different molecules, much like the mythical chimera is a blend of various animal parts.

A schematic representation of the CAR-T therapy is shown in Figure 1 ([3]) below.

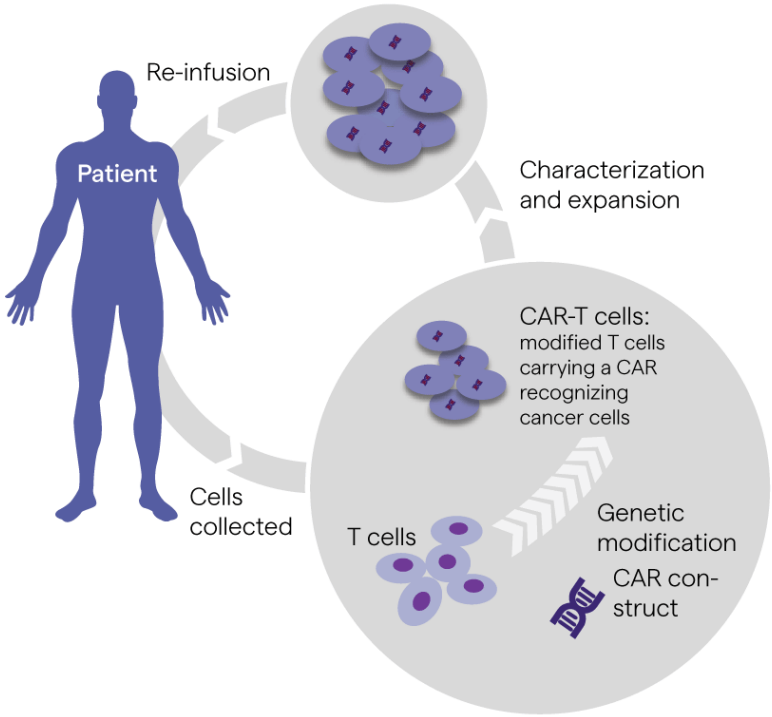

Figure 1. CAR-T therapy.

CAR-T is a customized treatment, tailored for each patient, and represents one of the most cutting-edge approaches to cancer immunotherapy [4].

B. Gene Therapy

Gene therapy involves modifying or replacing defective genes to correct genetic disorders or treat diseases. Among the main tools used to transfer genetic material to cells are viral vectors, that are viruses stripped of their contents and rendered harmless, then transformed into carriers for therapeutic genetic material. The viruses used are altered to prevent them from replicating, allowing them only to enter target cells and deliver genetic information to the cell nucleus. Instead of making the infected cell produce new viruses, the vector provides it with therapeutic genetic information, like a working copy of a gene.

The most commonly used viruses for creating vectors are lentiviruses and adeno-associated viruses (AAV):

- Lentiviral vectors are derived from the viruses of HIV, that causes AIDS. These vectors have been 'tamed' to retain their strong ability to infect human cells while being engineered so they can't replicate. Despite this modification, lentiviral vectors still have the ability to efficiently integrate into the host genome, ensuring that the therapeutic gene is expressed long-term and passed on to any daughter cells in a growing organism or tissue [5].
- AAV vectors are derived from small, non-pathogenic viruses that rarely cause inflammation, making them especially safe. Unlike lentiviral vectors, AAV vectors rarely integrate into the DNA once they enter a cell, remaining in the nucleus as separate genetic elements. There are many versions of AAV, both natural and synthetic, each with a tendency to target specific organs, allowing for targeted delivery of therapeutic genes to sites like the liver, heart and muscles [5].

It must be said that patients can potentially have antibodies to some viral vectors, so also non-viral vectors are used in gene therapy such as bacterial, lipid- and polymer-based vectors. Immune response is a key step in selecting an appropriate vector.

No matter what type of vector is used to deliver genetic information, the expression of the transgene in the intended target tissues is ultimately regulated by the promoter. The transgenes can contain the full copy of the gene of interest or the partial gene, depending on the situation [6].

The image below (Figure 2, [6]) provides a schematization of the mechanism of action of gene therapy using a viral vector to transport the transgene.

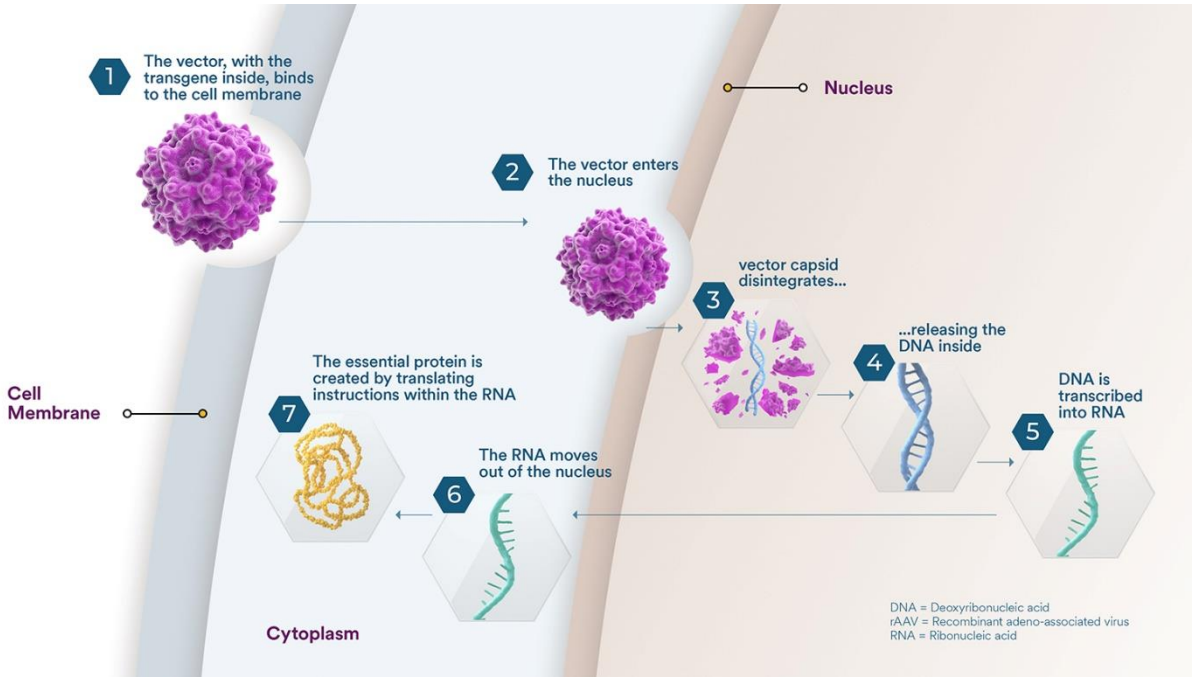

Figure 2. Mechanism of action of gene therapy with a viral vector.

There are two key approaches for administering gene therapy:

1) *In vivo*: this administration involves delivering the 'therapeutic gene' directly into the patient's body. It can be done through a local injection into the target organ or via a systemic injection into the bloodstream [7].
2) *Ex vivo*: this method involves correcting cells outside the patient's body. The process begins by extracting the target cells from the patient, then genetically altering them, and finally reintroducing them back into the patient [7].

A schematization of the two different approaches is shown in Figure 3 ([8]) below.

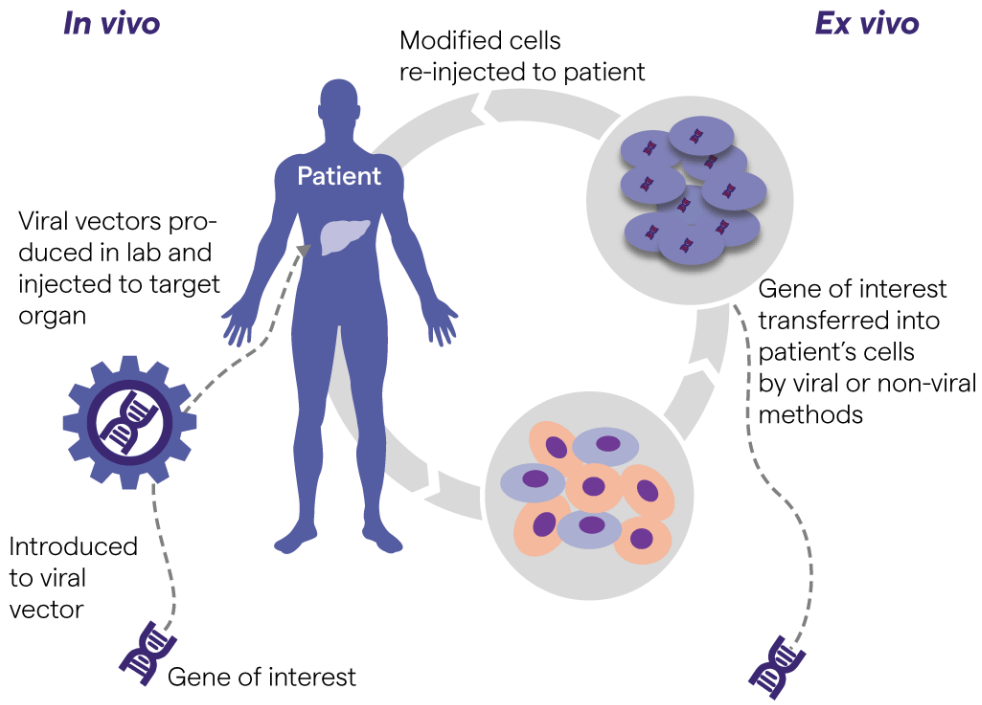

Figure 3. In vivo and *Ex vivo* methods for delivering gene therapy.

Gene therapy holds promises for treating inherited disorders like cystic fibrosis and muscular dystrophy, as well as acquired conditions like cancer.

C. Tissue Engineering

Tissue Engineering (TE) is a continually evolving field of research of ever-increasing interest in the sphere of regenerative medicine. This multidisciplinary science is based on the seeding of stem cells on special supports known as scaffolds, in combination with specific bioactive molecules in order to obtain functional tissues.

The term Tissue Engineering made its first appearance in common language around the seventies of the last century, univocally understood as the manipulation of tissues and organs. Over the years the term has taken on its current meaning, referring to that multidisciplinary sector that applies the principles and methods of engineering and medicine in order to develop biological substitutes for the maintenance, repair or regeneration of tissues or organs [9].

Any condition that leads to organ or tissue degeneration is a prime candidate for tissue engineering. Until recently, the only cure for such conditions was through organ transplants. However, transplants come with several drawbacks, including a shortage of donors, the risk of transmitting diseases, and the potential for rejection, where the immune system attacks the transplanted organ because it is seen as foreign. This can result in prolonged waiting times for patients, sometimes lasting years, during

which they may require immunosuppressive treatments. These treatments are not always successful, and in cases of rejection, there have been no alternative healing options. Therefore, TE initially emerged to create technologies that could bypass the limitations of organ transplantation. As said before, it uses biomaterials to construct scaffolds onto which cells can attach, grow, and eventually form tissues. The term "biomaterial" covers a wide range of substances, from glass to hydrogels, basically referring to the material that best mimics the tissue type. For instance, porous tantalum metal scaffolds are ideal for bone tissue engineering due to their strength and durability. On the other hand, polymer-based biomaterials have been employed to engineer soft-tissue organs, which is particularly beneficial for patients with end-stage organ failure [10].

In this broad branch of research, biomaterials such as sponges, membranes, foams, fibers and hydrogels are used with the aim of repairing skin, bone, nerve and vascular defects. In this sense, TE can be explored in more detail based on the organ to be improved or repaired. It is therefore possible to distinguish between:

1) **Skin Tissue Engineering (STE)**: this field is dedicated to regenerating the normal anatomy and physiology of the skin. Skin, the body's largest organ, is essential for protecting, regulating, sensing, and maintaining homeostasis. It helps control temperature, fluid balance, and metabolic processes, and acts as a barrier against pathogens and environmental threats. It has a complex, multilayered structure with various components like cells, fibers, veins, and hair follicles. When the skin sustains severe structural damage leading to significant loss of function and structure, its ability to self-regenerate becomes compromised. STE aims to create functional tissue by combining cells with mediator molecules like growth factors and biomaterials that support cell growth and proliferation. Recent developments in biomaterials have led to faster and more effective wound healing, contributing to better skin restoration. For example, chitosan and its derivatives are popular choices for creating functional scaffolds in this context due to their biocompatibility, strong bioactivity, appropriate degradation rates, and good mechanical properties. These materials can also be engineered to create multifunctional structures that closely resemble the extracellular matrix [11].
2) **Bone Tissue Engineering (BTE)**: it aims to use stem cells, innovative scaffolds, and biological factors to develop reliable and effective bone formation techniques for skeletal tissue regeneration. This approach is designed to improve the quality of life for older adults and those with bone-related conditions. Congenital abnormalities, cancers, trauma, rickets, osteomyelitis, osteoporosis, infections, and fractures can lead to loss of bone tissue and its

functions. Bone is a dynamic tissue with a natural ability to regenerate but this innate capacity is usually sufficient only for minor injuries like hairline cracks or certain types of fractures. BTE focuses on creating materials that can be implanted into bone defects, promoting regeneration by gradually being replaced with new bone tissue. These materials serve as a temporary framework for cellular activity and play a provisional role similar to the extracellular matrix until bone repair is completed. Common natural polymers employed to produce bone scaffolds include chitosan, collagen, gelatin, alginate, hyaluronic acid, cellulose derivatives, and silk fibroin [12].

Chitosan is a prime candidate for this role because it supports cell growth, is more biocompatible than synthetic polymers, and degrades into non-toxic byproducts. However, one of the main challenges with chitosan-based materials is their typically low mechanical strength, limiting their use in some applications. One efficient solution is to blend chitosan with other materials to address this issue: combining chitosan with ceramics, synthetic polymers, natural polymers, or other additives allows the creation of functional biomatrices that are suitable for BTE [11].

3) **Nerve Tissue Engineering (NTE)**: this field focuses on studying, developing, and applying materials for nerve repair. Damage to nerves caused by trauma, degenerative conditions, or genetic factors can lead to permanent disability and severely reduce patients' quality of life. NTE aims to create new, efficient, and reproducible methods for treating nerve injuries to restore sensory and motor functions [11].

   An important example of application in this field is the creation of injectable hydrogels that can fill damaged areas and support injured tissues without requiring complicated surgical procedures. However, injectable hydrogels have demonstrated some limitations, such as low solubility, difficult processability, and weak mechanical properties. Recent advancements in chitosan-based hydrogels aim to improve these aspects: researchers are exploring the potential of hydrogels with self-healing capabilities. Filling the cavity left by a spinal cord injury with these self-healing materials can serve as a bridge and a conduit for regenerating axons and myelin sheaths in the central nervous system, facilitating electrical signal transmission in the spinal cord. As a result, the regenerative environment provided by these self-healing materials could represent a significant step forward in repairing spinal cord injuries [13].

4) **Vascular Tissue Engineering (VTE):** it aims to produce engineered structures for the replacement or by-pass of damaged blood vessels. VTE is the research area on which this thesis has focused, and which will be explored in greater detail in the following chapters.

A schematic representation of the various fields of application of Tissue Engineering is provided below in Figure 4 ([11]).

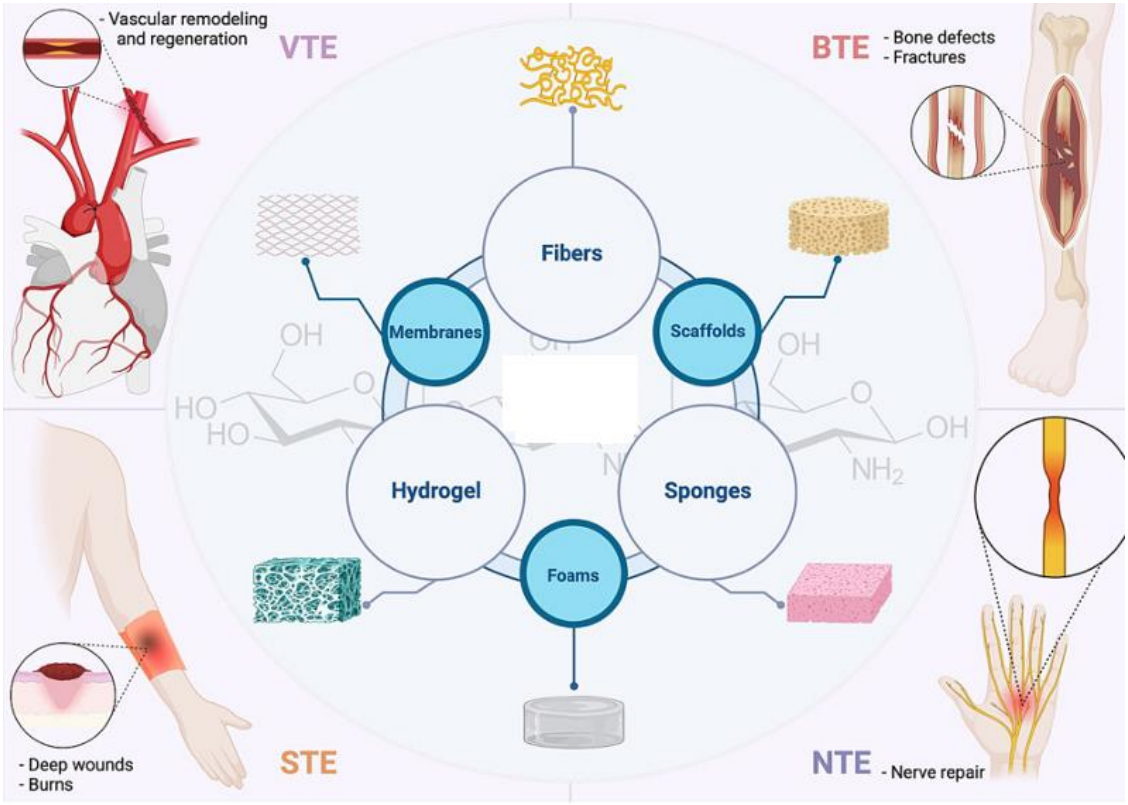

Figure 4. Biomaterials and areas of application of TE.

1.2 Vascular Conditions and Diseases

A vascular disease is a condition that impacts the arteries or veins, affecting blood flow by either obstructing or weakening the blood vessels, or even by damaging the valves in the veins. This can lead to reduced or completely blocked blood flow, which may harm organs and other body structures. Cardiovascular diseases (CVD) represent the leading cause of death worldwide, with nearly 20 million deaths according to the data collected by the Journal of the American College of Cardiology (JACC) in 2022. The compiled report, which analyzed the impact of 18 cardiovascular conditions and 15 risk factors in 21 regions of the world for a total of 204 nations, saw a huge increase in deaths, from 12.4 million in 1990 to 19.8 million in 2022 [14].

When examining the geographic spread of this problem, although vascular diseases are prevalent worldwide, certain regions in Asia, Europe, Africa, and the Middle East have the greatest levels of

mortality. Specifically Eastern European countries have the highest mortality rate, with 553 deaths per 100,000 people. The causes of such geographical differences lie in an opposite growth trend regarding people suffering from hypertension, one of the main triggers for the onset of CVD. In fact, in recent years there has been a decrease in the number of people with hypertension in industrialized countries, while in middle- and low-income countries, the number of people with hypertension has surged. The decrease in blood pressure seems to be due to better nutrition and early treatment, while the increase appears to be associated with unhealthy diets high in calories and saturated fats and low in fruits and vegetables [15].
Regarding the situation in Italy, cardiovascular diseases remain the leading cause of death. According to ISTAT data, in 2021, these pathologies have caused approximately 218 thousand deaths, accounting for 30.8% of all deaths, specifically 27.7% for males and 33.7% for females [16].

The rise in cardiovascular disease rates over the past few decades can be attributed to industrialization, which has shifted jobs from physically active to more sedentary roles. This, combined with a technology-driven culture that promotes longer work hours and less time for leisure activities, has led to a significant increase in CVD. Key contributing factors include physical inactivity, diets high in calories, saturated fats, and sugars, which are linked to atherosclerosis and metabolic issues such as metabolic syndrome, diabetes mellitus, and hypertension, conditions often found in individuals with CVD [17].

A study published in 2024 ([18]) further highlighted a link between SARS-CoV-2 infection and the development of cardiovascular issues. This study examined a large segment of the population, involving nearly 229000 individuals (32000 of whom had contracted Covid since January 2020) from the general practitioners' database of ASL 1 in Naples. The subjects, all over 18 years old, were followed for three years, from 2020 to 2022. The data obtained, which were compared with medical records from the same database for the pre-pandemic period from 2017 to 2019, showed that among those affected by Covid-19, there were twice as many cases of myocardial infarction, stroke, heart failure, atrial fibrillation, and myopericarditis.

Cardiovascular disease encompasses four main conditions [19]:

1) Coronary artery disease (CAD), also known as coronary heart disease (CHD). CAD occurs when the heart's need for oxygen-rich blood exceeds the supply due to a reduced capacity of the coronary vessels. This condition, primarily caused by atherosclerosis, involves the buildup

of plaque in the coronary arteries, leading to inflammation: the narrowing or blockage of these arteries from plaque can result in myocardial ischemia. If a plaque ruptures, it can form a blood clot, further restricting blood flow. A complete and sudden blockage of a coronary artery can cause a myocardial infarction, potentially leading to permanent heart muscle damage if not treated quickly [20].

2) Cerebrovascular disease, which is linked to strokes, also known as cerebrovascular accidents, and transient ischemic attacks (TIAs).
3) Peripheral artery disease (PAD), which primarily affects the arteries in the limbs and can lead to claudication.
4) Aortic atherosclerosis, which is connected with the development of thoracic and abdominal aneurysms.

Atherosclerosis, which involves the buildup of cholesterol plaques in the arteries, is the primary cause of cardiovascular disease as previously mentioned. These plaques can obstruct arteries, limiting the flow of oxygen and nutrients to vital organs like the heart, brain, and kidneys, as well as other tissues throughout the body.

Nevertheless, other risk factors can contribute to cardiovascular disease, some of which are hereditary, while others are often linked to poor lifestyle choices. The main risk factors can be divided according to different causes:

- Environmental causes, including air pollution, indoor pollution, lead exposure, temperature.
- Metabolic causes such as high blood pressure, cholesterol, overweight, blood glucose level, and kidney dysfunctions. To get an idea, dyslipidemia, which consists of elevated plasma cholesterol and triglycerides in the blood, affects about 25-30% of the global population, the same percentage of people affected by high blood pressure. Obesity characterizes 10-15% of the population, while diabetes impacts about 5% of the public.
- Behavioral causes such as diet, smoking, passive smoking, alcohol use, physical activity.

These risk factors significantly increase the likelihood of developing CVD by two to four times for each factor compared to someone in good health. The risk becomes even more alarming when two or more of these factors are present together, potentially raising the likelihood of cardiovascular disease by 10-20 times [21].

Also, oxidative stress, resulting from an imbalance between the production of reactive oxygen species (ROS) and the body's antioxidant defenses, is a key contributor to cardiovascular disease (CVD). ROS, produced during cellular metabolism and influenced by external factors like pollution and smoking, can damage lipids, proteins, and DNA. This damage affects endothelial function, leading to vasoconstriction, inflammation, and thrombosis, which in turn contribute to the development of atherosclerosis and hypertension [22].

Non-modifiable factors like family history, age, and gender can have varying effects. A family history of premature atherosclerotic disease in a first-degree relative before age 55 for males and 65 for females is recognized as an independent risk factor. There's evidence that gender may affect how CVD risk factors manifest. For example, women who smoke more than 20 cigarettes per day or have diabetes may face a higher risk of CVD compared to men with the same habits [23]. Additionally, the likelihood of developing CVD increases significantly with each passing decade of life.
Finally, HIV (human immunodeficiency virus) has also been linked to a higher rate and incidence of CVD [24].

1.3 Tissues in the vascular apparatus

To better understand the causes of vascular diseases, it is necessary to briefly describe the tissues of the vascular system.

Endothelial Tissue

The endothelium is the epithelial tissue that lines the cavities of the circulatory system, including blood vessels, lymphatic vessels, and the inner surface of the heart, forming a kind of diffuse organ within the body. Initially, the endothelium was thought to be an inert surface with the sole function of preventing blood clotting. However, in recent years, it has been discovered that the endothelium also plays a role in modulating vascular tone and blood flow in response to specific signals. Additionally, it plays an important role in angiogenesis and in regulating platelet activation and inflammation [25].
The endothelium has the typical structure of a simple squamous epithelium, consisting of a single layer of flat, polygonal cells known as endothelial cells or endothelia. These cells have their upper surface in direct contact with the blood (or lymph), while their base is anchored to the basal lamina, which connects them to the underlying tissues made up of smooth muscle and connective tissue.

Endothelial cells are extremely thin and tightly connected, creating a continuous, uninterrupted surface (Figure 5, [26]). Generally, these cells elongate in the direction of blood flow, especially in larger arteries. In smaller vessels, such as capillaries, they are characterized by remarkable thinness, often with a thickness of no more than 0.2 μm. The walls of capillaries often consist of just 2 or 3 endothelial cells, and in the smallest capillaries, a single cell is sufficient.

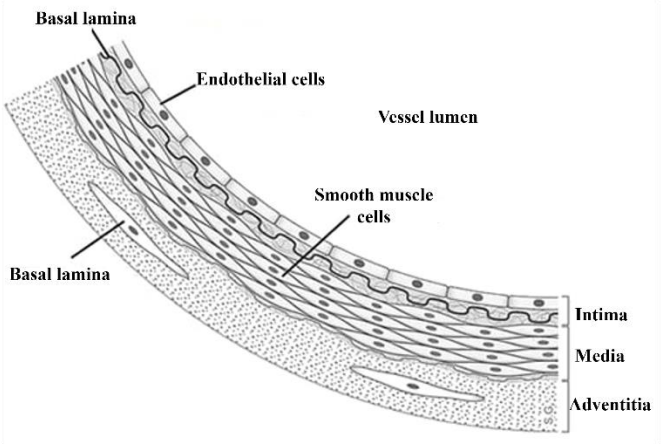

Figure 5. Endothelium's structure.

The endothelium performs numerous functions, which can be summarized as follows:

- It regulates the passage of substances between the extracellular fluid and the blood, acting as a semi-permeable barrier.
- It manages coagulation, fibrinolysis, and platelet aggregation, maintaining the balance of blood fluidity.
- It regulates the adhesion and infiltration of white blood cells.
- It controls the growth of smooth muscle cells in the tunica media and modulates the tone, permeability, and structure of blood vessels.
- It promotes the formation of new blood vessels, known as the process of angiogenesis.
- It regulates inflammatory processes and the oxidation of LDL.

The endothelium carries out its functions by producing various chemical mediators, which can be classified into vasodilators, which have antiproliferative and anti-thrombogenic effects and increase vessel lumen, and vasoconstrictors, which have the opposite effects. The primary mediator produced by endothelial cells is nitric oxide (NO), which is involved in the physiological regulation of vascular tone by exerting a vasodilatory action. NO also inhibits platelet activation, smooth muscle cell proliferation, and white blood cell adhesion.

Among the main anticoagulant mediators, in addition to nitric oxide, glycosaminoglycans and thrombomodulin can be mentioned. On the other hand, the most important procoagulant mediators include activators of Von Willebrand factor (which initiates platelet aggregation) and tissue factor thromboplastin (TF) (which triggers the extrinsic coagulation cascade).

If the normal function of the endothelium is compromised, endothelial dysfunction occurs, that is a condition characterized by the dominance of procoagulant and proinflammatory activities. This can lead to the development of atherosclerosis, hypertension, blood vessel damage, and thrombosis [25], [26].

Muscle Tissue

Smooth muscle tissue lines the walls of hollow organs and is a key component of blood vessels. Smooth muscle fibers are small and spindle-shaped, each containing a single nucleus located at the widest part of the cell. A distinctive feature of smooth muscle tissue is the presence of myofibrils (responsible for muscle contraction) arranged in various directions, which results in the absence of the transverse striations typical of skeletal and cardiac muscle tissue.

The contraction of smooth muscle cells is slow and sustained, occurring simultaneously throughout the muscle as if it were composed of a single fiber. Moreover, this contraction is involuntary and mediated by the autonomic nervous system, whose fibers innervate smooth muscle tissue (Figure 6, [27]). Specific chemical mediators, such as acetylcholine and norepinephrine, are released by the nerve fibers of the sympathetic or parasympathetic nervous system, signaling the muscle to contract. The smooth muscle in blood vessels is of the multiunit type, meaning that the cells are not electrically connected to each other through junctions, so each cell requires individual stimulation to contract. This mechanism allows for finer control and more graduated contractions.

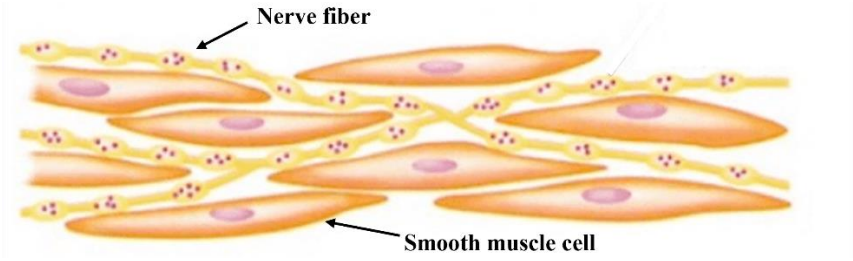

Figure 6. Arrangement and structure of smooth muscle cells.

Connective tissue

Connective tissue is a group of tissues responsible for connecting, supporting, nourishing, and defending various organs. The cells within this tissue are diverse, each with a specific function, but

they share the common characteristic of being dispersed within an extracellular matrix, rather than being closely packed together. We can distinguish between cells dedicated to the formation and maintenance of the matrix, such as fibroblasts, cells involved in the defense of the body, like macrophages and white blood cells, and cells with specialized functions, such as adipocytes, which store lipids as an energy reserve for the body.

1.4 Blood Vessels

1.4.1 Structure and characteristics

To better understand the pathogenesis of vascular diseases, it's crucial to first grasp the normal structure and function of blood vessels. Additionally, it should be noted that most vascular diseases have characteristic anatomical distributions, meaning they affect only specific types of blood vessels.

The cardiovascular system is the collection of organs responsible for transporting blood throughout the human body. It includes the heart, which acts as the blood pump and is the central element of the system, as well as the blood vessels (arteries and veins) and the lymphatic vessels.
Depending on the direction in which the blood flows, we can distinguish blood vessels as either arteries or veins:

- Arteries are responsible for carrying oxygenated blood (except for the pulmonary artery) away from the heart and to every part of the body. They have thicker and more elastic walls than veins because they must withstand the mechanical stress and high pressure caused by the heart's pumping action. Additionally, arteries are generally located deeper within the body than veins, and their pulse can be felt [28].
- The venous system is responsible for transporting deoxygenated blood (darker in color compared to oxygenated blood) back from the body to the heart, where it will then be directed to the lungs. Capillaries and venules are tasked with collecting deoxygenated blood, which is then passed on to the veins for transport to the heart. To help maintain the blood flow toward the heart, veins are often equipped with valves, which are absent in arteries. The walls of veins are thinner and less elastic than those of arteries, as the blood flow pressure is significantly lower. Veins are generally located closer to the body surface and often run parallel to arteries, except in the subcutaneous adipose tissues of the arms and legs, where only venous vessels are present. Overall, the venous system is more extensive and denser than the arterial system,

resulting in the fact that the venous system holds about two-thirds of the total blood volume [28][29].

The lymphatic vessels, similar to veins and located within the connective and muscle tissues throughout the body, are composed of thin and elastic membranes that form channels responsible for transporting and draining lymph. Lymph is an essential fluid for the proper functioning of the body, consisting of water, electrolytes, fat, glucose, proteins, and white blood cells. These vessels drain the fluid from the spaces between tissues and return it to the bloodstream via the thoracic duct [30].

The overall architecture and cellular composition of blood vessels are consistent throughout the cardiovascular system. However, certain structural features that reflect different functional roles are unique to specific types of vessels.

The walls of blood vessels are primarily composed of endothelial cells (ECs) and smooth muscle cells (SMCs), mixed with a variety of substances that form the extracellular matrix (ECM), such as elastin, collagen, and glycosaminoglycans. The relative amounts of these fundamental components vary throughout the vascular system, adapting locally to mechanical or metabolic needs. In arteries and veins, these components are organized into three concentric layers: intima, media, and adventitia [30] (Figure 7, [31]).

- Intima is the innermost layer of the artery. The internal lining in contact with the blood is made up of endothelial cells, arranged in a single layer of flattened cells that form an impermeable barrier, though it can become permeable in response to various stimuli. The integrity of the endothelium is crucial for maintaining the structural and functional properties of the vessel, as this single layer of endothelial cells is the only barrier between blood and the underlying thrombogenic tissues. The endothelium rests on the basal lamina, a layer of loose connective tissue composed of collagen, proteoglycans, elastin, and other matrix glycoproteins. The endothelium provides structural support and acts as a filter for exchanges between the vessel and the interstitium. The outermost layer of the intima is an elastic structure known as the internal elastic lamina, which consists of a fenestrated layer of dispersed elastic fibers arranged longitudinally. The spaces between these fibers allow smooth muscle cells to penetrate into the intima [32].
- Media layer is composed of alternating layers of smooth muscle cells and elastic fibers arranged in several concentric layers, with the relative amounts depending on the type of artery. For instance, elastic fibers predominate in large arteries, while smooth muscle fibers are more prominent in medium and small arteries. The media is relatively poorly vascularized;

in fact, the oxygen and nutrients required for muscular function are supplied by diffusion from the vessels in the adventitia [32].

- Adventitia is the outermost layer surrounding the arterial vessels. It is primarily composed of fibrous and/or elastic connective tissue, although its composition can vary depending on the type of artery. In large arteries (>7 mm), the adventitia is made up of fibrocytes and collagen fibers, mixed with numerous elastic fibers. Near the boundary with the media, these fibers become densely packed to form the external elastic lamina, a fenestrated elastic membrane similar to the internal elastic lamina. In medium-sized arteries (2.5-6 mm), the outer layer consists of fibrous connective tissue with intertwined bundles, interspersed with elastic fibers. In smaller arteries (<2.5 mm), the adventitia is less prominent and in the smallest vessels, it consists only of a few elongated cells aligned parallel to the axis of the vessel [32].

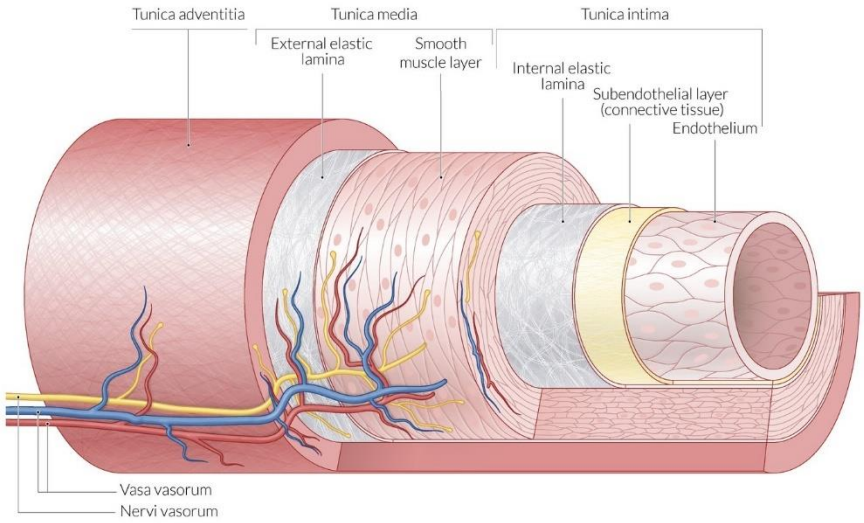

Figure 7. Graphical representation of the tunica intima, media, and adventitia.

The endothelial cells and smooth muscle cells that make up the vascular wall work in an integrated manner, influencing physiological responses to hemodynamic and biochemical stimuli. It is important to note that while endothelial cells share common characteristics throughout the vascular system, they differ morphologically depending on the specific function they perform. For example, they may be fenestrated to allow filtration in hepatic sinusoids, whereas they form an impermeable membrane in the central nervous system. Endothelial cells are characterized by having a non-thrombogenic surface, meaning they keep blood in a fluid state. They are also capable of metabolizing hormones, regulating

inflammatory processes, and influencing the growth of smooth muscle cells. Additionally, endothelial cells significantly influence the vasoreactivity of nearby smooth muscle cells by producing vasoconstricting or vasodilating factors.

Through the process of endothelial activation, these cells can respond to external stimuli by altering their normal constitutive functions and acquiring inducible functional properties. Various inducers of this mechanism include cytokines and bacterial products, hemodynamic stress, lipid metabolism products, and advanced glycation end-products. Viruses can also act as activators, prompting endothelial cells to produce growth factors or factors with procoagulant and anticoagulant activity.

Endothelial dysfunction occurs when there is an alteration in the endothelial phenotype, which can lead to vascular diseases such as thrombosis, atherosclerosis, or general vascular injuries. The natural process of vascular repair is carried out by smooth muscle cells, which can proliferate (if stimulated) and synthesize collagen, elastin, proteoglycans, and growth factors.

Endothelial cell dysfunction or loss leads to vascular injury, which in turn stimulates the recruitment and proliferation of smooth muscle cells: the ultimate result is a thickening of the tunica intima, which affects blood flow downstream. It is important to note that this response is observed in any kind of vascular damage or dysfunction [30].

Based on their structural characteristics and size, arteries can be divided into:

1. Elastic arteries: These are large caliber arteries located near the heart. They include the aorta and its major branches, such as the subclavian artery, the common carotid artery, the iliac artery, and the pulmonary arteries. They are characterized by walls rich in elastic fibers, enabling them to handle large volumes of blood coming from the heart [33].
2. Muscular arteries: These are medium-caliber arteries, including the smaller branches of the aorta, such as the coronary and renal arteries. They are characterized by a less elastic wall, but they are richer in smooth muscle cells, allowing them to regulate the blood flow through vasoconstriction (increasing blood pressure) and vasodilation (reducing blood pressure) [33].
3. Arterioles: These are small-caliber arteries responsible for supplying blood to the capillaries. Their walls consist of endothelial cells covered by a thin layer of smooth muscle cells. They have a diameter of about 50 to 100 μm and branch into terminal arterioles and metarterioles, with diameters of 10 to 50 μm, which deliver blood to the capillaries [33].

In general, the thickness of the arterial wall progressively decreases as the vessels become smaller. However, the ratio between wall thickness and the diameter of the vessel lumen, which is the internal

cavity of the artery through which the blood flows, increases, allowing muscular vessels to effectively control blood flow and pressure [30].

Capillaries are very small vessels with a diameter of about 5 μm, which is smaller than the size of red blood cells, typically 7-8 μm. They have thin walls composed of a single layer of endothelial cells surrounded by a basement membrane of cells similar to smooth muscle cells, called pericytes: overall, capillaries have a wide cross-sectional area, resulting in a relatively slow blood flow. These features allow for the efficient exchange of nutrients, such as oxygen and CO_2, between the blood and tissues. The number of capillaries varies depending on the metabolic activity of the specific tissue being supplied: the myocardium and the brain, which have high metabolic activity, exhibit the highest capillary density in the body [30], [33].

As previously described, veins collect deoxygenated blood and return it to the heart. Veins can be classified based on the part of the body in which they are located: thus, there are veins of the head, arm, leg, and abdomen.
Another classification, based on blood flow, divides veins into:

- Receptive veins: These veins have thin walls and receive blood by gravity. This group includes the veins of the head and neck, which collect blood from the upper part of the body. These veins then converge into the superior vena cava [33].
- Propulsive veins: These veins have thicker walls and are equipped with a swallow's nest valve system, allowing them to pump blood towards the heart against gravity (see Figure 8, [34]). These valves are shaped like pouches protruding inside the venous lumen: the pressure of the blood causes them to close, preventing backflow. Varicose veins reflect a loss of functionality and weakening of these valves, which can no longer prevent blood from flowing backward. This group includes the veins of the trunk and lower limbs [33].

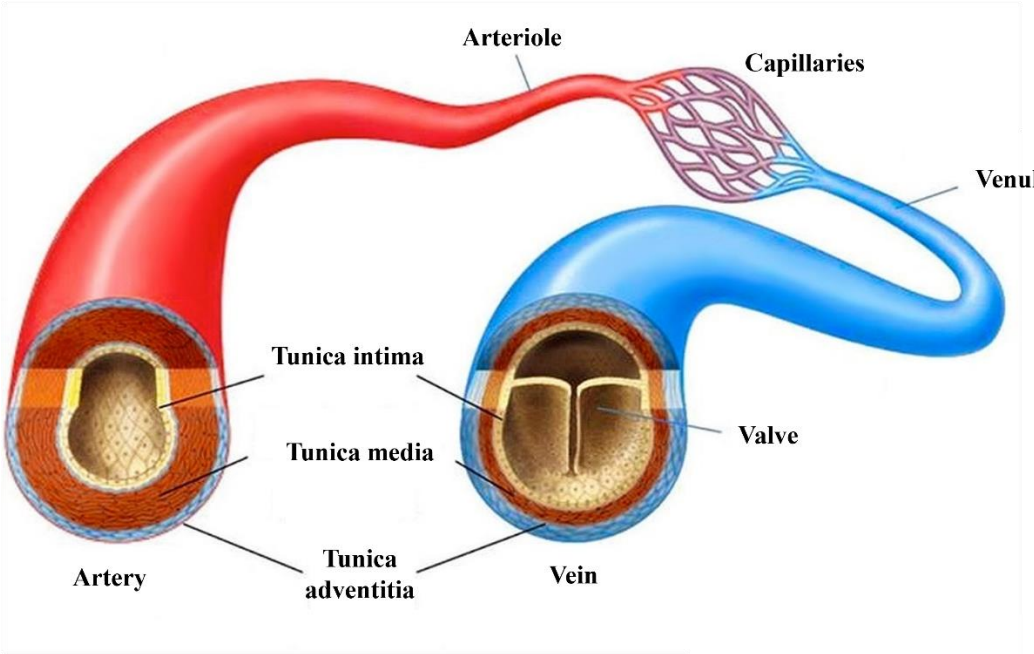

Figure 8. Structural difference between artery and vein.

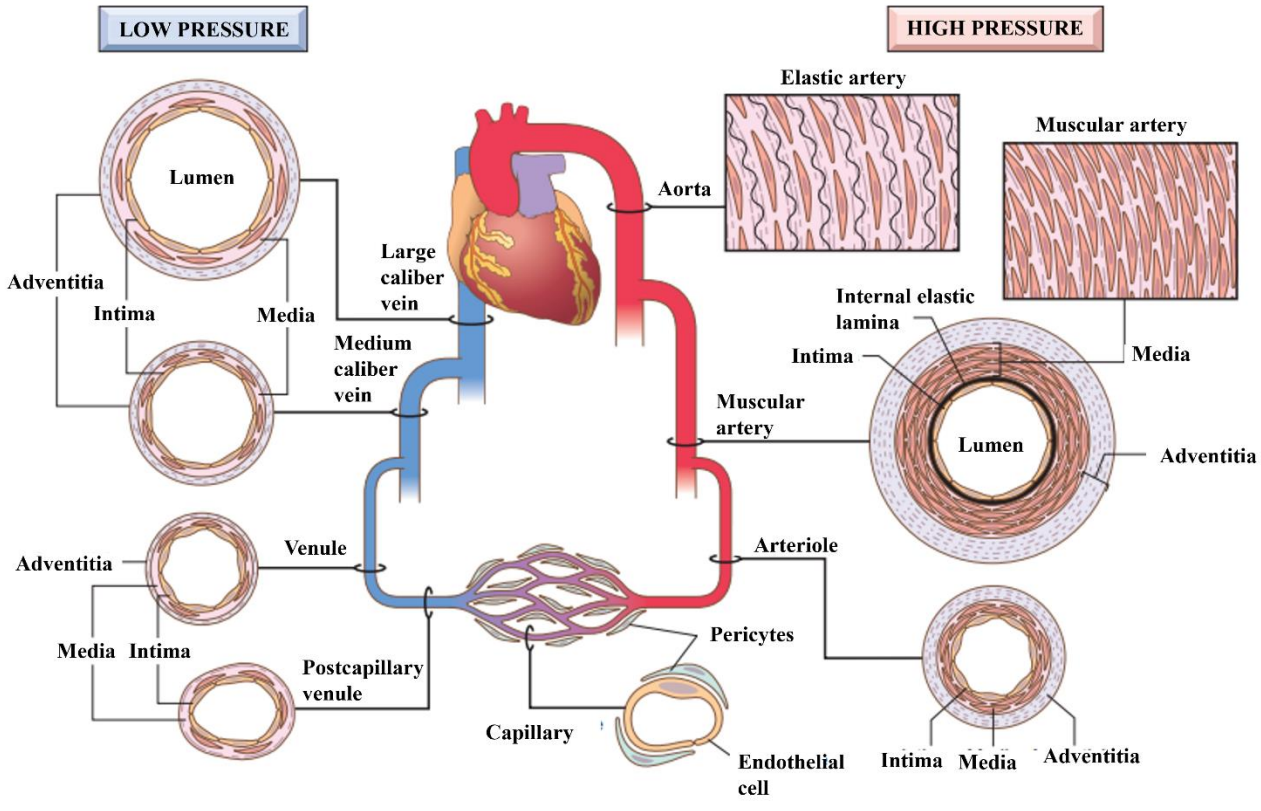

Figure 9. Representation of the basic organization of vascular structure.

The cardiovascular system delivers oxygen and nutrients to all the body's organs, tissues, and cells, while also removing carbon dioxide and waste products. Additionally, it transports white blood cells and other important molecules, such as hormones, allowing them to move between organs and tissues according to the body's needs.

The cardiovascular system is a closed and continuously active system, constituted by the heart and the blood vessels. The heart is a fibromuscular organ made up of two main pumps: the right heart, which pumps blood returning from the venous system to the lungs, and the left heart, which pumps blood from the lungs to the rest of the body.

The cardiovascular system is made up of two principal circuits: the pulmonary circuit, which includes the pulmonary blood vessels and those that connect the lungs to the heart, and the systemic circuit, which encompasses all the vessels that reach the other parts of the body. The pulmonary circuit features a network of capillaries that facilitates the exchange of nutrients and gases, such as oxygen and CO_2. In the pulmonary capillaries, oxygen from the air in the lungs enters the blood, while CO_2 exits the blood. The capillaries of the systemic circuit are found in all organs and tissues, where cells consume oxygen and produce CO_2. In these systemic capillaries, oxygen leaves the blood, and CO_2 enters. The flow in both circuits occurs simultaneously: as the right heart pumps blood to the lungs, the left heart pumps blood into the systemic circulation.

The stages of circulation can be summarized as follows:

1) The right ventricle pumps blood toward the lungs through the pulmonary artery. This artery bifurcates shortly after leaving the heart, directing blood to both the right and left lungs.
2) In the lungs, the blood becomes enriched with oxygen as it passes through the network of capillaries that cover the pulmonary alveoli.
3) The oxygenated blood then returns to the heart through the pulmonary veins (the only veins that carry oxygenated blood), which empty into the left atrium.
4) Subsequently, the oxygenated blood flows into the left ventricle, from where it leaves the heart again through the aorta.
5) Numerous branches of the aorta distribute the blood to the body's cells.
6) The deoxygenated blood then returns to the heart, collecting in the superior vena cava and the inferior vena cava, which both flow into the right atrium.
7) From the right atrium, the blood flows into the right ventricle, completing the circulation [35].

It is necessary to mention the existence of vascular anomalies, that are congenital diseases that originate from abnormal development during embryogenesis, and the type of pathology depends on

the embryonic stage during which it occurred. This definition includes both angiomas and vascular malformations.

Angiomas are swollen, reddish masses that result from a malfunction in the vessel-forming tissue, which, after completing its role in building blood vessels, turns into fibroadipose tissue. Although the lesion may increase in size over time, it typically does not pose a health risk.

Vascular malformations, on the other hand, are a more serious condition, and it is crucial to be aware of their presence, as failing to recognize them could lead to complications during surgical procedures. These are primarily unusual vascular networks, characterized by a higher-than-normal number of vessels, larger calibers, and an inverted overall architecture. These anomalies can affect all components of the vascular tree and can be classified as lymphatic, arterial, or venous [36], [37].

1.4.2 Coagulation

The endothelial cells lining blood vessel walls actively inhibit thrombotic events and serve as an anticoagulant surface. However, blood coagulation is a crucial process for the repair of blood vessels and is essential for maintaining tissue integrity. When an injury occurs, platelets immediately respond by forming a primary platelet plug to block blood loss. This plug is temporary and mainly serves to buy time for the activation of the coagulation cascade, a complex system of proteins that generates a stable blood clot necessary to stop the bleeding. Once the damaged tissue is repaired, the clot fully forms and is eventually removed through the process of fibrinolysis.

In the human body, there is a delicate balance between coagulation and anticoagulation: an excess of anticoagulation can lead to hemorrhages, while an excess of coagulation increases the risk of thrombosis, heart attack, and stroke. This balance must not be disrupted, even by medical devices in contact with blood, such as vascular grafts. However, these surfaces often promote thrombosis, shifting the balance toward increased coagulation.

When a vessel wall is damaged, the underlying matrix proteins are exposed, allowing circulating proteins, particularly fibrinogen, to aggregate. The enzyme thrombin plays a central role in thrombus formation by catalyzing the conversion of soluble fibrinogen into fibrin, which stabilizes and envelops the platelet plug. The fibrin network traps red blood cells, white blood cells, and platelets, transforming the plug into a stable blood clot.

Once the vessel or tissue damage is repaired, the fibrinolysis process degrades the clot [25].

More specifically, it’s important to mention that clot formation can originate from two different pathways: the intrinsic and extrinsic pathways, both of which converge at the enzyme thrombin.

Thrombin, which digests fibrinogen to form fibrin fibers that stabilize the clot as previously mentioned, is produced through the cleavage of the prothrombinase complex into FXa and FVa factors. The activity of prothrombinase begins in the presence of a negatively charged phospholipid surface, while thrombin, once produced, is activated by the presence of calcium ions (Ca^{2+}). Certain anticoagulant drugs, such as those based on citrate and EDTA (ethylenediaminetetraacetic acid), exploit thrombin's dependence on calcium ions: they act as chelators for Ca^{2+}, preventing thrombin from binding and thereby blocking blood coagulation. Thrombin can also promote the formation of additional thrombin by activating specific factors (FVIII or FXI), until a concentration sufficient for the creation of a stable clot is reached.

The inactivation of thrombin, necessary once the clot is stable, is achieved by binding with antithrombin (AT), forming a complex that is destined for degradation.

The intrinsic pathway of the coagulation process begins when blood comes into contact with a synthetic surface, particularly negatively charged surfaces, which easily induce thrombotic events and are thus rarely used *in vivo*. Essentially, in the intrinsic pathway, a series of inactive factors are sequentially activated, leading to a cascade of biochemical events that culminate in the activation of the FXa factor, which produces thrombin.

The extrinsic pathway, on the other hand, is triggered when the tissue factor thromboplastin (TF), a protein present on the membrane of smooth muscle cells in the subendothelium, is exposed following tissue damage at the vessel walls. In this pathway, TF also forms a series of protein complexes that sequentially lead to the activation of the FXa factor.

The endothelium is the ultimate non-thrombogenic material, so under normal physiological conditions, platelets simply bounce off endothelial walls as blood flows through vessels. However, when the endothelium is damaged, platelets come into contact with the underlying extracellular matrix and begin to adhere to this surface. This adhesion triggers a shape change in the platelets, causing them to aggregate and form a plug, which can lead to the development of a thrombus at the site.

When platelets no longer encounter healthy endothelium but instead detect the presence of subendothelium or a non-self-synthetic surface, they quickly bind to these "foreign" components. Typically, platelets follow the bloodstream until they reach a damaged area of the vessel where the underlying extracellular matrix is exposed. Collagen, one of the components of the matrix beneath the endothelium, is recognized by the platelets through receptors (integrin $\alpha 2\beta 1$) on their surface. This recognition leads to the binding of platelets to collagen and their subsequent activation.

Additionally, the binding between platelets and the matrix can also be facilitated by the interaction between the Von Willebrand factor (which binds to collagen) and the specific receptor (GP1B) on the platelets (Figure 10, [38]).

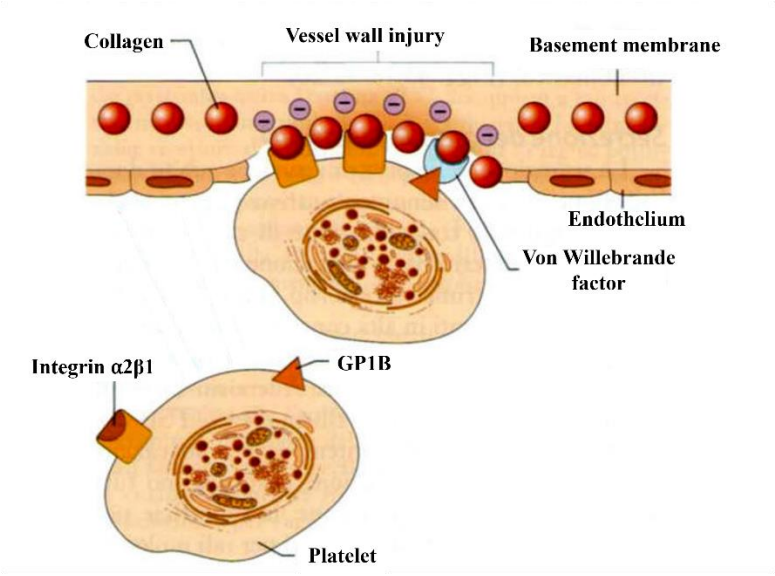

Figure 10. Mechanism of platelet adhesion to a vascular wall injury.

The surface of activated platelets becomes negatively charged, making it an ideal substrate for the propagation of the coagulation response: prothrombinase is activated, leading to the production of thrombin. Normally, the surface of platelets is spherical, but when they adhere to something, they flatten out to cover more surface area and quickly seal the breach. After activation, platelets can secrete various chemical activators, such as ADP, which further promote platelet adhesion.

In addition to binding to subendothelial layers when vessels are damaged, platelets also adhere to synthetic surfaces. In this case, the adhesion and subsequent activation of platelets result in significant morphological changes. They take on a "spike" shape, with protrusions extending from the main cell body, giving them a dendritic appearance. Preventing platelet adhesion and activation on synthetic surfaces is crucial to avoid the formation of clots on blood-contacting devices [39].

1.5 Pathologies of blood vessels

A. Atherosclerosis

Atherosclerosis is a disease that can affect the vascular systems throughout the body. It primarily involves the thickening and hardening of vessels caused by the accumulation of lipid plaques within the arterial walls.

The condition begins with damage to the endothelial cell layer that lines the vessel walls, which can be triggered by various risk factors, such as smoking, diabetes, hypertension, and/or elevated low-density lipoproteins (LDL). Following the damage to the endothelial layer, a series of pathophysiological events occur, which can be summarized as follows:

1) Endothelial cells no longer produce the correct amount of antithrombotic molecules due to the damage and become inflamed.
2) Pro-inflammatory cytokines are released.
3) Macrophages attach to the damaged endothelial cells through adhesion molecules like Vascular Cell Adhesion Molecule-1 (VCAM-1).
4) Macrophages release enzymes and oxygen radicals, leading to oxidative stress and the oxidation of LDL.
5) Additional growth factors are produced, stimulating the proliferation of smooth muscle cells within the affected vessel.

The oxidation of LDL, driven by inflammatory processes, oxidative stress, and macrophage activation, exerts a toxic effect on endothelial cells while simultaneously promoting the proliferation of smooth muscle cells.

Macrophages have several receptors on their surface that allow them to phagocytize LDL cholesterol; when they engulf oxidized LDL, they are known as foam cells. These foam cells are responsible for the initial injury to the vessel wall and contribute to the formation of a fatty streak. This streak triggers further inflammatory responses that increasingly damage the vessel wall. During this process, fibroblasts are also activated, releasing collagen into the fatty streak and leading to the formation of a fibrous plaque. If this plaque calcifies and protrudes into the vessel lumen, it causes an obstruction to blood flow. Moreover, some plaques may rupture before they fully obstruct blood flow, remaining clinically silent until the moment of rupture. When they rupture or fissure, they are referred to as complicated plaques and lead to the rapid formation of a thrombus, which can occlude the vessel, resulting in ischemia or infarction [40].

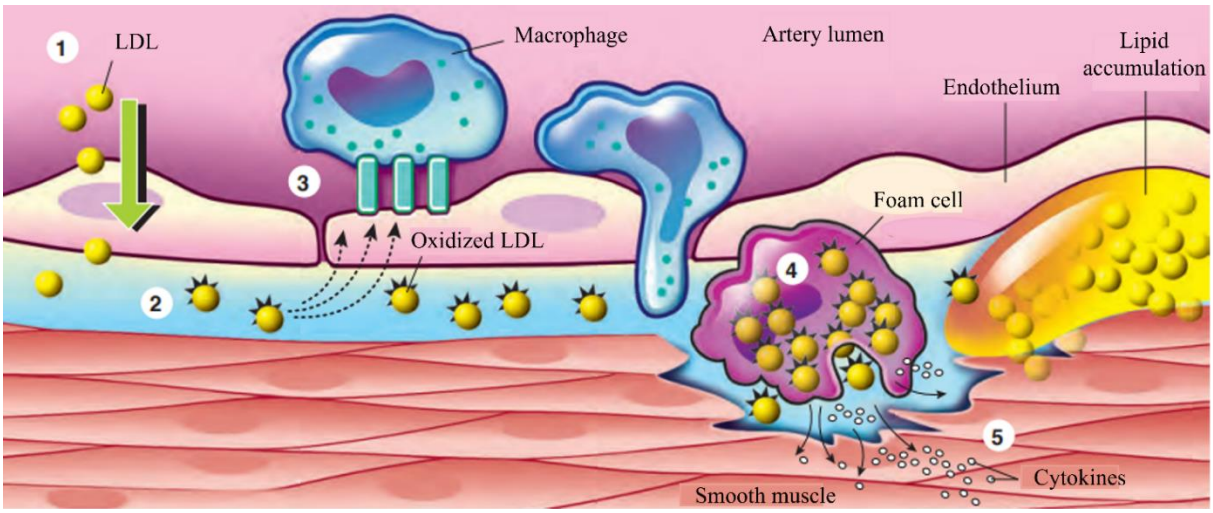

Figure 11. Oxidation process of low-density lipoproteins.

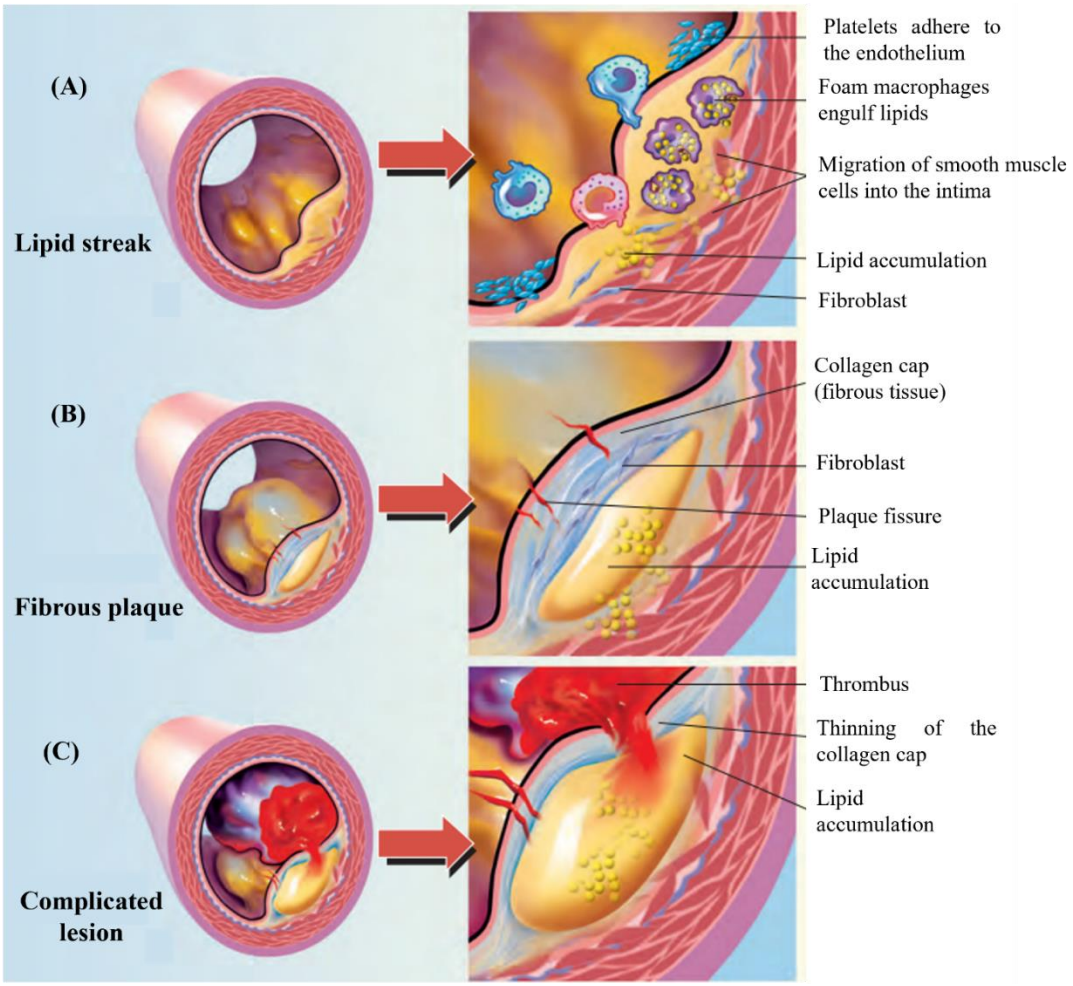

Figure 12. Atherosclerosis progression. (A) Formation of lipid streaks. (B) Fibrous plaque. (C) Complicated lesion.

B. Hypertension

Hypertension is a widely prevalent pathological condition characterized by a persistent increase in systemic arterial pressure. According to the Seventh Report of the Joint National Committee on Prevention, Detection, Evaluation, and Treatment of High Blood Pressure (JNC7), hypertension is defined as any condition where the average systolic pressure is 140 mmHg or higher, or the diastolic pressure is 90 mmHg or higher [41]. It must be said that systolic blood pressure is measured when the heart contracts and pumps blood into the arteries, while diastolic pressure is measured between two heartbeats, when the heart is relaxed and filling with blood. Factors that can contribute to the development of hypertension include aging, physical inactivity, and obesity. According to estimates from the National Health and Nutrition Examination Survey (NHANES) in 2018, 45.7% of the American population suffers from hypertension, a condition that significantly increases the risk of developing any cardiovascular disease or organ-specific diseases, such as myocardial infarction, kidney disease, and stroke [42].

The classification of hypertension used in Europe is presented in Table 1.

Table 1. Classification of the various hypertension conditions.

Category	**Systolic [mmHg]**		**Diastolic [mmHg]**
Optimal	<120	and	<80
Normal	120-129	and/or	80-84
High-normal	130-139	and/or	85-89
Grade 1 hypertension	140-159	and/or	90-99
Grade 2 hypertension	160-179	and/or	100-109
Grade 3 hypertension	>180	and/or	>110
Isolated systolic hypertension	>140	and	<90

It is important to note that this division into blood pressure ranges is arbitrary and primarily aims to simplify the diagnosis of hypertension. Additionally, it must be said that isolated systolic hypertension predominantly affects the elderly and results from the progressive stiffness of large arteries due to aging. In contrast, isolated diastolic hypertension is more common in younger individuals and is caused by the hyperactivation of the sympathetic nervous system, leading to vasoconstriction and increased peripheral resistance in the arterial vessels [43].

C. Aneurysm

An aneurysm is defined as a localized, permanent, and progressively enlarging dilation or bulging of the vascular wall. Most arterial aneurysms occur in the abdominal aorta due to the constant hemodynamic stress it endures, which causes its diameter to increase by more than 50% compared to the normal value. The primary cause of this condition is atherosclerotic disease, as plaques disrupt the structural integrity of the vessel wall. However, the risk of aneurysms can also be heightened by factors such as age, smoking, genetic predisposition, or hypertension. Hypertension, in particular, generates mechanical forces that weaken the arterial wall, contributing to its dilation. Other possible causes of aortic aneurysms include infections like syphilis, collagen disorders such as Marfan syndrome, and thoracic or abdominal trauma [44].

Aneurysms can be classified as true or false aneurysms (Figure 13, [40]):

- True aneurysms involve a weakening of the arterial wall that affects all three layers (tunics) of the vessel and can have a fusiform circumferential or saccular shape.
- False aneurysms occur when there is a communication between the intravascular lumen and the surrounding extravascular space due to the rupture of a point in the arterial wall. Outside the cavity, a blood clot forms, sealing the communication channel. These lesions can occur as a result of leaks between a vascular graft and a natural artery [40].

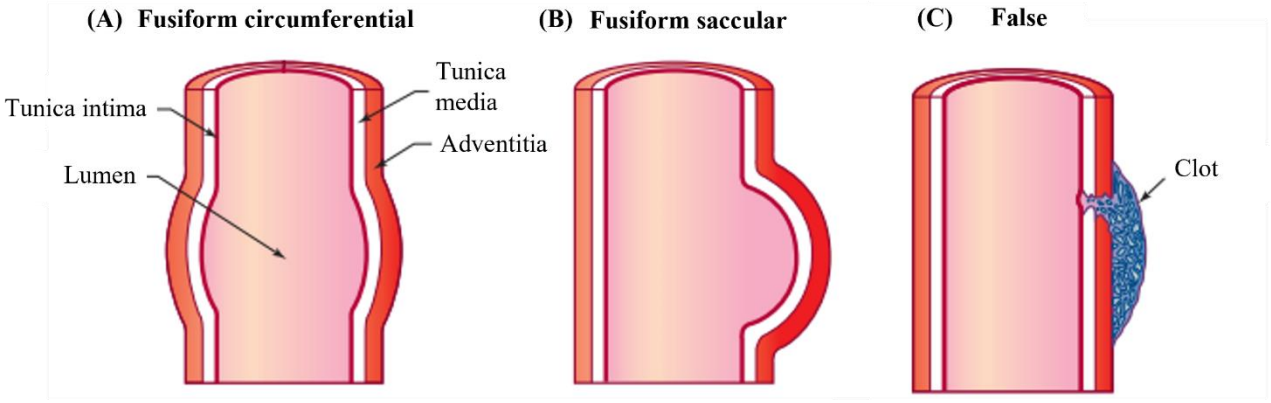

Figure 13. Longitudinal section of a vessel highlighting different types of aneurysms.

A further classification of aneurysms is based on their location within the vascular tree: thus, aneurysms can be referred to as cardiac, aortic, thoracic, or abdominal aneurysms.

As previously mentioned, the abdominal aorta is the most common site for aneurysm development. The dilation of this vessel follows an exponential growth pattern, with larger aneurysms expanding

more rapidly. The final stage of aneurysmal growth is the rupture of the aneurysm, which occurs when the internal forces within the aneurysm exceed the strength of the arterial wall. It has been shown that the risk of rupture is higher in saccular aneurysms than in fusiform ones, due to the greater stress exerted on the arterial wall at the site of the lesion [44].

D. Arterial thrombi

If conditions within the intravascular environment trigger the coagulation cascade, arterial thrombi can develop. Potential causes of pathological coagulation activation include alterations in the tunica intima due to atherosclerosis, infectious agents, the presence of aneurysms, traumatic events, or obstructions that cause blood stasis and accumulation.

The possible consequences of arterial thrombi on circulation include:

- Total artery occlusion, leading to ischemia in the tissue supplied by that artery.
- Fragmentation of the thrombus, which can cause a thromboembolic event, allowing the fragments to travel through the vascular system until they block a vessel [40].

E. Embolism

The term "embolism" refers to the movement and circulation of substances foreign to the blood within the bloodstream. An embolus, which can be a solid body like a thrombus that has detached from its original site, an air bubble, a cluster of fat, bacteria, or tumor cells, or even a liquid pocket, travels through the bloodstream until it lodges in a vessel, causing an obstruction due to its size.

Depending on the location where the embolus occurs, we can distinguish between blood embolism, which affects arteries, veins, and capillaries, and lymphatic embolism, which involves the lymphatic vessels [40].

F. Varicose veins and chronic venous insufficiency

Varicose veins are a disorder of the superficial venous system that involves the inability of blood to properly return to the heart. The primary causes include:

- Abnormalities in the venous wall, such as wear or damage to the valves inside the veins.
- Dilatation of the venous vessel due to the force of gravity acting on the blood in the lower limbs.
- Hypertensive conditions.

These factors can overlap: for example, the dilation process continues until the pressure inside the vein damages the valves, which can no longer maintain unidirectional blood flow, leading to increased hydrostatic pressure in the vein.

If the inadequate venous return becomes chronic, varicose veins can progress into chronic venous insufficiency (CVI). Blood stasis and high hydrostatic pressure within the vein cause inflammatory processes in the vein and surrounding tissue. Proper circulation is severely compromised by venous stasis, making it difficult to meet the cells' demand for oxygen and nutrients. The supply of these nutrients may cease entirely if further mechanical trauma occurs, leading to cell death by necrosis (known as venous stasis ulcers) [40].

G. Deep vein thrombosis

Deep vein thrombosis (DVT) refers to the formation of a thrombus in the large veins, particularly in the lower limbs, following the activation of the coagulation cascade. Factors that increase the risk of developing this condition include:

- Venous stasis, caused by obesity, lack of movement, or valve-related venous disorders.
- Trauma to the venous endothelium, resulting from medical treatments or surgical procedures.
- Factors that increase coagulation, such as hereditary disorders, pregnancy, oral contraceptives, or hormone therapies.

The venous thrombus forms due to the accumulation of coagulation factors under conditions of blood stasis within the vein, often near the valve. DVT is a potentially very dangerous condition because it can lead to pulmonary embolism, which occurs when a fragment of the thrombus breaks off and travels to the pulmonary circulation [40].

1.6 Treatment of vascular pathologies

A. Angioplasty

Angioplasty is a technique used in cardiology to widen the narrowed coronary arteries that reduce blood flow to the heart. It is a minimally invasive procedure, performed under local anesthesia, during which arterial dilation is achieved by inserting a balloon catheter that is then inflated at the site of the narrowed blood vessel. During the operation, the surgeon inserts the catheter into an artery and guides it to the site of the blockage. The exact location and extent of the blockage can be visualized using a contrast dye released from the catheter. The balloon is then inflated to widen the obstructed vessel, and a stent (a small expandable metal tube) may be inserted to allow blood to flow more freely and

to maintain the restored vessel diameter over time (Figure 14, [45]). This treatment is widely used to clear arteries of atherosclerotic plaques and it is adopted when the vessel's lumen occlusion is less than 70% [46].

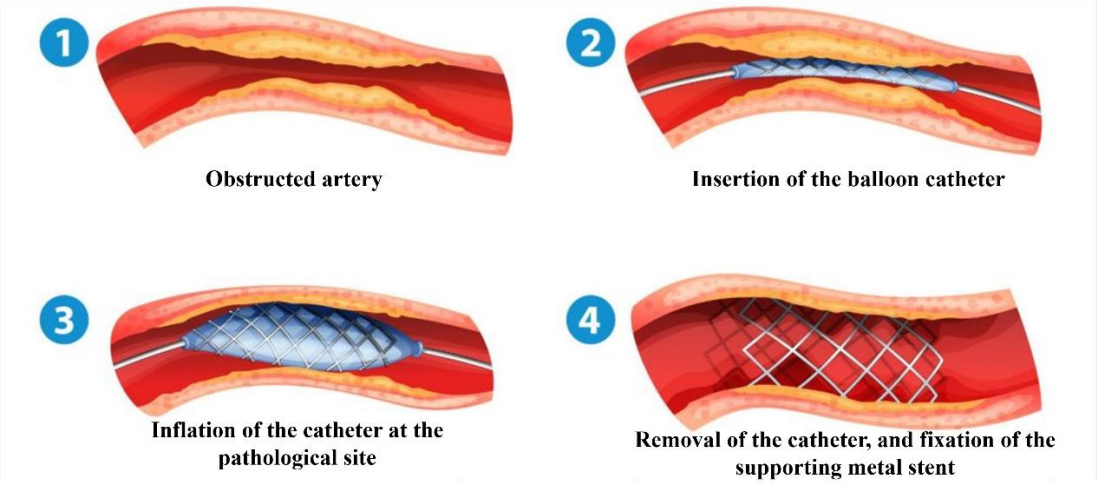

Figure 14. Schematic representation of the angioplastic procedure.

B. Coronary Artery Bypass

Coronary artery bypass surgery is performed to treat occluded or severely stenotic coronary arteries that cannot be managed with angioplasty. This procedure involves surgically creating arterial or venous grafts, which serve as alternative pathways for oxygenated blood to reach the heart, bypassing the obstructed vessel. Essentially, the vascular graft is used to bypass the diseased area, becoming a circuit parallel branch known as bypass (Figure 15, [47]). It is the most performed surgery worldwide for the treatment of vascular diseases, and the techniques used have been well-established for decades.

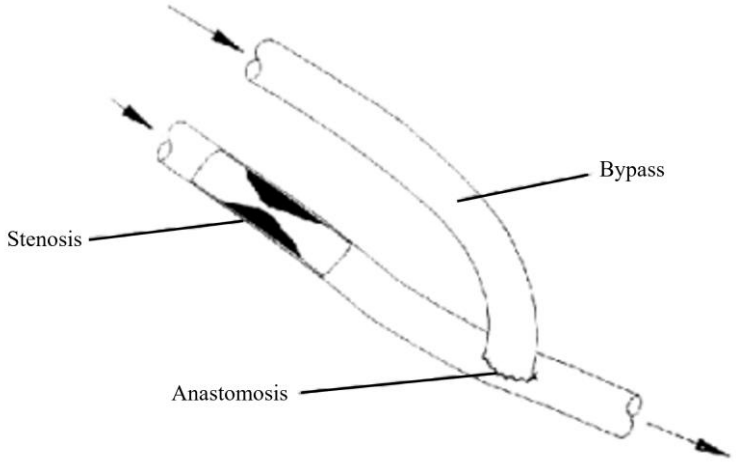

Figure 15. Schematization of a bypass, where the vascular graft delivers blood downstream of the stenosis.

The techniques used may or may not involve the use of a heart-lung machine: in the first case, the on-pump technique is employed, utilizing extracorporeal circulation, while in the second case, the off-pump method is used, meaning the surgery is performed on a beating heart. Additionally, a minimally invasive surgical technique for coronary bypass, known as MIDCABS (Minimally Invasive Direct Coronary Artery Bypass Surgery), can also be adopted.

The traditional on-pump technique involves a surgical incision in the chest wall, followed by clamping of the aorta (a process in which a clamp is placed on the blood vessel to temporarily close its lumen) and stopping the heart with a cardioplegic solution. This solution allows the myocardial cells to tolerate ischemia and reperfusion. To facilitate vascular anastomosis (the procedure to reestablish the continuity of blood vessels), the heart-lung machine is used to stop the heart and drain it of blood. Once the necessary vascular anastomoses are completed, the aorta is unclamped, and oxygenated blood flows again through the coronary arteries. Finally, normal heart activity is restored. During cardiopulmonary bypass, the patient must be given a high dose of heparin to prevent blood clotting in the bypass circuit. The main complications that can arise are due to the use of the heart-lung machine, which may trigger systemic inflammatory responses, leading to organ dysfunctions such as those affecting the lungs, kidneys, brain, or stomach. Additionally, the clamping and unclamping of the aorta can cause strokes due to emboli mobilization. Finally, arrhythmias may occur in the days following the surgery.

To overcome the complications associated with the traditional on-pump method, off-pump techniques have been developed that do not require the use of the heart-lung machine. These procedures allow for revascularization on a beating heart, using devices that stabilize a portion of the myocardium, keeping still the surgical site. Small intercostal incisions are made to perform the vascular anastomoses. Since the beating heart continues to demand oxygen, it remains sensitive to the interruption of blood flow during the operation. The risks associated with this process can be mitigated by using a temporary coronary shunt, which allows for blood perfusion distal to the surgical site. The off-pump technique is recommended for patients at higher risk of complications from extracorporeal circulation, such as those with severe aortic calcifications that make aortic manipulation dangerous or those with coagulation disorders.

The minimally invasive MIDCAB technique involves accessing the heart through small incisions, performed endovascularly with catheters inserted into the blood vessels. In this procedure, the aorta is not clamped in the traditional manner but is instead occluded using a balloon positioned at the tip

of the aortic catheter. This method is not suitable for multiple bypasses, and the rate of potential complications is similar to those of on-pump and off-pump techniques [48].

C. Carotid Endarterectomy

Carotid endarterectomy is performed in cases of carotid artery stenosis, which involves a blood vessel located laterally and bilaterally in the cervical region that is responsible for carrying blood to the head and brain. The lack of oxygen supply to the brain, leading to the death of brain cells, is caused by the closure or narrowing of the carotid arteries. The procedure is conducted on patients with at least 70% blockage of the carotid artery lumen. An incision is made in the neck near the affected artery, and the vessel is manually cleaned by removing the atherosclerotic plaque. This restores the vessel's lumen to its normal size, reestablishing proper blood flow to the head. Finally, the arterial wall is sutured using grafts or patches [49].

D. Sclerotherapy

Sclerotherapy is a treatment used for varicose veins, involving the injection of pharmacological solutions into the affected veins to induce their closure or to thicken their walls. The result is a reduction in blood pooling, which also halts the progression of varicose disease. Sclerotherapy is the only other effective method for treating varicose veins besides surgery [50].

During sclerotherapy, injections are made into the varicose veins, administering liquid solutions, formed by polidocanol alcohol, sodium tetradecyl sulfate, sodium salicylate, and chromated glycerin, to close them. However, in recent years, innovative solutions have been developed for sclerotherapy application:

- Use of endovenous sclerosing foam: The pharmacological solution is injected in foam form. Compared to traditional liquid solutions, foam can interact with the venous wall for a longer and more extensive period, allowing for a lower concentration of the injected drug. Additionally, the foam is visible via ultrasound, enabling precise tracking of the vein segment to be occluded and monitoring of the drug's progression and effects within the venous system.
- Transcutaneous laser treatment: A thin, low-energy laser beam is used to target the affected venous wall, causing it to thicken and close.
- Photochemical treatment: This is a hybrid solution combining the use of foam and transcutaneous laser. It is a personalized technique that allows for the minimal use of both the drug and laser energy, resulting in fewer side effects and requiring fewer treatment sessions for the patient [51].

E. Anticoagulants

Anticoagulant therapy is used for patients at high risk of developing blood clots. These medications alter the blood's ability to clot, making it more fluid and thereby reducing the risk of thrombus formation within blood vessels. The mechanism of action of these drugs involves interfering with the activation of clotting factors, which are necessary to initiate clot formation. These factors are activated when they come into contact with vitamin K: anticoagulants work by inhibiting vitamin K, preventing the coagulation process from starting. It is important to note that anticoagulant medications are highly specific to each patient in terms of dose and concentration, as an excessive dosage can lead to bleeding. Vitamin K can be used as an antidote in cases of anticoagulant overdose [52].

1.7 Vascular substitutes

Due to the increase in the average age of the population and the widespread prevalence of diabetes mellitus, arterial atherosclerosis has significantly risen in recent decades, making vascular diseases one of the leading causes of death in today's society. As a result, the focus of doctors and researchers has increasingly shifted towards revascularization procedures. In absolute terms, the most commonly used treatment remains endovascular and minimally invasive surgery. However, when it comes to complex arterial diseases or failed vascular interventions, there are still many unresolved cases. For example, in a standard lower limb bypass surgery, the autologous saphenous vein is typically used, while the internal thoracic artery is commonly employed for coronary bypass procedures [53]. The widespread use of these vessels for bypass procedures is due to the high primary patency (term that refers to the suitability of a conduit for the passage of gases or fluids through it) rates demonstrated at 5 years. However, a significant percentage of patients do not have suitable vessel characteristics for these options: vessels may not be easily accessible, as in the case of obese patients, or the combined procedure of vessel removal and bypass might be too lengthy and risky for the patient. This has driven researchers to focus on developing vascular substitutes that replicate the mechanical and functional properties of native vessels. The possible alternatives in this field are diverse and may include cellular or acellular components, either homologous or purely synthetic.

1.7.1 General requirements

The ideal vascular substitute should possess the following properties:

- Impermeability to blood.
- Absence of toxicity and immunogenicity.

- Biocompatibility.
- Resistance to thrombosis, meaning its surface should not activate the coagulation cascade to prevent lumen obstruction.
- Resistance to infection.
- Adequate elasticity and tensile strength.
- High compliance, meaning the graft can contract and expand radially in response to changes in blood flow pressure.

Additionally, from a technical standpoint, the ideal graft should be easy to implant, manageable, reasonably priced, and available in various sizes for emergency situations.

We can distinguish vascular grafts based on their size:

1) Large-caliber scaffolds: with a diameter greater than 6 mm.
2) Small-caliber scaffolds: with a diameter between 4 and 6 mm.

The human body reacts quite differently to the implantation of these two types of prostheses. In the case of large-caliber prostheses, blood flow moves faster and stays in contact with the vessel walls for a short time, unlike small-caliber scaffolds, which face more issues with hemocompatibility and a higher incidence of thrombotic events. The formation of blockages or the onset of hyperplasia is much more frequent in vessels with very small diameters.

To improve graft compatibility and limit undesirable effects, it is crucial that the size and mechanical properties closely match those of the original vessels. Otherwise, there could be disruptions in blood flow or improper transfer of pulsatile energy.

Another critical factor is the endothelialization of the prosthesis, which refers to the process of seeding the prosthesis with endothelial cells to reconstruct a natural endothelium and promote the formation of a new vessel. However, numerous challenges arise because the seeded cells struggle to adhere to the scaffold's surface and proliferate normally.

Lastly, to encourage the formation of the neointima, it is important that the graft wall has the correct porosity, although this is a difficult objective to achieve. Often, the neointima does not form, or the newly formed tissue grows excessively around the anastomoses, obstructing the vessel and leading to intimal hyperplasia [54].

The autologous vein is currently the best available material for prosthetic substitute because it offers a good combination of the aforementioned characteristics. However, it does not represent the gold standard, as venous grafts are prone to complications such as neointimal hyperplasia (a condition where the vessel narrows due to the separation between the internal and external elastic lamina, leading to smooth muscle hypertrophy), aneurysm, and atherosclerosis [55]. It is therefore necessary

to use artificial vessels, primarily made from materials such as ePTFE (expanded polytetrafluoroethylene) and Dacron (synthetic polyester fibers), which, however, do not offer the same performance as autologous vessels. Although satisfactory patency rates have been demonstrated, the main issues with these materials are the lack of endothelial cell growth within the artificial vessel and the different mechanical response between the elastic artery and the rigid graft. Additionally, while ePTFE and Dacron can be used for large-caliber vessels, they do not yield satisfactory results for small-caliber vessels. The search for materials suitable for small vessels that mimic the elasticity of native arteries remains one of the main objectives in tissue engineering [56].
Research into synthetic materials for the production of artificial blood vessels began in the second half of the 20th century. The materials initially tested, such as metal, glass, ivory, silk, and nylon, were unsuccessful because they led to thrombotic events and failed to meet the durability criteria of native vessels: it is therefore essential to find inert materials that interact as little as possible with the surrounding tissues and with the blood itself. [49].

A good vascular graft is composed of three fundamental components: the scaffold, which can be either biological or prosthetic, the extracellular matrix, and the endothelial cells. The scaffold must provide the basic mechanical structure on which cells can adhere and proliferate appropriately; it can either offer permanent support or be biodegradable, remaining intact until the blood vessel has properly reformed. The extracellular matrix must provide a suitable environment for the adhesion and proliferation of endothelial cells, which are crucial for ensuring an antithrombotic surface on the vascular substitute [56].
As mentioned earlier, vascular implants can originate from biological sources or be made from artificial materials, allowing for the following classification ([47]):

1) Biological prostheses:
    I. without chemical treatment.
    II. with chemical treatment.
    III. with synthetic support.
2) Synthetic prostheses made of:
    I. Polyethylene terephthalate (PET or Dacron).
    II. Polytetrafluoroethylene (PTFE or Teflon).
    III. Polyurethane.
    IV. Polydimethylsiloxanes (PDMSs).
    V. Bioresorbable materials.

However, both artificial and biological prostheses have significant drawbacks. Artificial prostheses require lifelong anticoagulant therapy and can lead to adverse effects such as thromboembolism and endocarditis. Biological prostheses, on the other hand, do not require anticoagulant therapy and offer better hemodynamic profiles, but they are limited by the potential for rejection due to the recipient's immune response. To prevent such adverse reactions, the tissue is treated with glutaraldehyde, but this treatment can cause cross-linking, cytotoxicity, and calcification, as well as damage to the collagen-elastin network and infiltration into the collagen matrix.

To address these issues, various decellularization techniques have been developed to remove cellular residues from the tissue. Common methods for eliminating donor cells include the use of triton-colate (TRICOL) and triton-taurodeoxycholate (TRITDOC) solutions [57].

1.7.2 Porosity

Porosity, defined as the degree of water permeability, is crucial for the patency of grafts, making the evaluation of this characteristic essential during the production of vascular grafts. However, it is challenging to accurately determine the spaces necessary for cell regrowth due to the varying pore sizes found in current synthetic matrices.

Experimental observations have shown that the interstitial pores of grafts often allow the entry of macrophages and other inflammatory cells but not connective tissue cells of similar size. This is because the development of connective tissue cells occurs after the growth of the endothelium. Therefore, to achieve a functional implant, the graft must have pores suitable for capillary growth and subsequent growth of other cells.

In experimental settings, it has been observed that the complete cellular regeneration of small-caliber vessels in ePTFE occurs only if the porosity is high enough to allow capillary growth. The central role of scaffold porosity in cellular regeneration has been the focus of numerous experiments, addressing both external and internal scaffold porosity [54].

Regarding external porosity, a two-month study ([58]) on the abdominal aorta of mice was conducted to compare the endothelial growth performance of 32 microporous polyurethane grafts with varying external porosity and 8 ePTFE grafts as a reference. The results indicated that all investigated prostheses showed rapid endothelial cell growth by the second week, although the PU scaffolds with higher porosity exhibited the highest growth rates. Additionally, PU grafts allowed the formation of a complete endothelial layer, whereas ePTFE grafts resulted in incomplete coverage.

As for internal porosity, several studies have demonstrated a correlation between this parameter and the likelihood of thrombogenic events: an internal wall with high porosity is less thrombogenic than

one with low porosity. Supporting this theory, a study comparing the hemocompatibility of cardiothane-51 (CA) grafts (composed of 10% polydimethylsiloxane and 90% polyether-polyurethane) with different internal porosities found that small-caliber grafts with high internal porosity led to less platelet adhesion, resulting in a lower risk of clot formation [59].

1.7.3 Compliance

Compliance is defined as the ability of a vessel to expand under increasing blood pressure and is a fundamental parameter for assessing the functional compatibility of vascular grafts. Compliance C can be expressed by the following equation:

$$C = \frac{\left(\frac{\Delta D}{D}\right) 100}{\Delta P} \tag{1}$$

where ΔD is the change in vessel diameter, and ΔP is the change in blood pressure.

It is important to remember that arteries possess elastic properties that allow them to radially dilate when blood pressure is at its systolic peak, and then return to their original shape during diastole. This arterial elasticity results in periodic blood accumulations, which in turn cause progressive dampening of the flow and pressure waves as they travel from the heart towards the periphery. The speed v at which these pressure waves propagate can be expressed by the Moens-Korteweg equation:

$$v = \frac{Es}{\rho D} \tag{2}$$

where E is the elasticity of the vessel wall,

s is the vessel thickness,

D is the vessel diameter,

and ρ is the blood density.

A different compliance between the native vessel and the artificial graft (which is stiffer and therefore has lower compliance) can lead to implant failure, resulting in two main consequences. The first concerns the discontinuity in the propagation speed of pressure waves at the interface between the artery and the scaffold: at this point, wave reflection and fluid dynamic discontinuities occur. The second consequence involves the stress exerted on the suture points of the anastomoses, due to the fact that the natural vessel expands radially while the prosthesis maintains its original shape [47].

1.7.4 Classification

1.7.4.1 Biological prosthesis

Biological vascular implants consist of segments of vessels harvested from the patient, donors, or animals, which are then treated chemically or otherwise and implanted as bypasses in the diseased vascular region. The harvested venous and arterial segments are preserved at 4°C or frozen for days or weeks before being used.

When harvesting from the patient, the saphenous vein from the leg, with a diameter between 4 and 6 mm, is primarily used for coronary bypass surgery. This venous graft is connected to the aorta and downstream of the blocked coronary artery. However, this solution has some disadvantages, as the saphenous vein, when used to replace an aortic segment, does not possess the same mechanical properties (pressure resistance and pulsatility) as the original artery. Additionally, to ensure adequate blood flow, it is necessary to either remove the valves within the saphenous vein without damaging the vessel wall or implant it in a reversed orientation.

Another biological graft harvested from the patient involves using the internal mammary artery for coronary bypass surgery. In this case, the procedure is easier to perform because it only requires cutting the mammary artery, located near the heart, and connecting it downstream of the blocked artery with a single anastomosis. However, allogeneic grafts have limited use because they tend to show low patency rates after just a couple of years.

If the patient does not have suitable blood vessels for the bypass, arterial or venous segments from external donors can be implanted. It should be noted that grafting vascular segments from cadavers may trigger inflammatory responses in the patient, potentially leading to the failure of the procedure. To prevent this, proper tissue preservation before the grafting and the implementation of immunosuppressive therapy are crucial.

An important example of a donor-based implant is the use of the human umbilical vein treated with glutaraldehyde for small-caliber bypass surgery. The umbilical vein is harvested from the umbilical cord within the first 24 hours after the baby's birth, treated with glutaraldehyde, and then fitted with a mandrel to maintain its shape before refrigeration[47].

Regarding vascular grafts of animal origin, Rosenberg was the first to conduct studies on the use of bovine carotid artery as a vascular prosthesis in humans [60]. Over the years, many researchers have explored this field. For instance, Huynh developed a vascular scaffold from collagen obtained from the mucosa of pig small intestine and type I bovine collagen. This scaffold was decellularized, treated with heparin, and implanted into rabbit aortas. The results were considered promising, as no thrombotic events occurred during the 90-day observation period before

explantation [61]. Another noteworthy example is the work by Clarke, who implanted decellularized bovine ureters into the canine aorta, achieving complete patency and absence of aneurysms and thrombi during the subsequent 10-month observation period [62].

A more advanced type of chemically treated biological implant involves vascular prostheses made from bovine pericardium. These prostheses are constructed by stitching a piece of bovine pericardium that has been pre-corrugated and treated with glutaraldehyde. The corrugation serves to keep the vessel flexible, reducing the risk of occlusion during bending movements [47].

1.7.4.2 Synthetic prostheses

Synthetic vascular implants are industrially produced using non-biological materials. The development of these artificial systems began with the aim of reducing the risk of rupture in abdominal aortic aneurysms, which, in the 1940s and 1950s, were treated with stainless steel piano wires inserted into the aneurysmal sacs or with epoxy resins.

In the field of synthetic tissues for vascular applications, it has been observed over the years that when these fibers are exposed to blood flow, fibrin tends to accumulate within the pores of the fabric. This fibrin deposition promotes the growth of fibroblasts from the vessel wall, facilitating the subsequent migration of endothelial cells. This process leads to the formation of an inner lining on the artificially manufactured prosthesis that closely resembles the natural endothelial surface of arteries.

Various materials have been used to create synthetic vascular prostheses, including Vinyon N, Nylon, Orlon, Dacron, and Teflon. However, due to issues such as the loss of mechanical properties, biological degradation, and manufacturing challenges, only Dacron has remained in use for these applications [47].

A. Polyethylene terephthalate (PET)

Dacron is the trade name for polyethylene terephthalate (PET), a type of polyester used in fiber form. Dacron is a condensation polymer obtained from ethylene glycol and terephthalic acid whose chemical structure is shown in Figure 16 ([47]).

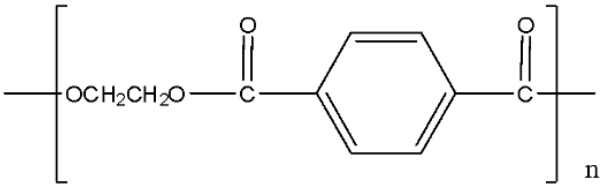

Figure 16. Chemical structure of Dacron.

PET was the first polymer employed as a material for vascular prostheses, available as early as 1957, and was immediately appreciated for its ease of handling and suturing. In the production of these prostheses, Dacron filaments were twisted to form threads, which were then knitted (that is woven) or crimped. Initially, the knitted form was preferred due to its porosity, which facilitated cell adhesion and growth. A further improvement was achieved by adding a series of perpendicular rings to the knitted structure, enhancing the anchorage of the prosthesis and the formation of neointima. However, the clinical evaluation of vascular prostheses made from woven synthetic fibers has highlighted the main advantages and disadvantages of this approach. A key factor is the flexibility of the prosthesis, which allows it to adapt to curves, such as when implanted near joints like the hip or knee. However, woven prostheses tend to occlude when subjected to flexion in these areas. To address this issue, corrugated prostheses, either accordion-shaped, with circular folds, or spiral corrugations, have been preferred. The corrugation enables the prosthesis to bend, allowing the outer surface to stretch and the inner surface to contract. Additionally, this design makes the prosthesis more adaptable to length variations during use, reducing stress on the sutures with the natural artery and simplifying the cutting process to the required length [47].

One of the key advantages of using PET is that it is chemically inert and highly hydrophobic, which reduces the risk of degradation by hydrolysis. Additionally, this polymer can be sterilized in various ways, such as steam autoclaving, ethylene oxide, or gamma radiation, without undergoing significant degradation [47].

Dacron grafts exhibit anisotropic behavior, meaning they respond differently depending on the direction of the force applied. When tensile strength tests are conducted on samples taken in longitudinal and circumferential directions, it is observed that both follow a similar pattern with an initial elastic phase followed by a nonlinear behavior. However, the numerical values differ: circumferential samples are stiffer, with less elongation at break and higher tensile strength. This anisotropy is attributed to the orientation and number of fibers in the samples, as well as the fact that stretching in the longitudinal corrugations promotes elongation in that direction.

The high circumferential stiffness of the graft helps dampen the pressure wave, potentially impacting the cardiac stroke, while the corrugated shape in the longitudinal direction helps mitigate this effect [63].

Factors such as manufacturing defects, improper storage, incorrect use during surgery, mechanical fatigue, and biodegradation, can lead to structural failure, although the risk is low. Manufacturing defects, such as excessive temperatures during spinning or overexposure to gamma or beta

radiation during sterilization, can compromise the graft's integrity. The areas where Dacron fibers are joined to form the circular structure are particularly vulnerable, as these points are subject to high stress during graft preparation. Additionally, the pulsatile blood flow causes progressive stretching and thinning of the Dacron fibers, leading to the eventual rupture of some fibers, a phenomenon more evident in small-caliber grafts.
Biodegradation is another factor that can compromise the graft's integrity. Over time, some fibers may weaken due to mechanical fatigue, attracting the attack of giant cells typical of foreign body reactions, which accelerates the degeneration of the graft [55].

B. Scaffold with fluorinated polymers

Teflon, the trade name for polytetrafluoroethylene (PTFE), is a synthetic polymer made up of fully fluorinated carbon chains. It is nearly inert to most chemical compounds and has a very low coefficient of friction.
In the biomedical field, Teflon, particularly in its expanded form (ePTFE), is used to produce vascular prostheses, especially as an alternative to the autologous saphenous vein, due to its very smooth surfaces, which are ideal for blood flow. The expansion of polytetrafluoroethylene involves stretching its chains by up to 800%, resulting in a structure that is more rigid, crystalline, hydrophobic, thermally stable, and with increased microporosity. However, Teflon grafts can be recognized by the body as foreign surfaces, triggering the coagulation cascade that leads to platelet adhesion and reduced conduit patency. To mitigate this issue, the internal surface is sometimes treated with covalently bonded heparin, which improves the conduit’s patency [64].

When comparing the stress-strain curves of woven PET and PTFE grafts with those of various segments of the aorta, both in the circumferential and radial directions, it becomes evident that the woven grafts are significantly more rigid than the aorta segments in the circumferential direction, while the behavior is more similar in the longitudinal direction. Additionally, among the woven grafts, those made of PET are found to be more rigid than those made of PTFE [47].
Despite numerous attempts to improve radial elasticity, most of the ePTFE and Dacron grafts currently available fail to match the elastic properties of the arteries they are connected to, often leading to intimal hyperplasia (IH) and stenosis. Intimal hyperplasia is a complex biological process characterized by an increase in the volume of the tunica tissue, caused by cellular proliferation triggered by inflammation at the graft's anastomosis site. It is believed that the issue of IH in these grafts is related to the difference in elastic modulus between the host artery and the

graft. This remains a critical concern for researchers, as most small-caliber grafts fail within five years, primarily due to obstruction caused by IH [65].

C. Polyurethane-based scaffold

In order to achieve better mechanical properties than those of Dacron and PTFE, polyurethane-based vascular grafts have been developed.

Polyurethanes are copolymers recognized for the presence of the urethane group [-NH(CO)O-], which results from the reaction between an isocyanate group and an alcohol group, and they are composed of two main components: the hard segment, typically made from a diisocyanate and a chain extender like a polyol, and the soft segment, which can be a polyol, polyester, polyether, or polycarbonate. The incompatibility between the hard and soft segments leads to phase separation within the polymer, forming a structure where rigid domains are embedded in a soft matrix (Figure 17, [54]). This configuration gives polyurethanes excellent physical properties, such as compliance and viscoelasticity, which are crucial for ensuring biocompatibility with blood and other tissues. The properties of polyurethane vary based on the proportion of these segments: with hard segment content between 15% and 40%, the material is elastomeric, while higher percentages make it thermoplastic with an increasing elastic modulus. The dimensions and characteristics of the material depend on the weight and chemical composition of the segments [54].

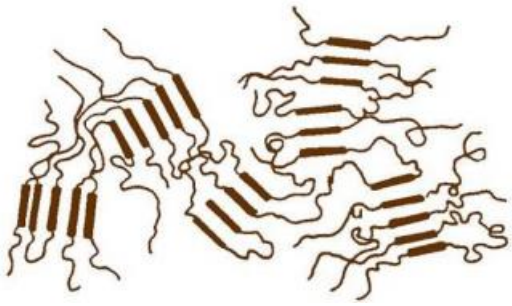

Figure 17. Typical structure of polyurethanes, where the soft segments (thin filaments) surround the hard segments (thick filaments).

During the production phase of polyurethanes, additives such as catalysts, auxiliaries, and stabilizers are used, which then remain in trace amounts in the final polymer. These components have not shown adverse effects, such as thrombogenic events, during implantation.

A challenge with polyurethanes based on polyether is that *in vivo*, they are prone to a phenomenon known as Biologically-Induced Environmental Stress Cracking (BIESC), where macrophages attack the ether groups, degrading the surface of the prosthesis and compromising its stability.
Therefore, the main drawback of using polyurethanes is the potential carcinogenic effect of their degradation byproducts. The component susceptible to degradation is the soft segment, specifically the ester, carbonate, or ether functional groups. One possible solution to mitigate this issue is to remove these functional groups by modifying the polyurethane production process. Over time, soft segments composed solely of hydrocarbons have been developed, leading to the creation of polycarbonate-urethane vascular grafts, which do not contain ether bonds and are therefore more stable and resistant to biodegradation [54]. Consequently, polyurethanes based on polycarbonate, such as ChoretaneTM or Chronoflex, which are resistant to BIESC, are now predominantly used.
Some polyurethanes are hemocompatible materials, particularly suited for producing small-diameter vascular grafts (internal diameter < 6 mm) using electrospinning, as they reduce the risk of thrombus formation or excessive neo-intima growth compared to Dacron and expanded PTFE grafts. The advantageous properties of polyurethanes come from the pore size of the internal surface and their ability to accommodate pulsatile blood flow.
Bioactive molecules are added to the internal surface of the grafts, bonded either covalently or ionically, to enhance hemocompatibility, reduce the risk of thrombosis, and promote the formation of a neo-intimal layer. Heparin is the most used substance for this purpose, but other anticoagulants, proteins, or tissue growth mediators are also employed [66].

D. Silicone-based scaffold

In recent years, silicones, also known as polydimethylsiloxanes (PDMS), have become increasingly used in biomedical devices. Silicone-based vascular prostheses are particularly noted for their excellent hemocompatibility. Additionally, they have low toxicity, good thermal stability, resistance to oxidation, and can be stretched considerably, although they are not very resistant to moderate and high stress.
Previously, materials such as PurSil (Ward et al., Polymer Technology Group, Berkeley, California, U.S.A.), which consists of a polyurethane matrix and silicones providing structural support, were developed. These materials have shown excellent properties, and studies conducted in Italy have yielded promising results. This success is partly due to the attention given to the vessel's microstructure, which significantly affects internal cell growth and the tendency to form

thrombi. Specifically, a highly porous vascular surface improves hemocompatibility by reducing platelet adhesion and the release of thromboglobulin-β into the plasma, a protein involved in platelet activation [67].

E. Bioresorbable scaffold

Bioresorbable stents are made from materials that can be absorbed by the body over time. Theoretically, the canonic non-resorbable stents should remain stable and unchanged, with no degradation or deposition occurring over time, whereas resorbable stents are designed to degrade completely at an appropriate rate. The resorbable part can be either the entire prosthesis or just the external coating, which may contain pharmacological agents that are gradually released during degradation.

The production of these implants involves the use of biocompatible, biodegradable metals and alloys such as iron, magnesium, and zinc, as well as polymers like poly-L-lactic acid (PLLA), poly-L-glycolic acid (PLGA), polycaprolactone (PCL), hyaluronic acid, or polyethylene oxide/polybutylene terephthalate (PEO/PBTP). This approach helps to eliminate the long-term presence of foreign materials in the body, thereby reducing the risk of foreign body reactions, avoiding complications, and lowering the costs associated with the reimplantation or removal of stents. The elderly, children, and diabetics can greatly benefit from this type of scaffold, as they are more prone to complications and challenges associated with repeated surgeries.

Ideally, bioresorbable stents provide the necessary mechanical support to the vessel during the healing period and fully degrade within 12 to 24 months. The degradation of bioresorbable stents must be predictable within a specified timeframe, and both the stent material and its degradation products must be biocompatible and non-toxic, ensuring maximum safety for patients.

Bioresorbable vascular scaffolds are typically made from metal alloys based on magnesium, iron, or zinc. In addition to the traditional biodegradable polymers like PLLA and PLGA, polymer blends based on polyhydroxyalkanoates (PHAs) have also been developed [68].

F. Innovative Polymers

Due to the lack of small-diameter vascular substitutes on the market, numerous studies are focused on finding suitable materials for this purpose. A recent study ([60]) explored the possibility of creating vascular prostheses made from bacterial nanocellulose (BNC) and medical polyurethane. Bacterial nanocellulose is a highly hydrophilic natural material with excellent hemocompatibility and a high Young's modulus, making it a good candidate for use in vascular scaffolds.

Additionally, combining it with medical polyurethane, which has excellent elastic properties as previously described, complements the characteristics required for an artificial vessel. The produced scaffold was composed of a BNC framework with polyurethane as the filling material. The results were promising, as the scaffold demonstrated good axial and radial mechanical strength, good suture resistance, and excellent cellular and blood compatibility. Tests conducted on rats over a period of 9 months showed no signs of blood flow obstruction, highlighting the great potential of combining these materials for creating small-diameter vascular substitutes [69].

Another innovative material for the production of vascular grafts is Poly(ethylene vinyl acetate) (PEVA), a copolymer composed of ethylene and vinyl acetate monomers. Its recent popularity is due to its high biocompatibility, flexibility, and ability to prevent the formation of clots or thrombi [70].

It is also important to mention the recent development of self-expanding stents made from shape-memory polymers (SMPs). These materials can return to their original shape even after significant deformations caused by external stimuli such as heat, light, or stress. In the context of angioplasty, these stents offer several advantages, including the elimination of the need for a balloon catheter, a simpler procedure, and consistent performance in treating the obstructed artery regardless of the operator. An example of this category is the polymer blend of polyurethane (PU) and polycaprolactone (PCL) [69].

1.8 Techniques for the production of vascular scaffolds

A critical phase in scaffold design involves selecting the appropriate fabrication technique. Each production method yields structures with distinct morphological, microscopic, and macroscopic properties, which can significantly influence the interaction of the biomaterial with cells and the host tissues.

Electrospinning

Electrospinning is a process that employs an electric field to produce polymeric fibers from a polymer solution. The polymer fluid, extruded through a syringe controlled by a volumetric pump, is subjected to a high-voltage electric field. This field generates an electrostatic force that overcomes the fluid's surface tension and viscous stresses, forming a jet that extends from the needle tip toward a collector,

typically metallic. As the charged jet travels through the electric field, it is stretched and aligned along the field's direction. During the time it takes for the jet to reach the collector, the solvent evaporates, enabling the deposition of solid polymeric fibers onto the collector's surface. For the production of vascular scaffolds, this technique employs a rotating cylindrical collector, allowing the controlled deposition of fibers in a tubular configuration.

Separation phase

Phase separation is a technique used to divide a polymer solution into two distinct phases: one enriched with polymer and the other with solvent. This process can be thermally induced or achieved through the addition of a non-solvent for the polymer, resulting in gel formation. The gel is then cooled to stabilize its morphology and subsequently freeze-dried to remove the remaining solvent. However, the fabrication of scaffolds through phase separation requires specialized equipment and does not allow for the creation of structures with aligned fibers.

3D printing

The fundamental principle of additive manufacturing is to create a product by adding material, which can be liquid, solid, or powder, layer by layer. The methods to achieve this can vary. The American Society for Testing and Materials (ASTM) has classified these technologies into several categories, among which we can mention for vascular applications: material extrusion, material jetting, and vat photoplymerization [71].

Material extrusion

Material extrusion is an additive manufacturing method in which material is selectively dispensed through a nozzle. This layer, usually composed of a thermoplastic melt, cools and serves as the foundation for the next layer. Fused Deposition Modeling (FDM) is a widely used material extrusion technique, with 3D printers that are easily available for purchase even for home use.

Extrusion bioprinting, employed in tissue engineering, typically uses syringe-based extruders without the heating elements found in standard FDM printers to prevent damage to biological materials. The printing solutions often include biopolymers or hydrogels containing cells. For the production of vascular structures, extrusion bioprinting can be followed by a cross-linking step using calcium ions. However, these tissues often lack the necessary cell density for successful *in vivo* integration and present additional challenges related to biocompatibility and biodegradation [72], [73].

Material jetting

Material jetting, also known as inkjet or drop-on-demand printing, is an additive manufacturing process in which droplets of material are selectively deposited. Waxy polymers and acrylic photopolymers with suitable viscosity for droplet formation can be processed and treated using this technique. The method essentially involves depositing droplets with high precision, which are then solidified through evaporation or reactions induced by heat or UV light.

In the field of bioprinting, hydrogel solutions are used, and the material jetting technique has been employed to horizontally print alginate tubular structures, with or without bifurcations. Although promising for printing microstructures, this technique has not yet been used to create functional vascular scaffolds. A significant advancement in this area is laser-assisted bioprinting, which allows for the deposition of cell-laden solutions with microscopic resolution. This method offers the advantage of computer-controlled precision, capable of creating microtissues. These technologies may, in the future, be applied to bioprinting capillary-like structures [74].

Vat photopolymerization

In vat photopolymerization, a liquid photopolymer contained in a vat is selectively hardened through light-activated polymerization. A photopolymer, also referred to as a light-activated resin, is a polymer that undergoes a change in its properties when exposed to light, typically in the ultraviolet or visible spectrum. This exposure triggers the linking of its molecular chains. One of the most well-known vat photopolymerization techniques is stereolithography (SLA or SL), widely used for biomedical applications due to its high precision. This method is primarily suited for photocrosslinkable resins, but recent advancements have allowed the use of photopolymer composites with ceramics.

In one study, a photocurable resin developed for SLA was used to create porous tubular structures with a diameter of less than 2 mm, which were then tested for biocompatibility. The scaffolds were functionalized with biomolecules, leading to the formation of an endothelial monolayer after cell seeding [75]. For the bioprinting of vascular grafts using vat photopolymerization, it is crucial to implement methods for removing cytotoxic substances, such as uncured resin, from the process.

DIW printer

Direct Ink Writing (DIW) is a 3D printing technique based on material extrusion, in which viscoelastic inks are used. The DIW printer uses a heated syringe that deposits ink onto a platform

moving along the x-y directions. The syringe features a nozzle, and LED light is used as the heating source.

A 2018 study employed this technique to produce a shape-memory elastomeric tube aimed at improving the vascular repair process [76]. Typically, an artificial vessel is sewn with biocompatible surgical sutures when implanted; however, this is a lengthy process that can lead to internal bleeding. The ink was prepared using a photocurable resin composed of aliphatic urethane diacrylate (AUD) and n-butyl acrylate (BA), along with a semicrystalline thermoplastic polymer (semicrystalline polycaprolactone (PCL)). Fumed silica-based nanoparticles were added as a rheological modifier. The 3D-printed scaffold was designed to have an external diameter significantly smaller than the internal diameter of the vessel and was implanted in the affected region of a blood vessel modeled with silicone. Once heated, the tube expanded to an external diameter slightly larger than the vessel's internal diameter. In practice, this vascular scaffold could tightly adhere to the vessel's inner surface, allowing blood to circulate normally and ensuring a very rapid repair process, thus reducing the risk of bleeding.

1.9 Imaging Techniques to visualize the correct positioning of Vascular Scaffolds

Following the implantation of the vascular prosthesis at the pathological site, it is crucial for the patient to undergo regular check-ups, initially frequent and then annually, to monitor the correct positioning and functioning of the scaffold.

There are various imaging methodologies that differ in the type of information provided, image resolution, invasiveness, and the type of contrast agents used.

Coronary Angiography

This is a radiological technique that employs X-rays and involves the selective injection of an appropriate radiopaque contrast agent to achieve opacification of the coronary tree. This methodology is used as the gold standard for visualizing coronary lesions, such as stenosis or aneurysms, but is also utilized to check the patency of aorto-coronary bypasses or previously implanted scaffolds. Coronary angiography is performed on an inpatient basis, during which the patient is positioned on a radiolucent table. During the procedure, the affected blood vessel is punctured with a needle, a guide wire is inserted, and a diagnostic catheter is positioned. At this point, the coronary ostium is cannulated, and a radiopaque contrast agent, which is usually an iodinated compound, is injected. By subsequently administering a small dose of X-rays, it is possible to obtain two-dimensional images

in which the lumen of the arteries appears opacified, allowing the identification of any condition that leads to luminal compromise. Although it is a high-resolution method, there are limitations in its use due to its invasiveness and the potential occurrence of some side effects. The use of contrast agents can, for example, cause chemotoxic effects related to their ionic content and viscosity. Additionally, local vascular damage may occur near the access site of the affected blood vessel [77].

Computed Tomography

Computed Tomography (CT) is a diagnostic imaging technique that uses a computer to process variations in X-ray intensity after they have passed through the body. It involves the intravenous injection of a contrast agent, allowing for three-dimensional imaging of the coronary arteries. The examination is performed on an outpatient basis, does not require patient hospitalization. The advantage of this technique is that it provides 3D images in a fast way, enabling visualization of the area surrounding the coronary lumen, thus overcoming the limitations of angiography. Additionally, it uses a relatively low amount of X-rays while still providing high diagnostic capability.

Similar to Coronary Angiography, the iodinated contrast agent is used to opacify the blood when visualized with X-rays. With this method, the scaffold appears as a radiopaque structure clearly visible on X-rays, allowing it to be distinguished from the vessel walls. It is also possible to analyze the adherence of the implant to the vessel wall. Additionally, the contrast agent helps verify that blood flow passes correctly through the stent, identifying any potential narrowing. The invasiveness of this technique is limited, but the downside is the exposure to ionizing radiation. Furthermore, small-caliber stents are more difficult to visualize because the lumen is very narrow, and the images do not always have sufficient resolution to clearly distinguish details within small spaces [78].

Magnetic Resonance Imaging

Magnetic resonance imaging (MRI) generates three-dimensional images of the body's internal tissues by applying powerful magnetic fields and radio waves. The images are produced because the hydrogen nuclei in water molecules and body lipids generate a response when subjected to a magnetic field and radiofrequency pulses. Fundamentally, protons in tissues typically rotate, generating weak magnetic fields oriented randomly. When the powerful magnetic field of the MRI is applied, their magnetic axes align along with that field. Following this, radiofrequency pulses are applied, causing the protons' axes to momentarily align in the opposite direction to the externally applied field, in a high-energy configuration. When the pulses are no longer applied, the protons relax, returning to their original alignment and releasing energy. The signal's magnitude, recorded by an antenna within the

MRI instrument, depends on the extent and speed with which the protons return to their original alignment (T1 relaxation) and the rate at which they release the previously acquired energy (T2 relaxation). These signals are analyzed by computerized algorithms and transformed into detailed anatomical images [79]. It has been demonstrated that T1 and T2 are influenced by the biochemical conditions of the tissue under examination, such as water concentration, pH, and the concentration of salts or fats. Consequently, an MRI scanner can compare these parameters between healthy areas and those that have undergone pathological damage within the same tissue, providing excellent contrast. The images obtained from the analysis can be weighted in T1 or T2, and in some cases, to improve visibility in the study of certain tissues, it is necessary to use a contrast agent that enhances the detectable signal. Contrast agents can be of type T1-CA or T2-CA. T1-CAs increase the signal of T1-weighted images by shortening the T1 relaxation time. The result in the image is a brighter and clearer area (hyperintense), in which the signal of the fatty tissues are enhanced. They are mainly used to identify inflamed areas or highly vascularized tumors. On the other hand, T2-CAs decrease the signal in T2-weighted images by shortening the T2 relaxation time. In the obtained image, where the signal from water is enhanced rather than that from lipids, this results in a darker area (hypointense). They are usually employed to detect specific accumulations, such as nanoparticles or hypovascular lesions [80].

Using this technique to visualize vascular scaffolds after implantation presents some challenges related to the material of the implant itself, which in most cases, if not modified in some way, is not visible to the radiomagnetic signal. For example, metallic stents made of stainless steel or cobalt-chromium alloys are not compatible with MRI, as they cause the formation of magnetic artifacts that create distortions and alterations in the images produced due to the interaction between the magnetic field and the material itself. This results in completely black areas that obscure the region surrounding the vessel of interest, preventing the evaluation of tissues and the distinction of anatomical structures. Additionally, investigating metallic stents with this technique risks may cause the heating of the implant or its unintended movement, creating a risk for the patient. Polymer scaffolds are more compatible with this analysis methodology; however, they must be appropriately modified to produce a detectable contrast, as otherwise, the signal produced in response to the application of the magnetic field is practically invisible. To overcome visualization issues, paramagnetic or superparamagnetic substances can be incorporated into the prostheses, capable of producing a visible and detectable response following the application of the magnetic field. The advantages of using MRI as an imaging methodology lie in the fact that it is a non-invasive technique, capable of providing three-dimensional images, does not require the use of ionizing radiation, and allows the visualization of soft tissues, thus

enabling the evaluation of the interaction between the scaffold and the surrounding tissues. The limitations concern the materials of the vascular implants, as previously described, the high costs of the analysis, and there may be greater difficulties in detecting small-caliber scaffolds, whose signal may be weak [81], [82].

IntraVascular UltraSound

IntraVascular Ultrasound (IVUS) is a widely used technique to verify the correct adhesion of the vascular prosthesis to the arterial intima. It is crucial to avoid any empty space between the scaffold and the vessel wall, as incomplete adhesion can reactivate the thrombotic process, causing another lumen occlusion. With the IVUS method, it is possible to acquire detailed cross-sectional/longitudinal images of the lumen using ultrasound. During the procedure, a very thin catheter with an ultrasound probe is inserted into the blood vessel of interest. This probe emits high-frequency ultrasonic waves that propagate through the surrounding tissues and bounce back differently depending on what they encounter, generating different echoes. These echoes are then processed to generate images where the arterial wall and its interaction with the scaffold are visible. A limitation of this methodology is that the implant material must be able to clearly reflect the ultrasound waves. For example, polymer prostheses generate a less distinct echo compared to metallic stents, but a possible solution is the incorporation of components, such as iron oxide nanoparticles, which can improve ultrasound contrast [83].

Optical Coherence Tomography

Optical Coherence Tomography (OCT) is a non-invasive technique similar to IntraVascular UltraSound but with 10 times greater resolution, using infrared light instead of ultrasound to identify different surfaces. In this method, a thin catheter containing a probe with optical fibers that transmit and receive light is inserted into the vessel of interest. To obtain images, the optical delay and the intensity of the light reflected by various tissues are measured. It is important to mention that the visual field must be made transparent because blood is not effectively penetrated by light, compromising the quality of the images. To address this issue, a small amount of saline solution, which is optically transparent, is infused through the catheter into the vessel, temporarily displacing the blood and allowing the image to be acquired [84].

2 Production and validation of polymeric vascular scaffolds

The primary objective of this thesis was the production of a polymeric scaffold suitable for use as a vascular graft. Electrospinning was employed as the fabrication technique, selecting an appropriate mix of polymers and solvents. After the fabrication phase, a conventional gelatin coating was applied. To validate the non-engineered scaffold, cell compatibility and blood clotting were first investigated. This preliminary study phase on the pure scaffold is crucial for advancing with the engineering of the graft for diagnostic purposes or its applicability in the treatment of vascular diseases.

2.1 Materials and methods

2.1.1 Preparation of polymeric solution

In order to produce the cardiovascular prostheses analyzed in this thesis work, two polymers were used: the poly (ε-caprolactone) (PCL) (molecular weight = 80000 g/mol) and the poly (glycerol sebacate) (PGS) (molecular weight = 2673 g/mol), synthesized following the protocol reported in Wang et al., 2002 [76]. All solvents and chemicals used, unless otherwise specified, were supplied by Sigma-Aldrich (St. Louis, MO, USA).

Two distinct polymer solutions were prepared, each with a concentration of 20% w/v, using a solvent mixture of chloroform and ethanol in a volumetric ratio of 9:1. For the samples containing quercetin, the ethanol used was previously dissolved with quercetin at a concentration of 5.5 mg/ml. The resulting solutions were placed on a magnetic stirrer under hood for one hour at a stirring speed of 500 rpm and at room temperature (25 ± 2°C). To obtain the final solution, the two preparations were mixed in a 1:1 v/v ratio at room temperature and stirred magnetically for at least 1 hour before the electrospinning technique. Since quercetin is a photosensitive material, the bottles used throughout the preparation process were wrapped in aluminum foil and kept away from light sources.

In addition to the samples with quercetin, control prostheses without quercetin were also produced. The same process was followed for these samples, with the ethanol solution not containing quercetin. This allowed for a direct comparison between the prostheses with and without the bioactive compound, to assess the specific contribution of quercetin to the material properties.

2.1.2 Electrospinning process

The electrospinning apparatus used for the production of cardiovascular scaffolds is shown in Figure 18 (Spinbow s.r.l., San Giorgio di Piano, Italia). The system consists of:

- a syringe pump (KDS-100, KD Scientific, Holliston, MA, USA);
- a high-voltage power supply (PCM series, Spellman, NY, USA);
- a 16-gauge flat-tipped needle;
- a cylindrical collector of 5.0 mm outer diameter and 13.0 cm in length.

The polymer solution is loaded into a 5 ml glass syringe (FORTUNA® OPTIMA®, Poulten & Graf GmbH, Wertheim, Germany) placed in the pump, which enables both the control of the volume to be electrospun and the pumping speed; then, the solution is pumped from the syringe to the flat-tipped needle through a capillary tube. An electrode connected to the needle allows to electrically charge the polymer mixture as it exits the capillary. This charging accelerates and stretches the jet of solution under the influence of the external electric field. As the solution travels towards the collector, it thins out and forms continuous solid fibers as the solvent rapidly evaporates. The tubular scaffold is formed by the random deposition of charged fibers onto the cylindrical collector.

For each prosthesis produced, a polymer electrospinning volume of 2 ml was set on the pump at a speed of 1.10 ml/h. As characteristic parameters of the electrospinning device, the generator was configured to a voltage of 17.0 kV, while the rotation and translation speed of the collector were set, respectively, to 500 rpm and 600 mm/min. The needle and the collector were adjusted to a vertical distance of 18 cm between them. Furthermore, to facilitate the easy removal of the prostheses at the end of the process, a small amount of vaseline was applied to the collector.

The operating conditions adopted in the electrospinning process for each scaffold produced are summarized in Table 2 below.

Table 2. Process conditions set during electrospinning.

Volume to be electrospun [ml]	2 or 2.5
Flow rate [ml/h]	1.1 or 2.2
Voltage applied to the electrodes [kV]	17
Rotation speed of the collector [rpm]	500
Translation speed of the collector [mm/min]	600
Vertical distance needle-collector [cm]	18

As can be seen from Table 2, it was necessary to adjust the operational parameters, such as the volume to be electrospun and the flow rate of the pumped solution, in order to achieve the same tubular scaffold structure under different environmental conditions. The variations in temperature and humidity, which fluctuate throughout the day and across seasons, had a direct impact on the electrospinning process. Consequently, tailored adjustments were made to ensure consistency in scaffold production, demonstrating the sensitivity of the technique to ambient conditions.

At the end of the electrospinning process, scaffolds were placed in a desiccator overnight to allow the complete evaporation of the solvents.

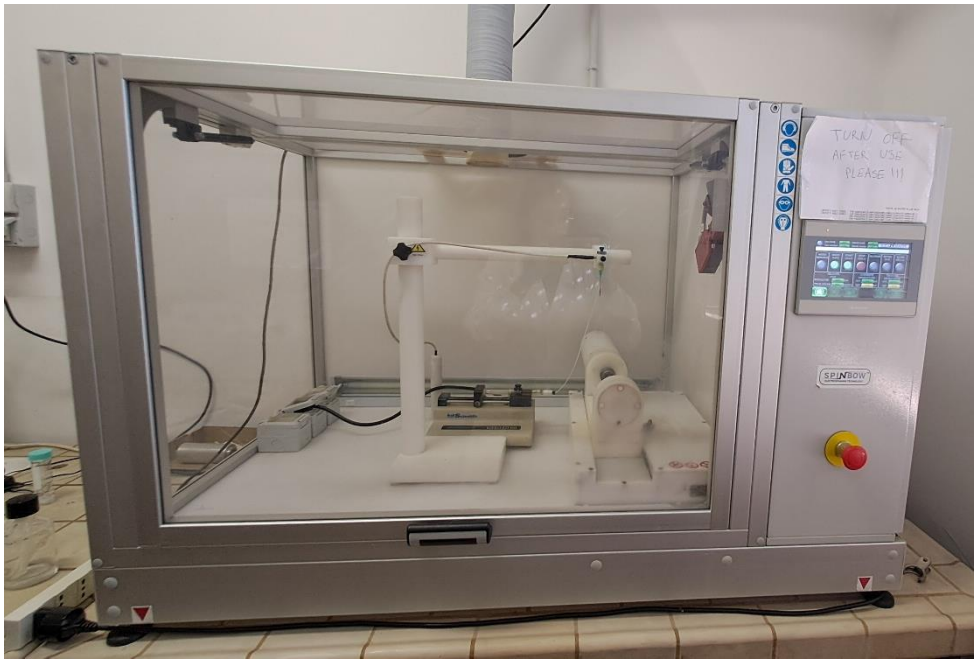

Figure 18. Electrospinning system used for the production of cardiovascular scaffolds.

2.1.3 Conventional coating process

All the scaffold produced through the electrospinning process has a porous structure. To decrease the bioprosthesis's permeability to liquids, a thin gelatin coating must be applied to fully cover the scaffold.

The conventional coating method, consistently used by the research group, involved immersing the scaffolds in a gelatin solution while utilizing a mechanical stirrer to achieve uniform coverage and even distribution.

First, a solution of gelatin from bovine and porcine bones (Sigma Aldrich, St. Louis, MO, USA) was prepared in deionized water at a concentration of 67 mg/ml, which represents the maximum solubility value of gelatin in water. This solution was heated to approximately 60 °C to fully dissolve the gelatin. Subsequently, the electrospun prosthesis was placed on a collector connected to a mechanical stirrer

(KIRK 510 Bicasa, Italy). The coating process was completed by immersing the collector containing the prosthesis in the gelatin solution, which was maintained at approximately 40 °C by a hot water bath placed on a magnetic stirrer. The stirrer was set to a speed of 135 rpm, while the overall coating process times were varied. After the immersion period in the gelatin solution, the scaffolds were dried under UV light, using different durations and settings to observe any potential changes in the overall coating.

The configuration used for the mentioned process is shown in Figure 19.

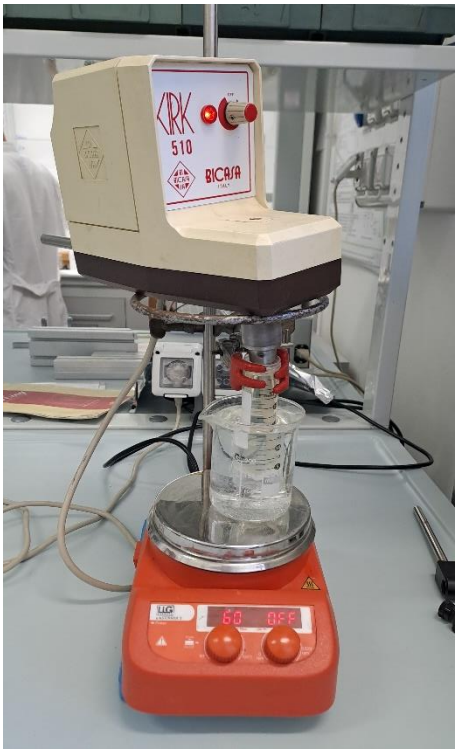

Figure 19. Configuration for gelatin coating with mechanical agitation.

Immersion times were set at either 1 hour or 4 hours. Additionally, as a further variable during the dip-coating process, the scaffold drying method was modified. In all cases, UV light was applied for 1 hour of drying; however, the scaffold positioning was adjusted to be either horizontal (laid flat along its length on the work surface) or vertical (supported at only one end on the work surface).

The tests conducted using the dip-coating method are summarized in Table 3.

Table 3. Variation of Parameters in the conventional coating Process.

BATCH	$C_{gelatin}$ [mg/ml]	$t_{coating}$ [h]	t_{UV} [min]
1	67	1	60 vertical
2	67	1	20 vertical + 40 horizontal
3	67	1	60 horizontal
4	67	4	60 horizontal

2.1.4 Scanning Electron Microscopy (SEM) analysis

The scanning electron microscope (SEM) allows for the examination of the sample's morphology and structure, including identifying the crystalline shapes of its components.

SEM is a technique, non-destructive for the sample, that utilizes a beam of electrons to interact with the atoms of the analyzed material. This interaction allows for the generation of images with extremely high magnification, surpassing the resolution limits of optical microscopy, and achieving atomic-level resolution.

The limitation of optical microscopy lies in its inability to observe two points that are closer together than the wavelength of photons, which falls in the range of hundreds of nanometers within the visible spectrum. However, since electron microscopy uses electrons, which have a wavelength approximately three orders of magnitude smaller than visible light, the resolution limit of the electron microscope is much higher. It is therefore a widely used tool for investigating microstructures and, when combined with microanalysis (EDS), it allows the determination of the chemical compositions of both organic and inorganic materials [85].

A Scanning Electron Microscope (SEM) is composed of several essential parts:

- Electron Source: This is usually a tungsten filament that generates the electron beam needed for scanning.
- Column: It contains multiple lenses that guide and focus the electron beam. There are two main electromagnetic lenses in this system: the condenser lens and the objective lens. The condenser lens controls the electron beam's intensity, adjusting the number of electrons (or

beam current) that pass through a specified aperture. The objective lens then focuses the electrons onto the sample's surface.

- Detectors: These components capture the signals produced when the electron beam interacts with the sample. They are vital for creating images and for determining the sample's composition.
- Sample Chamber: This chamber houses the samples to be examined, which are placed on a movable stage for precise positioning.
- Vacuum System: This system, typically including a pre-vacuum pump, maintains a high vacuum in both the column and the sample chamber. The vacuum is crucial to prevent the electron beam and generated signals from interacting with gas molecules, which could distort the image and reduce analysis accuracy.

During operation, electrons are emitted from the source at the top of the column and accelerated downward. They pass through the series of lenses and apertures, which shape them into a fine, focused beam. This electron beam then strikes the surface of the sample. At each scanning point, the electron beam interacts with the sample within a region that usually resembles a pear or a droplet in shape. This interaction generates signals, which are picked up by the detectors in the SEM, allowing the creation of detailed imaging of the sample.

The most commonly used signals in SEM are:

- Backscattered Electrons (BSE): These are produced through elastic interactions between the incident electron beam and the atomic nuclei of the sample. BSEs are those electrons, coming from material depths of a few μm, that are reflected back with energies between 50 eV and the initial incident energy. They primarily carry compositional information. Captured by the Backscatter Detector (BSD), these electrons create an image where the grayscale correlates with the sample's composition. Darker areas in the image correspond to lighter elements (with lower atomic numbers), while brighter areas indicate heavier elements (with higher atomic numbers), which produce a stronger signal.
- Secondary Electrons (SE): They are emitted from the sample's surface layers, in the order of thickness of 10 nm, due to the inelastic collision with the electron beam. During this interaction, some energy is lost, resulting in secondary electrons with much lower energy than backscattered electrons, typically between 0 and 50 eV. The Secondary Electron Detector (SED) produces an image that emphasizes surface characteristics, offering a detailed, three-

dimensional topographical view of the sample. However, it does not provide information about the composition of the sample.

- X Rays: They have specific energies depending on the elements in the sample, with intensity correlating to element concentration. They can be detected and differentiated by wavelength (WDS) or energy (EDS), offering detailed insights into the composition, quantity, and distribution of sample elements [86].

The structure of the pure scaffolds produced has been examined using the SEM microscope model S-2500 Hitachi (Figure 20), capturing images at various levels of magnification. This type of SEM is based on the emission of secondary electrons, which are captured by a detector, converted into electrical impulses, and sent to a monitor, specifically a cathode ray tube screen, where a digital image of the sample can be displayed. For the proper conduction of the SEM analysis the primary requirement is that the samples must be conductive. To meet this criterion, the material to be analyzed needs to be coated with a 30 nm thick layer of gold. To achieve this, a Polaron SEM coating system (Figure 21) has been utilized. The main unit of Polaron houses a high voltage power supply, a vacuum manifold, and measuring instruments. A workchamber is mounted on top of the principal unit. The top plate assembly of the glass workchamber holds the target material to be sputtered onto the specimen holder.

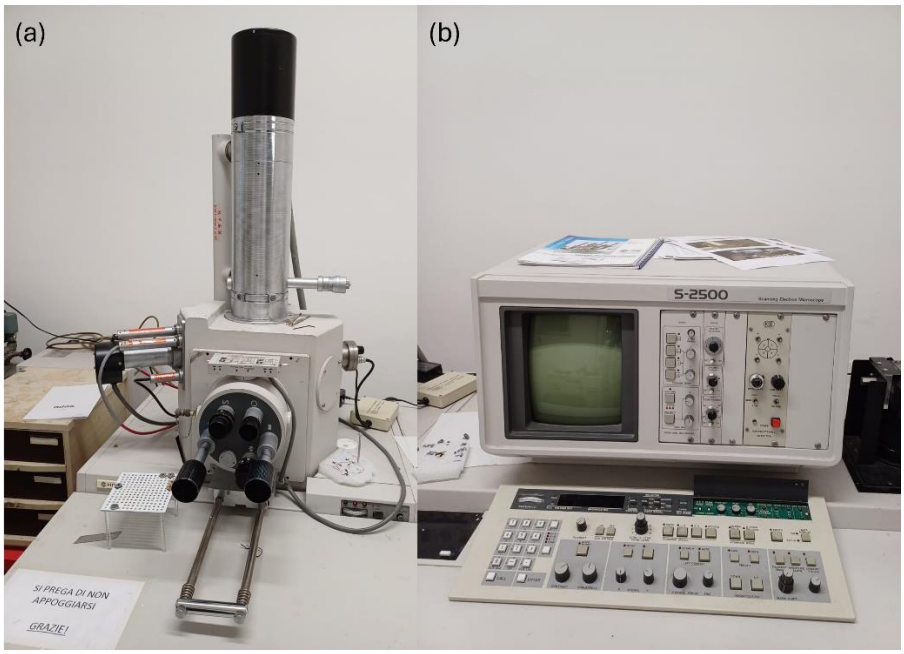

Figure 20. Scanning Electron Microscope Hitachi model S-2500. (a) Column and sample chamber, (b) monitor for image creation.

Figure 21. Polaron SEM coating system.

2.1.5 Fourier Transform Infrared Spectroscopy

To characterize the polymer material of the produced prosthesis, FTIR spectroscopy (Fourier Transform Infrared Spectroscopy) (Nicolet iS50 Analytical FTIR Spectrofotometer) was employed, capable of identifying the various chemical compounds present in the scaffolds. The advantage of this analysis lies in the rapid data acquisition, requiring only a small sample volume.

FTIR is a vibrational spectroscopy that has evolved from traditional infrared IR spectroscopy. IR spectroscopy is a technique that absorbs radiations in the range between the visible and microwave regions to analyze chemical bonds within substances. It reveals the presence of various functional groups in a compound by producing distinct signals.

To correctly interpret an IR spectrum, it's important to examine the position, intensity, and shape of the absorption bands. The position of the bands, measured in wavenumbers or wavelength (expressed in cm^{-1}) on the x-axis, corresponds to the specific vibrational frequencies of chemical bonds and functional groups in the molecule. The intensity of the bands, shown as percent transmittance or absorbance on the y-axis, indicates how much IR radiation is absorbed and can reflect the concentration of the functional group. The shape of the bands offers insights into the sample's purity and molecular interactions. Narrow and sharp bands suggest a consistent chemical environment, while broader bands may point to hydrogen bonding or other interactions. Additionally, the presence of secondary peaks can signal overlapping vibrations or similar functional groups.

Several factors can affect the number of bands seen in an IR spectrum. These include absorption frequencies that fall outside the detectable range, very weak frequencies, the merging of two bands, overlapping bands, or a lack of change in the dipole moment. Conversely, factors such as overtones,

that are bands resulting from vibrations beyond the fundamental ones, can increase the number of observed bands.

Considering these aspects, the IR spectrum is typically divided into specific regions of interest:

- 4000-3000 cm^{-1}: Corresponds to hydrogen-containing bonds (such as O-H, N-H, C-H).
- 3000-2000 cm^{-1}: Reflects the presence of triple bonds.
- 2000-1500 cm^{-1}: Indicates double bonds (like C=O, C=C).
- 1500-1000 cm^{-1}: Associated with single bonds (such as C-Cl, C-O).
- 1000-400 cm^{-1}: Known as the fingerprint region, which is unique to each compound and helps in its identification.

FTIR spectroscopy can be equipped with additional instrumentation for specific analytical needs, including attenuated total reflectance (ATR), micro and macro imaging. ATR-FTIR spectroscopy investigates samples at a depth of 0.5-5 μm from the surface of the internal reflection element, using materials such as diamond, silicon, or germanium. In this study, the spectra of the produced electrospun scaffolds were acquired using a diamond crystal with attenuated total reflectance (ATR) with 100 scans in the range of 400-4000 cm^{-1}. The acquisition of each spectrum was preceded by background correction. The background spectrum was measured and subsequently subtracted from the analysis results.

2.1.6 Thermogravimetric Analysis (TGA)

Thermogravimetric analysis (TGA) was used to monitor the weight variations of the samples as the temperature increased, in order to determine the quantity of the different substances present in the produced scaffolds.

During the analysis, the sample is subjected to a predefined thermal cycle, and its weight variation is recorded as a function of temperature. By operating in an inert atmosphere, it is possible to detect the weight loss of the sample at the temperatures where specific degradation reactions occur, usually involving the formation of gaseous compounds. Knowing the temperatures at which these reactions take place and evaluating the weight loss, it is possible to calculate the percentage of the compound that has undergone transformation.

In our case, the analysis was performed using the Thermal Analysis System STA200 Hitachi (Figure 22), with nitrogen as the inert gas. The samples were heated from room temperature to 800 °C at a rate of 10 °C/min.

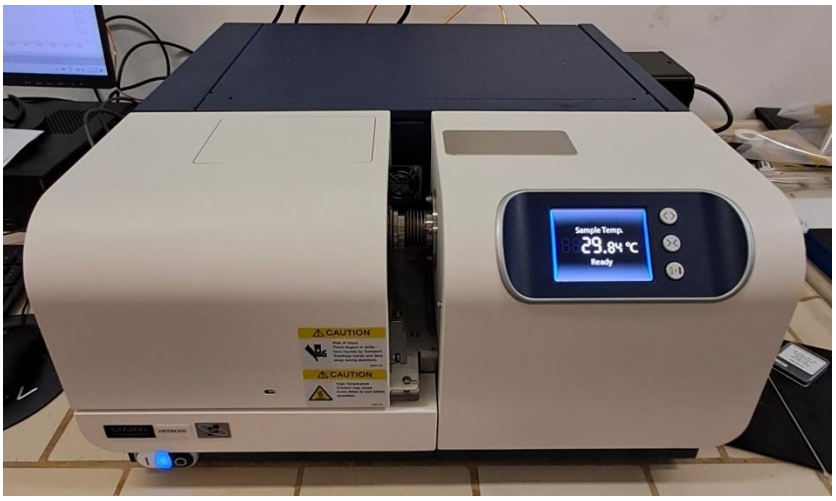

Figure 22. Thermal Analysis System STA200 Hitachi.

2.1.7 Cell viability

The cell compatibility test was conducted to evaluate the biocompatibility of our polymeric material designed for prosthetics. This analysis is crucial, as it determines whether the material is cell-friendly, which can significantly influence the success of the prosthesis in clinical applications. Specifically, we aimed to assess cell viability, proliferation rates, and the overall response of the cells to the polymeric materials. Understanding how the cells interact with our materials, whether they die, proliferate, and how quickly they do so, provides insight into their suitability for biomedical applications.

For this study, we conducted tests on two types of prosthetic materials: the bare prosthesis made of PCL:PGS with quercetin and the same scaffold coated with gelatin. The comparison between these two materials aimed to determine whether the incorporation of gelatin improved the cell compatibility. To prepare the samples, the polymeric materials have been cut into circular discs, ensuring uniformity for the experiment.

To ensure sterility and prevent contamination during the tests, we prepared a sterilization solution consisting of PBS (phosphate-buffered saline) and a 1% v/v mix of penicillin and streptomycin antibiotics. Working under a biological safety cabinet to maintain a sterile environment, we immersed the samples in 3 ml of the sterilizing solution and performed an initial wash for 15 minutes. After this first wash, we replaced the 3 ml of solution with another 3 ml of fresh sterilizing solution and conducted a second wash for 8 minutes. This was followed by a third wash, carried out in the same manner for an additional 8 minutes.

After completing the washes and removing the sterilizing solution, the samples were placed to dry on a petri dish. Once the samples were properly arranged on the dish, they were ready to be seeded with cells.
This rigorous sterilization protocol is essential to ensure that any subsequent cell growth is due solely to the interactions with the polymeric materials and not influenced by external microbial contamination. The outcomes of this cell compatibility test will help determine the viability of our polymeric materials for future biomedical applications.

After the sterilization of the samples, the next step involved seeding them with endothelial cells to assess the biocompatibility of the polymeric materials. The goal was to evaluate the cellular response to the materials, specifically whether the cells adhered, proliferated, or died.
The endothelial cells, initially cultured in T-flasks, required detachment, counting, and subsequent seeding onto the polymeric discs. First, the exhausted culture medium was removed from the flasks. The cells were washed with PBS (Phosphate Buffered Saline) to eliminate any residual medium, and the PBS was discarded after the wash. To detach the adherent cells, 1.5 ml of trypsin was added to each flask, followed by incubation at 37 °C for 5 minutes, allowing the trypsin to break down the proteins that held the cells attached to the flask surface.
After the incubation, fresh medium containing serum was added to neutralize the trypsin, and the entire content of the flasks, including the medium, cells, and trypsin, was transferred into Falcon tubes for centrifugation. To separate the cells from the solution, the Falcon tube was centrifuged at 120 RCF (Thermo Scientific SL 8 Centrifuge) for 8 minutes with soft acceleration. Centrifugation causes the cells to collect at the bottom of the tube, forming a cell pellet, while the supernatant (the liquid above the pellet) contains the remaining medium and neutralized trypsin. This separation is crucial as the supernatant contains unwanted substances that need to be discarded, while the pellet is composed of the viable cells required for seeding.
After centrifugation, most of the supernatant was carefully removed, leaving just a small amount to avoid disturbing the cell pellet. Fresh medium (5 ml) was added, and the cells were gently resuspended by pipetting to create a homogeneous suspension. This ensured that the cells were evenly distributed and ready for counting and seeding.
For cell counting, a 10 µl aliquot of the cell suspension was transferred to a Burker counting chamber, which was covered with a glass slide. The cells appeared as small black or yellow dots under the microscope, and this visual aid was used to determine the number of cells in the suspension.

Based on the cell count results, a solution of fresh medium containing approximately 15000 cells per well had been prepared for seeding. Under the biological hood, 200 µL of this solution was pipetted into each well of a 96-well plate, where the sterilized polymeric discs had already been placed. The plate contained PCL:PGS samples, PCL:PGS with quercetin samples, empty wells without any polymer material which acted as positive control to observe the cells' natural growth behavior on the plastic surface of the plate.

To measure cell viability, the CellTiter 96® AQueous One Solution Cell Proliferation Assay protocol was used. This colorimetric technique quantifies the number of viable cells in cytotoxicity assays. Its primary reagents include a novel tetrazolium compound, (3-(4,5-dimethylthiazol-2-yl)-5-(3-carboxymethoxyphenyl)-2-(4-sulfophenyl)-2H-tetrazolium inner salt; MTS) and an electron coupling reagent (phenazine ethosulfate; PES), which together form a stable complex. Specifically, the MTS compound is bioreduced by cells to produce a colored formazan product that is soluble in the culture medium.

To conduct the assay, 20 µl of reagent were added to the wells containing the material samples with cells, followed by incubation at 37°C. Sampling was performed after 1, 2, 3, and 7 days by taking 100 µl from each well, and absorbance at 492 nm was measured in a microplate reader (microplate reader Infinite 200® PRO, Tecan, Männedorf, Switzerland) to determine the quantity of formazan produced.

2.1.8 Hemocompatibility

The evaluation of hemocompatibility was performed to assess whether the polymeric materials used in vascular prostheses cause hemolysis, which is a critical factor for blood-contacting applications. The test measures the absorbance of hemoglobin released following the lysis of red blood cells (RBCs): a higher absorbance indicates a greater degree of hemolysis caused by the interaction between the RBCs and the material. The goal is to ensure that the hemolysis percentage remains low, indicating the material's compatibility.

In this study, different samples were tested: control PCL/PGS, coated PCL/PGS, PCL/PGS with quercetin, and coated PCL/PGS with quercetin. All experiments were conducted in triplicate for each sample.

The samples were prepared by cutting the materials into small circular discs, which were then placed into separate Eppendorf tubes. Each disc was immersed in 1 ml of PBS for 10 minutes to ensure washing. After the PBS wash, it was removed, and 1.2 ml of red blood cells was added to each tube.

The tubes were then incubated at 37 °C for 2 and 3 hours with gentle agitation to prevent sedimentation of the RBCs.

Following incubation, 150 µl of the mixture from each Eppendorf tube was collected and centrifuged for 7 minutes at 3000 rpm. The purpose of centrifugation was to separate the RBCs from the supernatant. A red-colored supernatant would indicate RBC lysis caused by the material. After centrifugation, 100 µl of the supernatant from each tube was transferred into a 96-well plate, and the absorbance was measured at 540 nm using a microplate reader (microplate reader Infinite 200® PRO, Tecan, Männedorf, Switzerland) to quantify the released hemoglobin.

The percentage of hemolysis has been calculated for each sample using the following equation:

$$Hemolysis\ [\%] = \frac{(A_s - A_b)}{(A_p - A_b)} * 100 \tag{3}$$

where A_s is the sample Absorbance,

A_b is the absorbance of negative control,

A_p is the absorbance of positive control.

In this protocol, fresh PBS buffer and deionized water were used as the negative and positive control, respectively.

2.1.9 Blood clotting

The blood clotting test was conducted to assess the pro-coagulant behavior of the polymeric materials used in vascular grafts. Evaluating blood clotting is essential to determine if the material promotes or inhibits coagulation, which is a critical factor for blood-contacting medical devices. Materials that excessively trigger clot formation can cause thrombosis, leading to potential clinical complications. On the other hand, materials that do not induce sufficient clotting could pose risks in cases where clot formation is necessary for wound healing or hemostasis.

In this study, six types of samples have been analyzed: control PCL:PGS, PCL:PGS with quercetin, control scaffold coated with gelatin, quercetin scaffold coated with gelatin, Dacron, and ePTFE (expanded polytetrafluoroethylene). ePTFE was included due to its widespread use in vascular applications, particularly as a graft material in surgeries, providing an additional reference point to evaluate the performance of the experimental materials. All tests were conducted in triplicate for each sample.

The samples were prepared by cutting the materials into small discs, which were then immersed in 1 ml of PBS and incubated at 37°C for 10 minutes to wash the materials. After the washing step, the PBS was removed. Subsequently, 30 µl of human blood and 3.75 µl of 0.2M $CaCl_2$ were added to each well containing the material samples. The plates were incubated at 37°C, and blood clotting was assessed at different time intervals: 30 minutes, 1 hour, and 2 hours.

At the end of each respective incubation period, 3 ml of deionized water was added to each sample. This step induces osmotic shock: red blood cells outside the clot burst due to the influx of water, while those trapped within the clot remain intact, as they are protected by the fibrin matrix that forms the clot, along with platelets and red blood cells. The degree of redness in the sample after the water addition indicates the amount of free red blood cells that have lysed. A redder sample signifies less clot formation, meaning the red blood cells were not captured in a clot and were lysed upon water exposure.

To assess blood clotting indirectly, the percentage of hemoglobin released into the solution has been measured. A higher hemoglobin release indicates that fewer clots were formed, meaning more free red blood cells were lysed. After the addition of deionized water, 150 µl of the solution was taken from each sample and centrifuged at 1000 rpm for 5 minutes. Then, 100 µl of the supernatant was transferred into a 96-well plate for spectrophotometric analysis, and absorbance was measured at 540 nm using a UV/vis microplate reader (microplate reader Infinite 200® PRO, Tecan, Männedorf, Switzerland).

The sample containing blood without any material was used as the reference for calculating the Blood Clotting Index (BCI). The BCI was calculated as follows:

$$BCI\ [\%] = \frac{A_s}{A_r} * 100 \tag{4}$$

where A_s is the absorbance of the supernatant in sample material,

A_r is the absorbance of the supernatant in the reference sample.

To evaluate morphological changes in Red Blood Cells (RBCs) following contact with gelatin coated scaffolds, 0.5 ml of a 5% (v/v) RBC suspension was incubated with the scaffolds at 37°C for 6 hours. After incubation, the samples were centrifuged at 850g for 7 minutes, and the RBCs were fixed with 4% formaldehyde at room temperature for 2 hours. The fixed RBCs were then subjected to a

dehydration process by sequential immersion in ethanol solutions with increasing concentrations (50%, 60%, 70%, 80%, 90%, and 99.7%) for 5, 10, 15, 20, 25, and 30 minutes, respectively. Following dehydration, a small volume of the RBC suspensions was placed onto coverslips, allowed to air-dry, sputter-coated with gold, and subsequently observed using Scanning Electron Microscopy (SEM). A commercial gauze was used as reference material for comparison.

2.2 Results and discussion

2.2.1 Coating process

The different tests conducted using the dip-coating method have been compared by calculating the percentage mass variation, defined as follows:

$$mass\ variation\ [\%] = \frac{m_{post-coating} - m_{pre-coating}}{m_{pre-coating}} * 100 \quad (5)$$

where $m_{pre-coating}$ and $m_{post-coating}$ represent the mass of the prosthesis before and after the coating process, respectively. The results obtained for the different batches tested are shown in Table 4 below.

Table 4. Results of conventional gelatin coating in terms of mass variation %.

BATCH	$C_{gelatin}$ [mg/ml]	$t_{coating}$ [h]	t_{UV} [min]	Mass variation [%]
1	67	1	60 vertical	116.21
	67	1	60 vertical	10.07
	67	1	60 vertical	23.90
	67	1	60 vertical	16.98
2	67	1	20 vertical + 40 horizontal	71.45
3	67	1	60 horizontal	17.85
	67	1	60 horizontal	26.76
4	67	4	60 horizontal	9.92

The results obtained from testing four different operational conditions for the conventional coating method highlight its inherent limitations. Despite using the same gelatin concentration (67 mg/ml), the process showed significant inconsistencies in the amount of coating deposited, as reflected by the wide variability in the percentage of mass variation across batches. For instance, under identical coating conditions (batch 1), the percentage mass variation ranged from 10.07% to 116.21%, demonstrating a lack of reproducibility. Similarly, when increasing the coating duration from 1 to 4 hours (batch 4), the expected increase in deposited coating mass was not observed. This indicates the absence of a predictable trend correlating operational conditions with coating deposition. Additionally, at the experimental level during the UV drying phase, the operator's manual skill significantly influences the process, constituting an additional factor of variability in the mass of the deposited coating.

Such variability underscores the non-standardizable nature of this method, which fails to provide control over the coating deposition even under fixed parameters. This lack of precision is particularly problematic in commercial and industrial settings, where accurate knowledge and control of the deposited coating mass are essential for quality assurance and scalability. Furthermore, inconsistencies in the results, such as the decrease in deposited mass with prolonged coating times, suggest inefficiencies in the process and highlight the need for alternative, more reliable coating techniques.

2.2.2 Morphological analysis

The structural characterization, especially in tissue engineering, places significant emphasis on assessing the microscale thickness of individual fibers within the scaffold matrix. This is particularly relevant for fibrous biomaterials, where the diameter of each fiber becomes a defining feature in terms of mechanical and biological performance. Representative SEM images were collected for all the scaffolds produced.

To analyze the dimensional distribution of the fibers, ImageJ software was employed to measure fiber diameters, with a minimum of 100 fibers sampled per scaffold type to ensure reliable statistical data. The presence of quercetin did not interfere with the proper formation of fibers during the electrospinning process and did not affect the fiber dimensions, which showed an average diameter comparable to PCL/PGS scaffolds (see Table 5 for reference). This can be attributed to the fact that quercetin is fully dissolved within the polymeric solution used for electrospinning.

The application of the gelatin coating did not result in any morphological changes to the scaffold fibers. The analysis of average fiber diameters reveals that the addition of the gelatin coating caused

a slight increase in the mean diameters compared to uncoated scaffolds. SEM images of the coated scaffold further confirm the coating process, as certain regions of the prosthesis (highlighted with red arrows in Figure 23(c)) show visible evidence of gelatin coverage. The presence of gelatin is also supported by the increased roughness of the fibers, which appear less smooth compared to those in uncoated scaffolds. This wettability of the scaffold surface by gelatin is attributed to the presence of hydrophilic PGS within the polymeric blend, contrasting with the hydrophobic nature of PCL, which alone would render the surface non-wettable.

The results obtained are shown in Figure 23 below.

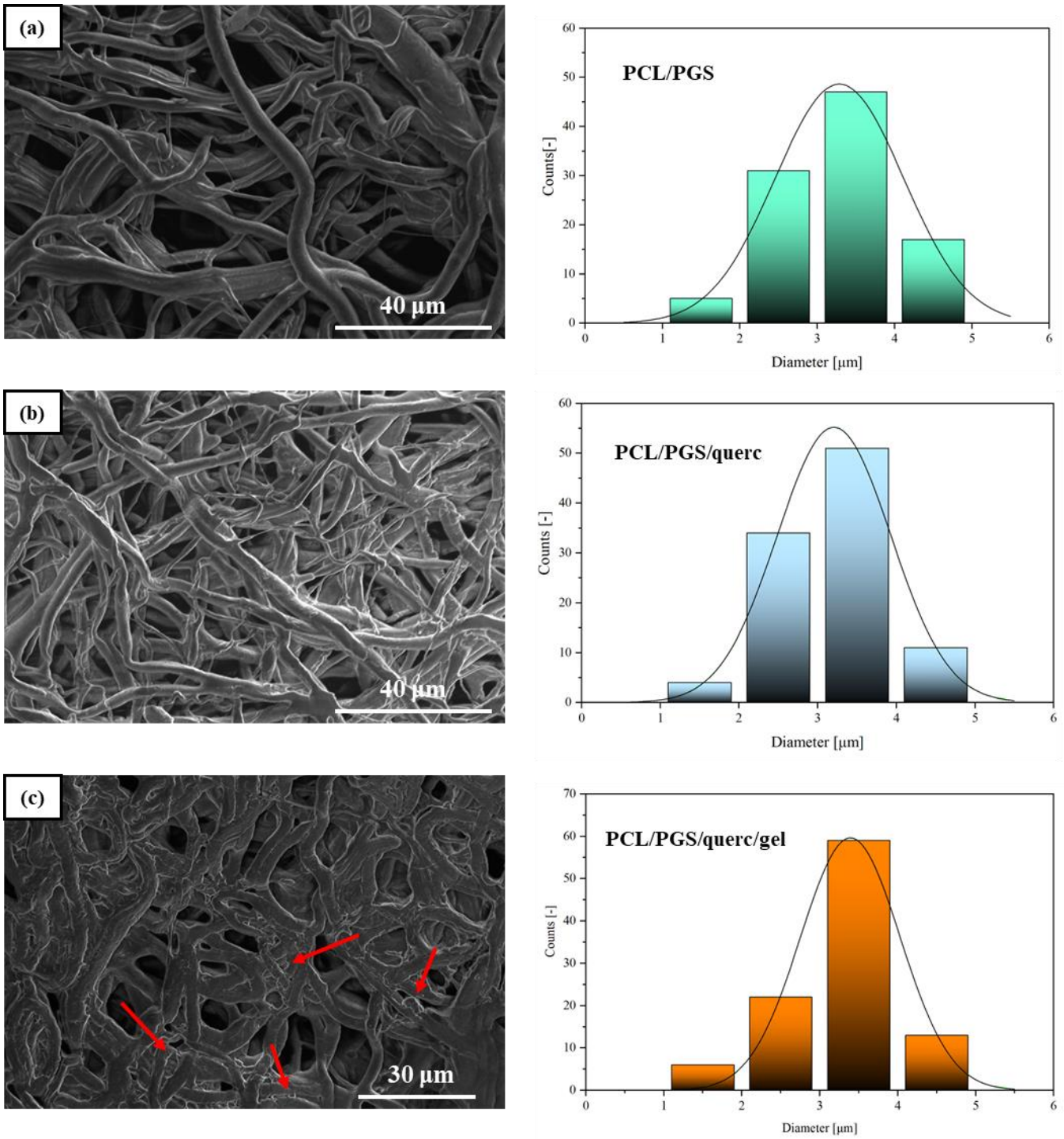

Figure 23. SEM images and dimensional distribution curves for: (a) PCL/PGS; (b) PCL/PGS/querc; (c) PCL/PGS/querc with gelatin coating.

Table 5. Fiber diameter of polymeric scaffolds. Results are reported as mean of 100 measurements ± standard deviation.

Sample	Mean Fiber Diameter [µm]
PCL/PGS	3.247 ± 0.758
PCL/PGS/querc	3.205 ± 0.672
PCL/PGS/querc/gel	3.398 ± 0.573

2.2.3 FTIR analysis

In Figure 24, the FTIR spectra of quercetin, PCL, and PCL/PGS/querc scaffold are presented. This spectroscopic analysis enabled verification of the actual presence of each component within the prostheses and allowed investigation of any changes in the polymer matrix resulting from the addition of quercetin.

The pure spectra of PCL and quercetin allowed the identification of their specific characteristic features. In the PCL spectrum, a distinctive peak at 1720 cm^{-1} is observed, attributed to the carbonyl ester group C=O. Additionally, a strong absorption peak appears at 1163 cm^{-1}, corresponding to the stretching of the C-O-C group. Peaks at 2867 and 2945 cm^{-1} are associated with the symmetric and asymmetric stretching of the C-H alkane group.

In the quercetin spectrum, the broad absorption band visible in the range 3100-3550 cm^{-1} is attributed to the stretching of OH groups. In the range of 1400-1600 cm^{-1}, numerous medium-intensity multiple bands can be identified, corresponding to the stretching of C=C bonds present in the aromatic rings of the structure. The peaks in the range of 1150-1300 cm^{-1} are associated with the vibration of the C-O bond present in the phenolic ring. The weak bands visible in the range of 600-800 cm^{-1} are attributed to the vibration of the hydroxyl (OH) groups attached to the aromatic rings.

In the spectrum of the PCL/PGS/quercetin scaffold, a weak broad band in the range of 3100-3550 cm^{-1} is identified, corresponding to the vibration of OH groups present in both PGS and quercetin. In the range of 2850-2950 cm^{-1}, characteristic peaks of C-H bond stretching are identified. It is noted that the intensity of these bands is higher compared to the PCL sample, as the alkane C-H groups are present in both PGS and PCL. At 1721 cm^{-1}, a high-intensity peak is observed, corresponding to the vibration of the C=O bond of the ester group, present in both polymers. The intensification of this peak is attributed to the additional presence of PGS in the polymer blend. In the range of 1150-1250

cm^{-1}, medium-intensity peaks associated with the stretching of C-O-C groups present in both PCL and PGS are identified.

From the overall comparison between the spectra of quercetin, PCL, and PCL/PGS/quercetin, an intensification of the characteristic peaks of the polymer components was observed, confirming the incorporation of both PGS and quercetin. Furthermore, it was verified that the addition of quercetin to the polymer blend does not influence the chemical structure of the scaffold.

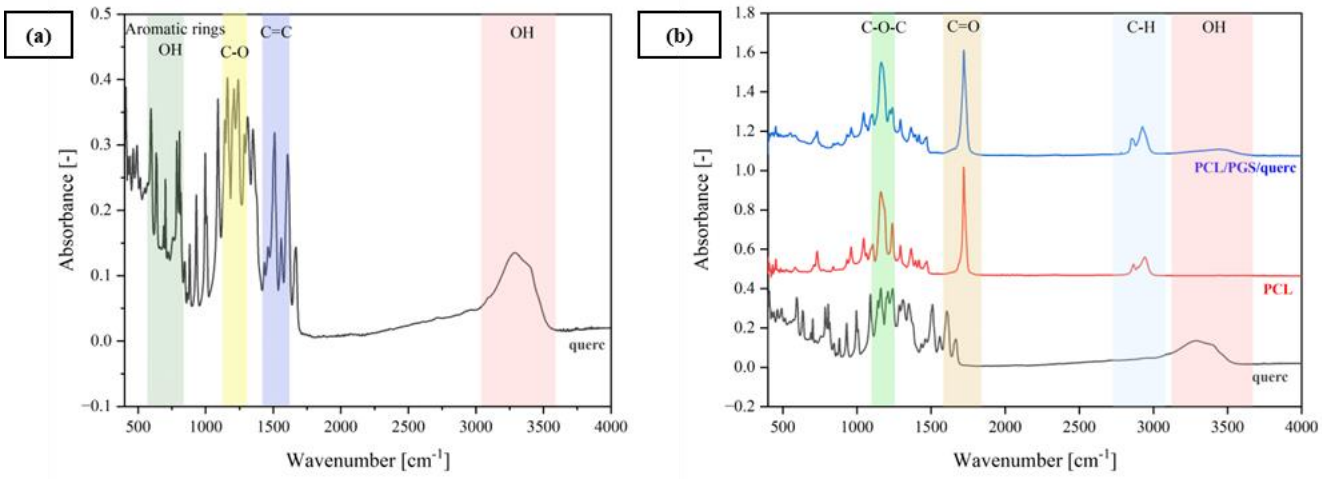

Figure 24. FTIR spectra for: (a) quercetin; (b) PCL and PCL/PGS/querc scaffolds.

2.2.4 TGA analysis

Thermogravimetric analysis was conducted on the produced scaffolds as an additional method to confirm the presence of individual components and to quantify the amount of quercetin incorporated into the structure.

TGA was performed on quercetin, neat PCL, neat PCL/PGS scaffold, and PCL/PGS scaffold containing quercetin. The resulting thermogravimetric curves are shown in Figure 25 and in Figure 26. The thermal parameters of the investigated materials reported in Table 6, including onset degradation temperature, offset degradation temperature, peak degradation temperature, and weight loss percentage, were derived from the TG and DSC curves. According to ASTM E2550, the onset temperature is defined as the point on the TGA curve where the first deviation from the baseline is observed before the thermal event. The offset degradation temperature represents the temperature at which material degradation is complete. The endothermic peak, on the other hand, represents the point at which the material undergoes its maximum rate of degradation, indicating the temperature where the sample's mass loss is most intense.

First of all, it must be noted that PCL/PGS scaffold and PCL/PGS/querc prosthesis have generated almost the same TGA curve, again confirming that the presence of quercetin didn't modify the chemical structure of the bared PCL/PGS scaffold.

For all samples, an initial weight loss step occurred at around 60 °C, corresponding to chloroform or ethanol loss from the analyzed structures. Specifically, the loss of solvent molecules begins at 30 °C for PCL/PGS/querc fibers, at 58.7 °C for PCL fibers, at 61.5 °C for PCL/PGS fibers, and at 69 °C for quercetin, and extends respectively till 65.4 °C, 66.7 °C, 71.4 °C and 106.1 °C.

Regarding quercetin, its main thermal degradation is observable between 209.8 °C and 378.5 °C with a weight loss of 37.3%, due to the onset of its thermal oxidation. This is also evident in the DSC curve in Figure 26(b), where quercetin presents an exothermic peak at 342.6 °C, associated with the release of energy during its oxidative decomposition. Notably, a preceding endothermic peak at approximately 317.2 °C is also observed, likely corresponding to preparatory chemical changes, such as the scission of weaker chemical bonds, that facilitate the subsequent oxidative degradation.

Pure PCL fibers exhibited a principal stage of weight loss within the temperature range of 217.4–416.3 °C, accounting for 97.1% of the total mass loss, which is associated with the large-scale thermal degradation of the polymer chains. This event corresponds to the breakdown of the ester bonds in the PCL structure, leading to the formation of volatile degradation products. Furthermore, the DSC analysis revealed an endothermic peak at approximately 350.5 °C, indicating the energy required for bond scission during this process.

The thermal degradation profile of the PCL/PGS blend shows a principal stage of weight loss within the temperature range of 176.5–478.3 °C, as seen in the TG curve. This broader degradation range, compared to pure PCL (217.4–416.3 °C), indicates the influence of the PGS component, which introduces additional degradation pathways and interactions between the two polymers. The earlier onset of degradation suggests that the PGS component lowers the thermal stability of the blend, possibly due to its lower degradation temperature or increased hydrophilicity. Additionally, the DSC curve for PCL/PGS exhibits an endothermic peak at 415.8 °C, which is slightly higher than the 350.5 °C peak observed for pure PCL. This shift may reflect enhanced thermal energy requirements for breaking the mixed polymer chains, indicating stronger intermolecular interactions or a more complex degradation mechanism introduced by the PGS.

The thermal degradation of the PCL/PGS/querc scaffold occurs primarily within the temperature range of 182.8–483.1 °C, as indicated by the TG curve. Compared to the PCL/PGS blend, the addition of quercetin leads to a slight increase in both the onset and final degradation temperatures. This suggests that quercetin, although thermally active, may stabilize the polymer matrix to some extent

by interacting with the PCL and PGS chains. In the DSC curve, the endothermic peak at 410.2 °C for PCL/PGS/querc is slightly lower than the 415.0 °C observed for PCL/PGS. This downward shift could indicate that quercetin reduces the energy required for the blend's thermal events, possibly due to its incorporation altering the polymer chain interactions.

By comparing the TGA curves of the PCL/PGS and PCL/PGS/querc samples at a temperature range where degradation of both structures occurs, the mass loss associated with quercetin was quantified at 1.55%. This value directly corresponds to the amount of quercetin incorporated into the scaffold. Given that the sample mass analyzed during the TGA test was 9.431 mg, it can be deduced that the mass of incorporated quercetin is 0.1462 mg.

The findings from this analysis indicates that incorporating quercetin only slightly affects the thermal stability of the electrospun PCL/PGS scaffold, likely due to the relatively low amount of quercetin present.

Table 6. TGA thermal parameters.

Sample		**T_{onset} [°C]**	**T_{offset} [°C]**	**Endothermic peak [°C]**	**Weight Loss in the range $T_{onset} < T < T_{offset}$ [%]**
quercetin	First step	69	106.1	-	1.09
	Second step	209.8	378.5	317.2	37.3
PCL	First step	58.7	66.7	-	0.28
	Second step	217.4	416.3	350.5	97.1
PCL/PGS	First step	61.5	71.4	63.7	0.49
	Second step	176.5	478.3	415.8	98.5
PCL/PGS/querc	First step	30	65.4	63.7	0.39
	Second step	182.8	483.1	410.1	98.5

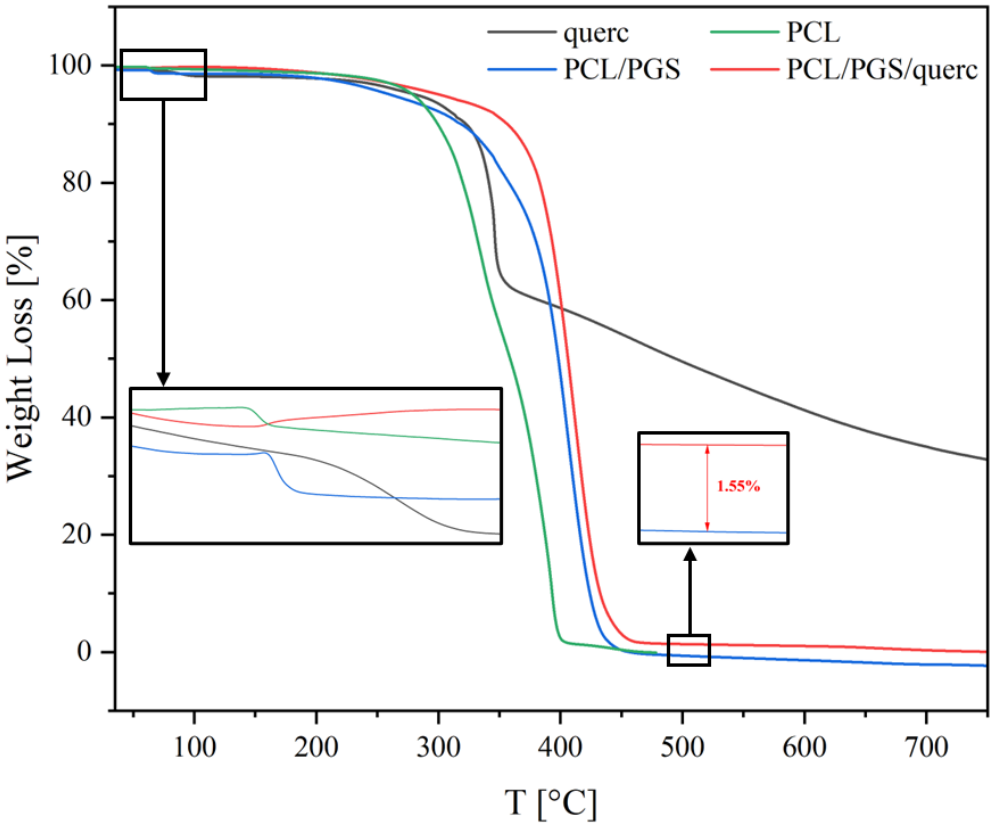

Figure 25. TG curves for analyzed samples.

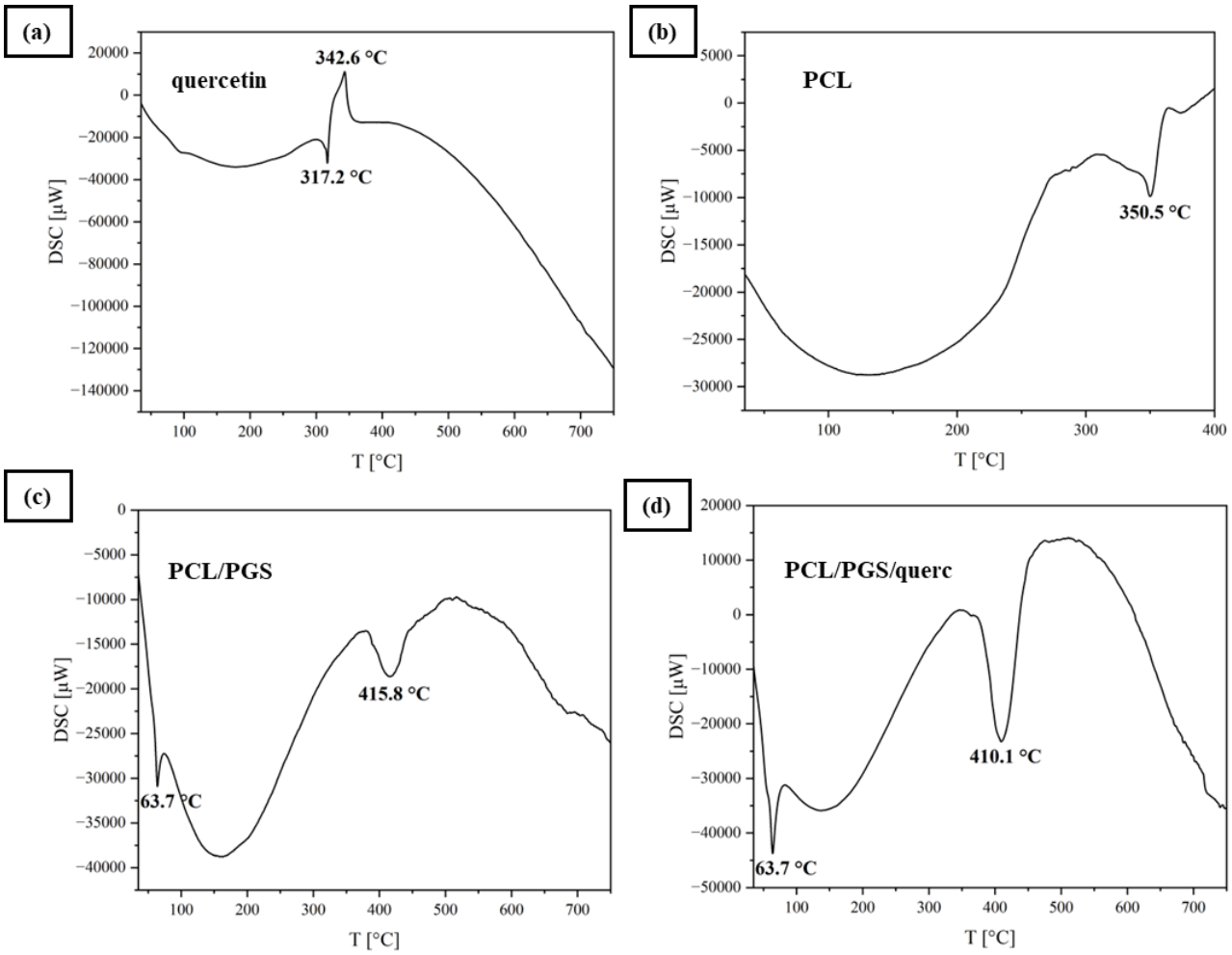

Figure 26. DSC curves for: (a) quercetin; (b) PCL; (c) PCL/PGS; (d) PCL/PGS/querc.

2.2.5 Cell compatibility

Various studies have indicated that gelatin can improve the biocompatibility of biomaterials by promoting cell adhesion and proliferation. In our experiment, a gelatin coating was applied exclusively to the external surface of the scaffold with the specific aim of reducing water permeability. The PCL/PGS/quercetin and the gelatin coated scaffolds were evaluated in terms of biocompatibility by exposing them to human endothelial cells to assess the non-toxicity of the polymeric material. The results, shown in Figure 27, indicate that the electrospun scaffolds produced did not interfere with cell viability during the 7-day period investigated. Specifically, the analysis of the gelatin-loaded scaffold results suggests that the amount of gelatin released during this time frame is not cytotoxic, nor are any other potential by-products released from the scaffold. After the first 2 days, a notable increase in cell viability was observed, while after a week, there were no statistically significant differences between the cells grown on a tissue culture plate and those grown in the presence of our scaffolds.

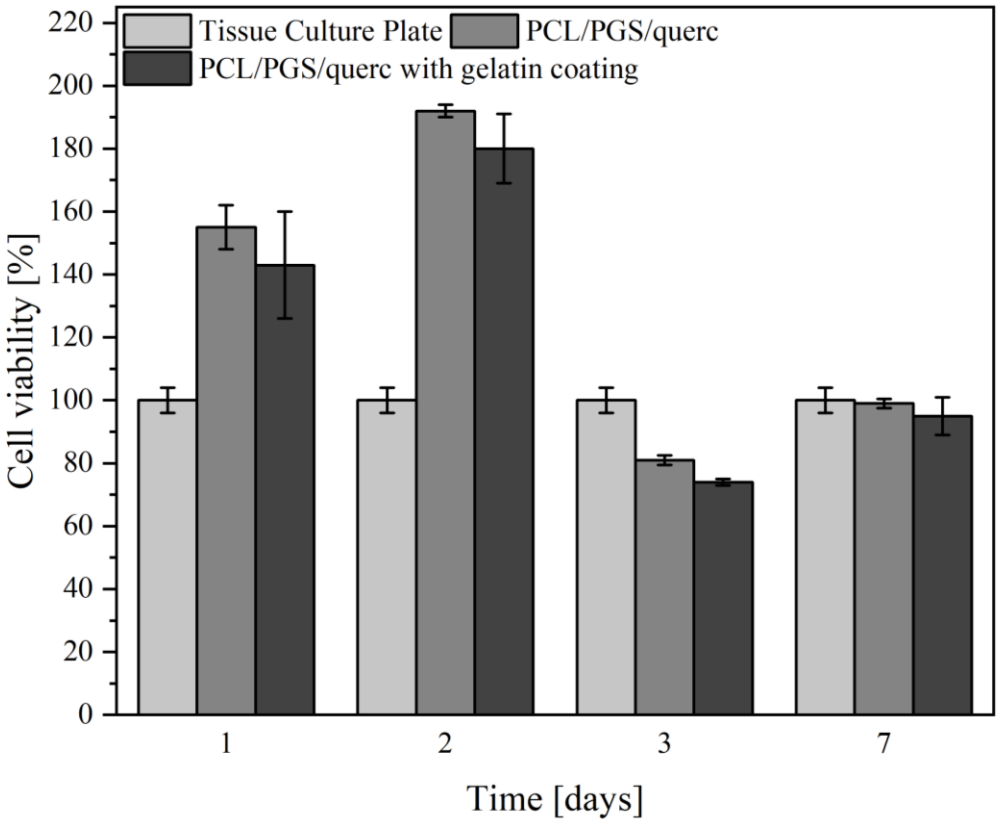

Figure 27. Cell viability test on PCL/PGS/querc and gelatin coated scaffolds on human endothelial cells. The Tissue Culture Plate served as positive control.

2.2.6 Hemocompatibility

To evaluate the hemocompatibility of the produced electrospun scaffolds, the percentage of red blood cells that ruptured upon contact with the polymeric material was calculated. More precisely, the percentage of hemolysis, which represents the amount of hemoglobin released when erythrocytes rupture upon contact with the prosthesis, was evaluated. The results obtained are shown in Figure 28, where it can be seen that the gelatin-coated scaffolds showed a significant decrease in the percentage of hemolysis compared to the other samples at both investigated times, respectively 2 and 3 hours. This behavior is attributed to the presence of the gelatin coating, which reduced the scaffold's porosity and provided a more uniform surface roughness. In any case, the results obtained are considered satisfactory for all produced scaffolds, as the percentage of hemolysis is <5 for all samples, indicating highly hemocompatible materials.

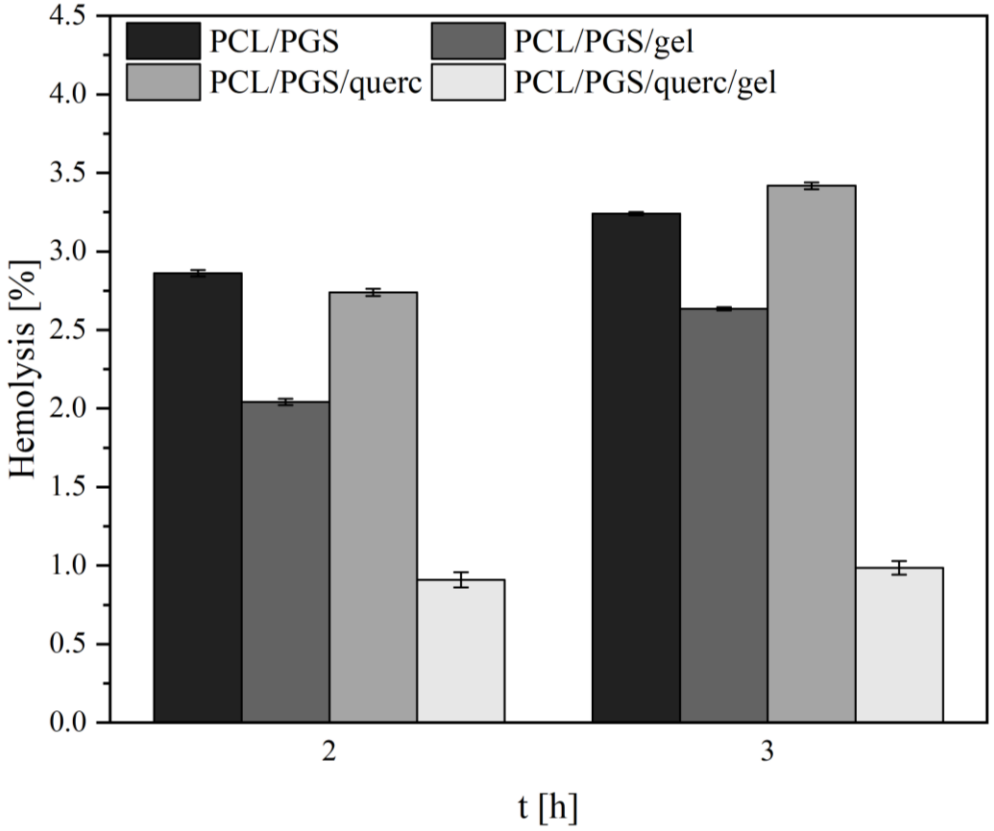

Figure 28. Hemolysis ratio of electrospun scaffolds with and without gelatin coating.

2.2.7 Blood clotting

The coagulation capacity of a material *in vitro* can be expressed through the blood clotting index (BCI %). This index value indicates the material's ability to form a thrombus upon contact with blood; specifically, a low BCI value reflects a low propensity for thrombus formation. In the context of cardiovascular prostheses, it is desirable for the produced scaffolds to neither promote nor facilitate thrombus formation when exposed to blood flow.

Coagulation tests were conducted on the electrospun scaffolds, and the results are displayed in Figure 29(b). As expected, the reference polymer materials, polyethylene terephthalate (PET or Dacron) and expanded polytetrafluoroethylene (ePTFE), exhibited a low thrombus formation capacity after 60 minutes, with BCI values of 20.72 ± 0.72% and 12.24 ± 1.05%, respectively. After 120 minutes, the BCI values slightly decreased to 17.62 ± 2.97% for PET and stabilized at 13.07 ± 0.92% for ePTFE. Among the electrospun scaffolds produced, the PCL/PGS and PCL/PGS with quercetin samples displayed nearly identical BCI values, reaching 19.05 ± 2.55% and 19.25 ± 1.99% after 60 minutes, and 17.73 ± 0.88% and 16.43 ± 2.72% after 120 minutes, respectively. These results suggest that the inclusion of quercetin does not impact clot formation and thus does not encourage thrombotic events.

The gelatin-coated scaffolds showed slightly higher BCI values compared to the uncoated prostheses. Specifically, the PCL/PGS control scaffold with gelatin coating exhibited a BCI of 22.13 ± 1.45% after 60 minutes and 14.81 ± 0.64% after 120 minutes. Similarly, the PCL/PGS scaffold with quercetin and gelatin coating had a BCI of 29.61 ± 7.15% after 60 minutes and 19.60 ± 5.30% after 120 minutes.

The observed decrease in BCI% over time highlights a positive attribute of the tested scaffolds in terms of blood compatibility. Initially, higher BCI% values at the 60-minute mark indicate that the material supports the formation of thrombi to a degree, potentially due to initial interactions with blood components such as platelets and clotting factors. However, as time progresses, a reduction in BCI% at 120 minutes suggests that the scaffolds do not excessively promote or sustain coagulation, an essential quality for cardiovascular applications.

Overall, these findings are satisfactory, as no significant thrombogenic activity was observed with the produced scaffolds, confirming that the selected polymer blend shows promising potential for cardiovascular applications.

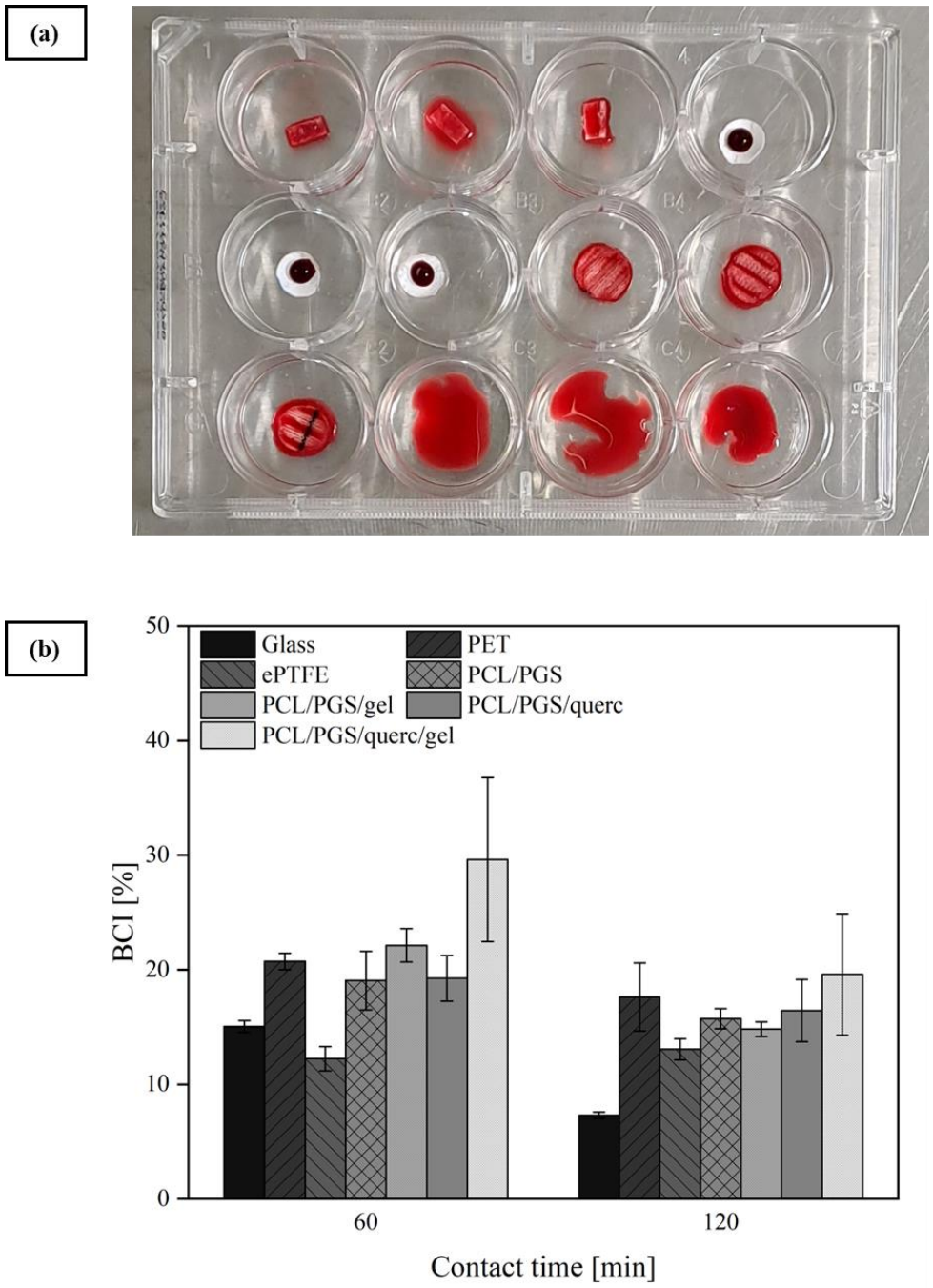

Figure 29. (a) Photograph from the *in vitro* blood-clotting measurement; (b) Blood clotting index after 60 and 120 minutes for reference materials and for electrospun scaffolds.

The morphological assessment of red blood cells (RBCs) after interaction with the gelatin-coated scaffolds was conducted using Scanning Electron Microscopy (SEM). This analysis aimed to evaluate the hemocompatibility of the scaffold by observing potential morphological alterations in RBCs that could indicate stress or damage caused by contact with the material.

SEM imaging, shown in Figure 30, predominantly revealed RBCs with a morphology consistent with early-stage echinocytosis. While some spicule formations were evident, the cells largely retained their

characteristic biconcave shape, suggesting that the interaction with the scaffold induced only minor alterations. This observation points to a relatively low level of stress exerted on the RBCs, likely attributable to the biocompatibility of the gelatin coating. Early-stage echinocytosis is typically characterized by minor irregularities that might result from surface interactions with the scaffold. These alterations may be influenced by the surface properties of the gelatin-coated scaffold, such as its roughness, or hydrophilicity. However, the absence of advanced echinocytosis or stomatocytosis indicates that the scaffold material does not determine a significant disruptive effect on RBC integrity.

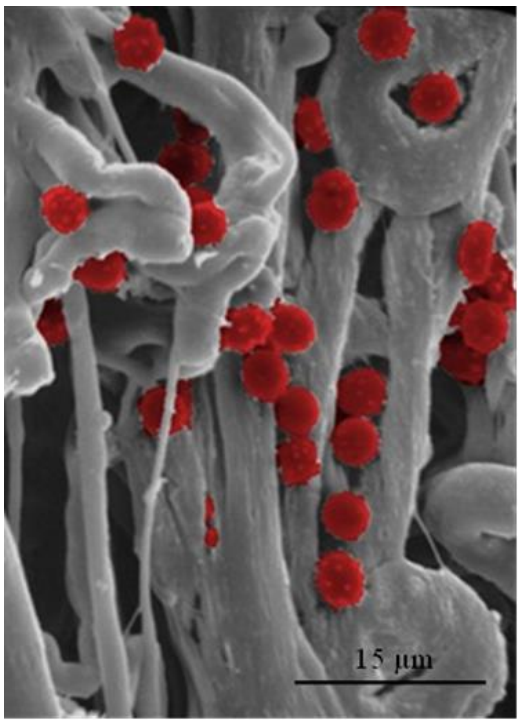

Figure 30. Morphology of RBCs after being in contact with gelatin coated scaffold.

3 Bioengineering of scaffolds for therapeutic applications

To successfully apply polymeric scaffolds in vascular applications, it is essential to perform a coating process, as polymeric prosthesis cannot be implanted in their bare form. To ensure the functionality and reliability of the produced tubular scaffolds, an appropriate surface coating is essential. Such a coating is needed to address the intrinsic challenges of polymer-based prosthetics, including limited hemocompatibility and excessive water permeability.

Despite advancements with synthetic materials like polyethylene terephthalate (Dacron) and expanded polytetrafluoroethylene (ePTFE) in large-diameter grafts, small-diameter vascular replacements (<5-6 mm) still face significant challenges. These smaller grafts often suffer from complications, such as thrombosis and intimal hyperplasia, primarily due to the absence of a native endothelial layer post-implantation, which is crucial for preventing clot formation and hyperplastic growth. This lack of a native endothelial layer on the graft surface promotes platelet adhesion and thrombus formation, limiting the graft's long-term success and biocompatibility.

Applying a natural biopolymer coating can provide a biomimetic surface that encourages cellular adhesion and minimizes thrombosis. Gelatin, derived from the thermal denaturation of collagen, has been widely employed in vascular graft applications due to its biodegradability, biocompatibility, and cost-effectiveness. Gelatin's structural similarity to collagen, a primary component of the extracellular matrix, makes it an ideal candidate for vascular prostheses, as it offers the biological cues necessary for cell adhesion and proliferation. These properties have led to its use in diverse medical applications, such as drug delivery systems and wound healing dressings. For fibrous scaffolds, gelatin can also reduce water permeability, addressing a critical limitation of electrospun vascular constructs, which often allow excessive water transfer [87], [88].

The conventional method used by the research group for gelatin coating of scaffolds, tested in the current thesis work as described in Chapter 2.1.3, has consistently been non-specific. The primary aim was to achieve the deposition of gelatin on the polymer structure, but it was not feasible to predetermine the deposited amount. This approach proved challenging to replicate and standardize, as the final outcome was directly influenced by the operator's manual skills. However, after the conventional gelatin coating method, an attempt was made to induce polymer fiber expansion within the scaffold. This approach aimed to facilitate deeper and more uniform penetration of the gelatin into the scaffold's structure, potentially enhancing the coating's uniformity and adhesion to the fiber surface.

In this study, a novel gelatin-coating technique was applied to the PCL:PGS tubular scaffolds with embedded quercetin, aiming to achieve a repeatable, effective coating method that allows for the application of a known amount of gelatin by adjusting the process parameters.
A layer-by-layer coating technique was adopted, which is innovative in the context of cardiovascular prosthetic applications, using alternating layers of gelatin and tannic acid. This novel approach, while more complex, offers potential advantages in terms of coating stability, surface control, and the biofunctional properties of the scaffold. The inclusion of tannic acid, a polyphenolic compound with antioxidant and antimicrobial properties, may further enhance the scaffold's therapeutic potential by providing additional functional characteristics. The LbL technique, though relatively unexplored for vascular graft applications, allows for more precise control over layer thickness and composition, which can be advantageous in optimizing the scaffold's surface characteristics.

3.1 Materials and methods

To develop a standardized and reproducible coating process, tubular PCL/PGS scaffolds with embedded quercetin were produced as detailed in Chapter 2.1.2. Once the scaffolds were obtained, the initial experiment focused on expanding the polymer fibers. This approach aimed to allow gelatin to adhere more effectively to the scaffold through conventional coating methods by first acting on expanded fibers. Subsequently, the innovative layer-by-layer (LbL) coating method was implemented, offering an advanced alternative coating strategy.

3.1.1 Expansion of scaffold fibers

In this thesis work, experiments were conducted to expand the polymeric fibers within the scaffolds with the goal of enhancing gelatin penetration and ensuring a more uniform distribution within the fiber structure. The approach was based on methods observed in literature ([85], [86]), where sodium borohydride ($NaBH_4$) in an aqueous 0.1M solution was successfully employed to induce the expansion of polymer fibers, resulting in notable alterations in the material's structure. Specifically, these studies demonstrated that immersing two-dimensional polymer matrices in $NaBH_4$ solution can cause the fibers to expand significantly, creating a transformation from a two-dimensional matrix into a three-dimensional scaffold structure. This expansion is typically driven by $NaBH_4$'s role as a foaming agent, releasing gas within the fiber network and generating internal pressure that can modify the fiber architecture, enhancing porosity and facilitating internal access for subsequent treatments.

In the current study, PCL/PGS scaffolds embedded with quercetin were used for this method. The $NaBH_4$ solution was prepared in water, and scaffold samples were immersed for varying periods of 5 minutes, 30 minutes, 2 hours, and 4 hours. However, after each immersion, no observable changes in either shape or structure of the samples were detected. The lack of response to the $NaBH_4$ solution appears to stem from the hydrophobic nature of PCL, which resists interaction with the aqueous NaBH4 medium. This nonpolarity likely prevents the solution from effectively infiltrating the polymer fibers and generating the necessary internal pressure to prompt structural modification.

The reference literature suggests a viable alternative by recommending the preparation of $NaBH_4$ solution in a nonpolar solvent such as methanol, which would likely enhance interaction with hydrophobic polymers like PCL. However, methanol was not pursued in this study due to its cytotoxicity and incompatibility with vascular applications, where maintaining biocompatibility is essential. Methanol-based treatments would likely compromise the material's suitability for *in vivo* use, especially in applications involving direct blood contact, as in vascular grafts.

3.1.2 Novel coating method

3.1.2.1 Reactants used

The substances used in the tested coating techniques were gelatin and tannic acid.

Gelatin is a natural hydrophilic polymer derived from the denaturation of collagen, obtained by breaking down collagen's triple-helix structures into single strands through hydrolysis processes, which can be either acidic (Type A gelatin) or basic (Type B gelatin). Collagen is one of the most abundant matricellular proteins in the extracellular matrix (ECM) of arteries, contributing to the structural integrity of the blood vessel wall and facilitating the release of growth factors for vascular cells. The differentiation in gelatin production methods from collagen leads to different release profiles for these growth factors. A major advantage of gelatin over collagen is its lower immunogenicity, while still retaining the functional groups that promote essential biological processes such as cell adhesion, migration, proliferation, and differentiation.

In the context of vascular applications, gelatin exhibits favorable characteristics for the creation of grafts due to its high biocompatibility. Moreover, its ease of processing in combination with other materials enables the creation of structures that support blood flow and resist thrombosis, thus improving the effectiveness of ready-to-use vascular grafts [84].

Tannic acid (TA) is a plant polyphenol known for its astringent, antioxidant, antimicrobial, antiviral, and anti-inflammatory properties. Its molecular formula is $C_{76}H_{52}O_{46}$, and structurally

it's formed by a decagalloyl residue consisting of a center D-glucose molecule esterified at all five hydroxyl moieties with two gallic acids (Figure 31).

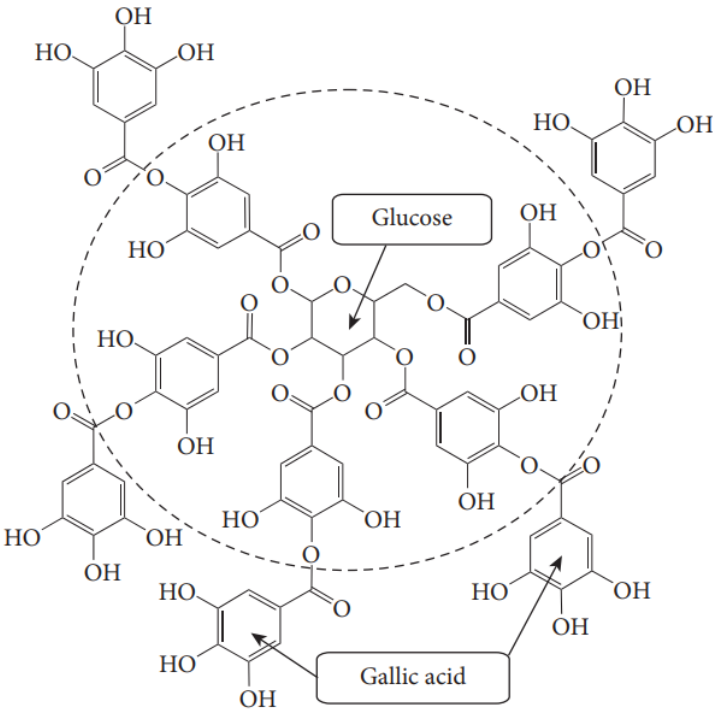

Figure 31. Chemical structure of TA, where the circle indicates pentagalloylglucose and the core structure of TA.

In vascular applications, it is crucial that the gelatin used as a coating for scaffolds maintains its integrity to ensure continuous and controlled release of growth factors. However, its biodegradation by matrix metalloproteinases (MMPs) is one of the main drawbacks for gelatin-based vascular scaffolds. To address this issue, numerous studies have been conducted to identify bioactive molecules that can stabilize gelatin, with tannic acid emerging as the most promising candidate. Tannic acid can prevent gelatin degradation by cross-linking it and inhibiting MMP activity. Additionally, its natural anti-inflammatory and antioxidant properties make it a suitable component for inclusion in vascular implants [86].

3.1.2.2 Layer by layer coating process

Another possibility in order to cover with gelatin the surfaces of the fibers' scaffolds is through layer-by-layer (LbL) self-assembly. This proceeding offers two key benefits:

(i) it enables precise regulation of the chemical composition and structure of films, as each layer is deposited according to a predetermined LbL method;

(ii) it is especially well-suited for producing large-area films on irregular or curved surfaces.

Layer-by-layer (LbL) assembly is a sophisticated technique where complementary multivalent species can be alternately adsorbed onto a substrate through electrostatic interactions, hydrogen bonding, halogen bonds, coordination bonds, charge-transfer interactions, biospecific interactions, cation-dipole interactions, or a combined interaction of the cited forces. A wide variety of materials can be utilized in this method to form building blocks, including graphene oxide, polypeptides, natural polymers, synthetic polymers, polymeric microgels, particles, dendritic molecules, organic components, block copolymers, and complexes of these species, regardless shape's and size's substrate. This method is particularly promising in biomaterials and can be successfully applied for biomedical coatings, because it enables the creation of highly complex and customized coating compositions of nanoscale thin films. Furthermore, unlike other molecular deposition techniques, LbL assembly occurs in water at room temperature, preserving the functionality of sensitive biomolecules like proteins and nucleic acids.

LbL multilayers can uniformly coat structures as small as 10 nm diameter gold nanoparticles, surfaces with intricate nanoscale features, but also large-scale macroscopic three-dimensional objects. Importantly, these multilayer thin films can be designed to exhibit high biocompatibility levels both *in vitro* and *in vivo*, accommodating various organic and inorganic nanomaterials alongside small and large molecules. Another noteworthy capability is the possibility to incorporate drugs into different layers of the substrate, thereby facilitating drug delivery [89].

A multilayer film can be created by alternately immersing a charged substrate into aqueous solutions of oppositely charged materials, with intermediate steps of rinsing in water and drying. Every time the object is submerged, it accumulates a layer of electrically charged particles from the liquid, which also flips the object's surface charge. This reversal makes it possible to apply a subsequent layer with a charge opposite to the previous one. Although it's common to dry the object after each coating, this step can be omitted to simplify the LbL assembly process. Physical and chemical characteristics can be tailored by adjusting deposition conditions, such as temperature and pH of the dipping solution, and altering the polymers' composition. Another thing to keep in mind is that the deposition times of the dipping LbL assembly process can be significantly reduced if polymers with rapid adsorption kinetics are used or when it is not necessary to achieve saturation adsorption of the polymer layers [23].

For the coating of cardiovascular prostheses, the layer-by-layer dipping technique was employed using aqueous solutions of gelatin from bovine and porcine bones and tannic acid (Sigma Aldrich, St. Louis, MO, USA).

Tannic acid binds with proteins through hydrophobic interactions. It must be mentioned that hydrophobic interactions refer to the interactions formed between hydrophobic groups in an aqueous environment due to both enthalpic and entropic effects, causing these groups to aggregate to minimize exposure to water molecules. Specifically, regarding tannic acid, it begins by attaching to hydrophobic areas formed by the side chains of amino acids in proteins: this initial interaction is primarily due to hydrophobic forces. Following this, hydrogen bonds are formed between the phenolic groups of tannic acid and the protein's amino acid chains. It has been shown that proteins with a high content of proline are particularly likely to bond with tannic acid because of their affinity for hydrophobic interactions [90].

Gelatin, being especially rich in proline and 4-hydroxyproline, can establish strong and diverse bonds with tannic acid (see Figure 32, [90]), including hydrogen bonds as well as hydrophobic interactions, allowing to achieve satisfactory results using the layer-by-layer coating technique [91].

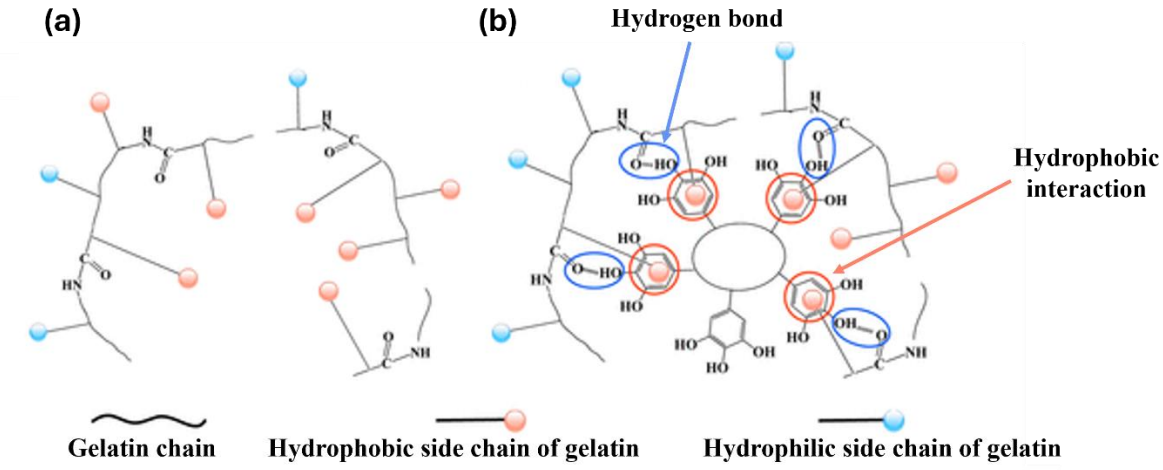

Figure 32. (a) Chemical structure of the protein of gelatin. (b) Interactions established between gelatin and tannic acid.

Various concentrations of gelatin were tested, while the concentration of tannic acid was kept constant at 0.125 g/ml. In the initial phase, to select the best operating conditions and to understand the influence of gelatin concentration on the amount encapsulated in a single layer,

preliminary tests were conducted on sample pieces of 0.5 × 1 cm size obtained from previously electrospun scaffolds. These samples were subjected to LbL coating with gelatin concentrations of 41.6 mg/ml, 10.4 mg/ml, and 5.2 mg/ml: concentration values lower than the maximum solubility of gelatin in water (67 mg/ml) were chosen, previously used in conventional coating. Furthermore, during the initial phase of experimentation, two different methods for drying the coated material were tested: lyophilization (Alpha 1-2 LDplus, Germany) and air drying.

Lyophilization, also known as freeze-drying, is the gentlest method for drying products. It relies on sublimation, a physical phenomenon where a substance transitions directly from a solid to a vapor without going through a liquid phase. The main advantage of this method is that the product does not deteriorate because it is not heated to high temperatures, which could, for example, activate biosynthetic pathways that would degrade important or relevant molecules in the analysis.

In order to deposit one layer of the coating of gelatin and tannic acid onto the polymeric scaffolds, the following steps were followed:

1) immersion of the prosthesis for 1 minute in the gelatin solution contained in a 15 ml falcon tube in a horizontal position;
2) immersion of the prosthesis for 30 seconds in the tannic acid solution contained in a 15 ml falcon tube in a horizontal position;
3) keeping the prosthesis in a horizontal position in the air for 1 minute before the drying phase;
4) drying phase, conducted according to one of the following methodologies:
   (a) lyophilization for 4 hours of the samples previously frozen for 15 minutes;
   (b) air drying under ambient conditions for 6 hours.

In the initial phase of the study, it was observed that freeze-drying caused embrittlement of the polymer material constituting the prosthesis. Consequently, in all subsequent tests, air drying was used instead, as it is simpler, less expensive, and capable of maintaining the mechanical properties of the scaffold.

The mentioned steps were subsequently repeated until the desired number of layers was achieved.

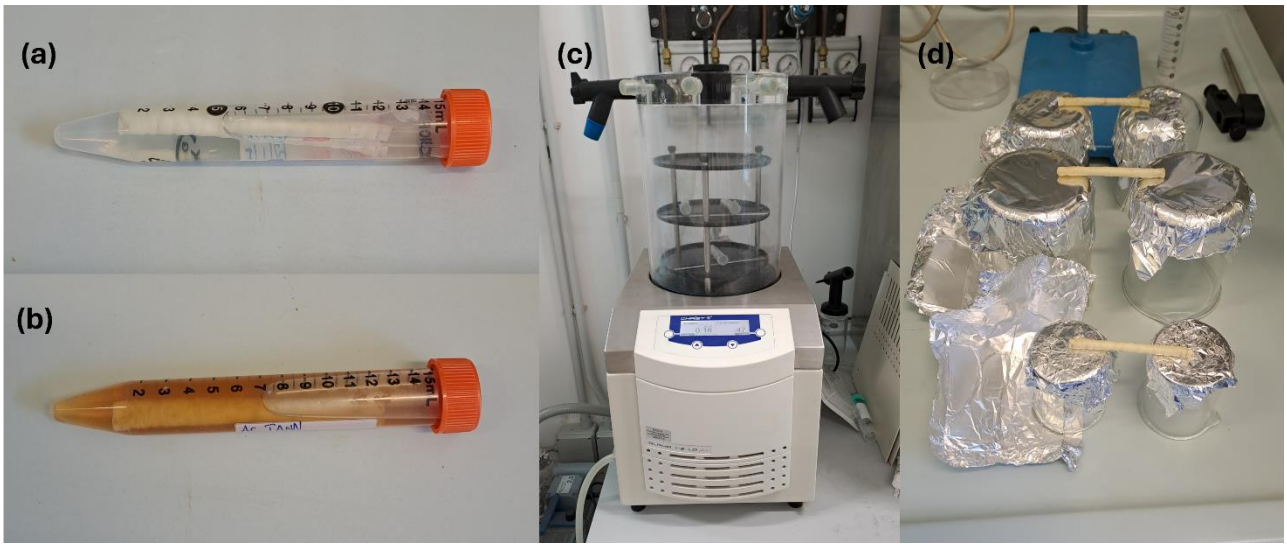

Figure 33. Configuration of the LbL coating process adopted. (a) Immersion of the prosthesis in the gelatin solution. (b) Immersion of the prosthesis in the tannic acid solution. (c) Drying by lyophilization. (d) Air drying at room conditions.

3.1.3 Scanning Electron Microscopy (SEM) analysis

The morphological characteristics of the LbL coated scaffolds were examined using a scanning electron microscope (SEM), following the same method reported in Chapter 2.1.4. The analysis was performed on scaffolds coated with lower and higher gelatin concentration, respectively equal to 5.2 and 41.6 mg/ml.

SEM images were taken to capture detailed surface features and to analyze the coating uniformity and fiber structure integrity post-coating.

3.1.4 Fourier Transform Infrared Spectroscopy

The FTIR analysis conducted on the LbL-coated scaffolds aimed to confirm the presence of gelatin and tannic acid on the scaffolds and verify the effectiveness of the LbL coating method in introducing these substances onto the surface.

Ensuring the presence of these components within the polymeric matrix is crucial to confirm that the electrospun scaffolds benefit from the antioxidant properties of tannic acid and from the high biocompatibility of gelatin.

In the FTIR spectra, characteristic peaks associated with gelatin, such as amide I (around 1650 cm^{-1}) and amide II (around 1550 cm^{-1}), and the phenolic groups of tannic acid, which generally appear around 1500–1600 cm^{-1}, are expected indicators of successful coating application.

FTIR analyses were conducted on scaffolds coated using the layer-by-layer technique with gelatin concentrations of 5.2, 10.4, and 41.6 mg/ml. The comparison among the different gelatin concentrations allows for verification of the successful application of the coating and investigation of potential trends or patterns in the developed process as this parameter varies.

3.1.5 Thermogravimetric Analysis (TGA)

Thermogravimetric analysis (TGA) was employed to evaluate the thermal stability and composition of the scaffolds coated with the layer-by-layer method. This technique provided critical insights into the quantity of gelatin and tannic acid incorporated into the coating, which directly influences the scaffold's structural integrity and biodegradation profile. For reference, a TGA analysis of pure tannic acid was also conducted to identify characteristic decomposition profiles that could be compared to those observed in the coated scaffolds. All the analyses were conducted following the method reported in Chapter 2.1.6.

TGA is commonly used to analyze composite materials because it allows for the identification and quantification of individual components based on their distinct decomposition temperatures and weight loss patterns. In this study, the presence of gelatin and tannic acid in the scaffold was confirmed by observing specific weight loss events corresponding to their thermal degradation, which typically occurs at the characteristic temperatures where proteins and polyphenolic compounds break down.

3.1.6 Hydrophilicity test

To evaluate the hydrophilicity of the produced polymeric scaffolds, the contact angle was measured, which is the angle formed between a liquid droplet and the material's surface. This value provides information about the interaction between the material's surface and liquids. High contact angle values (greater than 90 degrees) generally indicate a hydrophobic surface, while low values identify a hydrophilic material. For vascular scaffolds, it is necessary that they possess adequate hydrophilicity to increase biological compatibility, promoting the process of cell adhesion. The contact angle values with a water droplet were evaluated for scaffolds based on PCL, PCL/PGS, PCL/PGS with quercetin, and scaffolds coated with the layer-by-layer coating. The analysis was carried out using an optical microscope (Vision SX45 Elite Microscope, Leica Microsystems), quantifying the change in the contact angle between the surface and the liquid at the initial moment of the test and after some time following their interaction. By comparing the investigated materials, it is possible to determine how

the polymer composition, the inclusion of specific substances like quercetin, or the application of the coating influence the surface properties.

3.1.7 Quantification of bioactive compounds

The application of the layer-by-layer coating with gelatin and tannic acid has raised the issue of how to individually detect the presence of these components, keeping in mind that the quercetin present in the scaffold can also act as an interferent. Different methods have been tested to quantify tannic acid and quercetin together, which are both polyphenolic compounds, thus trying not to consider the contribution of gelatin. The identification of the appropriate methodology is crucial for the release studies conducted on the scaffold, as described in the following chapters.

3.1.7.1 UV spectroscopy

In order to determine the amount of bioactive compounds released from the scaffold during the release tests, UV/visible spectroscopy was initially tested.

UV/Vis spectroscopy focuses on the absorption of light within the visible region (350–700 nm) and the near ultraviolet (200–350 nm) of the electromagnetic spectrum. It can also extend into the far ultraviolet (10–200 nm), though this requires operating under vacuum or in an inert gas atmosphere, as atmospheric oxygen can obscure the signals from other substances at these wavelengths. This technique is a form of electronic spectroscopy because the absorption of UV/Vis radiation by molecules can trigger energy transitions in the outer electrons, whether they are involved in bonding or not.

For this type of analysis, Jenway Genova Analyser was employed. This spectrophotometer, which is equipped with a Xenon lamp as light source, has a single-beam configuration, meaning that the dispersing system sends a single beam to the cuvette containing the sample. The downside of this configuration is that for each measurement and each wavelength, it is necessary to repeat the blanking process with the spectrum of the blank, that is the solvent in which the sample is dissolved.

To determine whether UV/vis spectroscopy is a suitable method for individually detecting the components of the coating, absorbance measurements were conducted on pure solutions of tannic acid and gelatin at 212 nm, that is the characteristic peak of TA. The results indicated that the method successfully detected absorbance not only in tannic acid solutions but also in gelatin solutions. This outcome reveals a limitation of the analytical approach, as it is unable to isolate the absorbance contributions of tannic acid from those of gelatin when both components coexist in a sample. Consequently, this method does not allow for the independent quantification of

bioactive compounds in the presence of gelatin, highlighting the need for an alternative analytical strategy to ensure accurate characterization in composite systems.

3.1.7.2 Folin Ciocalteu assay

An attempt was made to estimate the amount of bioactive compounds released from the scaffolds using the Folin-Ciocalteu assay, widely used in literature to determine the content of phenolic compounds.

The prosthesis samples with the LbL coating were immersed in 6 ml of deionized water, subjected to an ultrasonic bath for 15 minutes, and heated to around 50 °C for 15 minutes to promote the release of bioactive agents from the polymer matrix. Then, 0.5 ml of Folin-Ciocalteu reagent, 1 ml of sodium carbonate solution and 2.5 ml of deionized water were added. The content was vortexed and left in the dark for 1 hour. Finally, the absorbance of the sample was measured at 725 nm in glass cuvettes to determine the concentration of polyphenols using a calibration curve. The same procedure was performed on a pure gelatin solution with a concentration of 5.2 mg/ml. The spectrophotometric reading at 725 nm of the gelatin sample gave a positive result, highlighting the limitation of the protocol in being able to individually detect the bioactive components present in the coated scaffold.

3.1.7.3 Ferric Chloride assay

Another method explored for quantifying bioactive molecules was the Ferric Chloride protocol, which allows for the determination of polyphenols present in a sample through protein precipitation.

As outlined in the Folin-Ciocalteu protocol, the prosthesis samples with LbL coating were immersed in 1.5 ml of deionized water, placed in an ultrasonic bath for 15 minutes, and then heated to approximately 50°C for another 15 minutes to facilitate the release of bioactive compounds from the polymer matrix. After this step, 0.5 ml of the samples appropriately diluted in deionized water were added to 2 ml of SDS-triethanolamine solution (SDS 5% v/v in distilled water, triethanolamine 1% v/v in distilled water). The solution was gently stirred, followed by the addition of 0.5 ml of ferric chloride (0.01M $FeCl_3$ in 0.01M HCl), and then mixed again immediately. The absorbance at 510 nm of the samples was read 15/30 minutes after the addition of ferric chloride, using the reagent mix of the assay and pure deionized water instead of the sample as blank. To derive mass values from absorbance data, an appropriate calibration curve was constructed using solutions with known concentrations of tannic acid prepared in the reagent

mix of the protocol. To verify that the assay does not detect gelatin, a pure gelatin solution was analyzed using the same protocol, resulting in no absorbance. This finding confirms that the Ferric Chloride assay can specifically detect polyphenols without interference from gelatin.

3.1.7.4 BCA assay

A test was conducted to detect only the portion of gelatin present in the release medium using the BCA assay, in order to subtract it in a subsequent phase and obtain the contribution of only polyphenolic substances.

The BCA assay is based on the addition of a copper solution and a bicinchoninic acid solution in volumetric proportions of 1:50 to the protein solution to be analyzed. The assay relies on the reduction of Cu^{2+} copper ions by the proteins. The resulting Cu^{1+} copper ions then react with bicinchoninic acid to form a purple-violet complex, known as the BCA-Copper complex. The color is measured at a wavelength of 562 nm, and the absorbance of the complex formed between copper and bicinchoninic acid is directly proportional to the protein concentration of the sample. Specifically, in the tests conducted in this thesis work, both the gelatin solution at a concentration of 5.2 mg/ml and the tannic acid solution at a concentration of 0.125 g/ml were analyzed using the BCA assay. The protocol resulted in the coloration of both samples, thus highlighting the impossibility of using this assay to detect only gelatin in samples where both components are present.

3.1.8 Antioxidant activity

The antioxidant activity of the produced scaffolds, attributed to the presence of tannic acid in the structure, was investigated using both the DPPH and ABTS protocols. Both assays work by transferring hydrogen atoms or electrons from antioxidant molecules to neutralize radicals, which contain an unpaired electron. The primary difference between the two methods lies in their solubility and sensitivity. DPPH is more soluble in organic solvents, such as ethanol or methanol, making it suitable for assessing lipophilic antioxidants. Conversely, ABTS is soluble in both organic compounds and water, allowing the analysis of hydrophilic antioxidants as well. Furthermore, ABTS is more sensitive than DPPH, enabling the measurement of samples with lower antioxidant concentrations.

3.1.8.1 DPPH assay

The anti-oxidation performance of the produced polymeric prostheses was measured by investigating their scavenging effects on free radicals.

The DPPH assay involves the use of the 2,2-diphenyl-1-picrylhydrazyl radical, which has an unpaired electron on a nitrogen atom. This reagent must be properly diluted in solution and then reacted with the sample to be analyzed.

This protocol allows for the measurement of the reducing activity of antioxidant molecules against DPPH, which is characterized by a purple color that fades in the presence of an antioxidant agent. The antioxidant molecule exerts its effect by transferring a hydrogen atom (that is the ability to transfer an electron) to the radical. The discoloration obtained, which can be quantified by the decrease in the absorbance peak in the UV/Vis spectrum at 517 nm, is proportional to the antioxidant content in the sample.

First of all, a 0.1 mM DPPH solution was prepared using pure anhydrous ethanol as the solvent. Since the DPPH reagent is light-sensitive, every step was carried out by covering the glassware used with aluminum foil. For each type of sample, measurements were performed in triplicate to ensure consistent results. The tested samples included control PCL/PGS prostheses, PCL/PGS prostheses loaded with quercetin, and PCL/PGS with quercetin prostheses coated with gelatin using the layer-by-layer method with a gelatin concentration of 5.2 mg/ml over three coating cycles. Additionally, solutions of tannic acid at 0.125 g/ml, gelatin at 5.2 mg/ml, and quercetin at 5.5 mg/ml in ethanol were analyzed for comparison.

The solid samples were accurately cut to obtain uniform portions of 10 mg, while for liquid samples, a volume of 100 µl was used. Each sample was mixed with 3.9 ml of the DPPH solution and then incubated in darkness for one hour at 30°C with continuous shaking at 150 rpm, ensuring adequate interaction with the DPPH radicals. After incubation, absorbance was read at 517 nm in 1 ml plastic cuvettes, using pure anhydrous ethanol as blank. Absorbance measurements of the pure DPPH solution were also recorded before and after incubation to provide a baseline for comparison.

The antioxidant activity AA was calculated using the following formula:

$$AA\ [\%] = \left(1 - \frac{A_{sample}}{A_{DPPH}}\right) * 100 \tag{6}$$

3.1.8.2 ABTS assay

The ABTS assay is an established method to assess antioxidant activity by measuring the ability of samples to scavenge the ABTS radical cation (ABTS•+), which has an unpaired electron on a nitrogen atom and exhibits a distinct blue-green color at 734 nm. This color fades in the presence of antioxidants as they neutralize the radical through the transfer of an electron or a hydrogen atom, which allows for quantification of the antioxidant effect. This protocol is extensively used to assess the antioxidant activity of both water- and oil-soluble compounds.

Since ABTS is light-sensitive, the entire preparation and testing procedure were carried out in the dark, using aluminum foil to cover glassware.

To begin, a 7 mM ABTS stock solution was prepared by dissolving 0.0959 g of ABTS in 25 ml of deionized water. A 140 mM potassium persulfate solution was then made by dissolving 0.3775 g of potassium persulfate in 10 ml of deionized water. After that, 25 ml of the ABTS solution was mixed with 440 µl of the potassium persulfate solution, and this mixture was kept refrigerated in darkness for 16 hours. After this period, this stock solution was diluted with deionized water to achieve an absorbance of approximately 0.7 at 734 nm, yielding the working solution for the assay.

The samples analyzed included control PCL/PGS prostheses, PCL/PGS prostheses with quercetin, and PCL/PGS prostheses coated using the layer-by-layer method with gelatin (5.2 mg/ml) over three coating cycles. Additionally, tannic acid (0.125 g/ml) and gelatin (5.2 mg/ml) were tested as individual reference solutions. All measurements were performed in triplicate to ensure accuracy and reliability.

For solid samples, a 10 mg portion was used, while 50 µl was taken for each liquid sample. To each sample, 1 ml of the ABTS working solution was added. After 2 minutes, absorbance readings were taken at 734 nm using 1 ml plastic cuvettes, with deionized water as the blank reference.

The antioxidant activity, expressed in terms of Radical Scavenging Activity (RSA), was calculated similarly to the DPPH method, using the following equation:

$$RSA\ [\%] = \left(1 - \frac{A_{sample}}{A_{ABTS}}\right) * 100 \tag{7}$$

3.1.9 Release of bioactive compounds from scaffold in static conditions

An *in vitro* release study of the bioactive components from the scaffold with layer-by-layer coating (gelatin concentration of 5.2 mg/ml) was conducted under static conditions. For the release medium

study, an analytical technique was employed that does not distinguish individual components but instead considers the cumulative contribution of quercetin, gelatin, and tannic acid.

Tannic acid was used as the reference component, assuming that gelatin and quercetin exhibit similar behavior. This approximation can be considered valid because tannic acid and gelatin exhibit characteristic peaks in their respective UV spectra within the same wavelength range, overlapping with one another. Consequently, during the initial phase of the study it was necessary to obtain the characteristic spectrum of tannic acid to determine its specific absorption wavelength. To achieve this, several solutions of tannic acid in PBS at different concentrations were prepared and analyzed using UV/Vis spectroscopy (PerkinElmer Lambda 25). Only spectra with absorbance values below 1 and free of noise were considered valid.

For the release study, all material samples were weighed before the start of the analysis. The analyses were conducted in triplicate to obtain reliable values with their respective standard deviations.

The release media from coated LbL scaffolds were measured by UV/vis spectrophotometer (Jenway Genova Analyser). Specifically, the coated scaffolds with gelatin concentration of 5.2 mg/ml were put into falcons and immersed in 4 ml of PBS buffer solution, and then placed in a 30 °C incubator with a speed rotation of 150 rpm. The sampling was conducted at 30 minutes, 1 hour, 2 hours, 3 hours, 4 hours, 6 hours, 8 hours, and 24 hours. At each sampling time, 1 ml of the falcon solution was taken to be analyzed subsequently, and simultaneously 1 ml of fresh solution of PBS was added again to the solution to maintain total volume inside the falcon constant.

The samples were analyzed using quartz cuvettes and UV absorbances at 212 nm were measured using PBS as blank, while the concentration was obtained from equation of standard regression curve of TA in PBS. The specific wavelengths of 212 nm was determined through spectroscopic analysis of the characteristic peaks of TA in PBS. From the concentration data and knowing the volume of the sample taken at each time point, it was possible to calculate the mass quantities released at each sampling.

To obtain the cumulative release curve, the percentage P_t of substances released at a given time t was first calculated using the following formula:

$$P_t[\%] = \frac{W_t\ [\mu g]}{W_{coated\ scaffold}\ [\mu g]} * 100 \tag{8}$$

where W_t is the mass of components released at time t,

$W_{coated\ scaffold}$ is the mass of the coated prosthesis used for the release.

The cumulative release percentage C_t was calculated as follows:

$$C_t[\%] = \sum_{i=t_0}^{t} P_{t_i} \tag{9}$$

The static release profile was studied by applying nonlinear fitting with various mathematical models, which are detailed in the following sections. The significance of these models lies in their application in both the formulation design phase and in experimentally confirming the release mechanism of a pharmaceutical product.

a) Higuchi Model [92]

$$C_t = k_H\sqrt{t} \tag{10}$$

where k_H is the Higuchi release constant. In this model, the release of the drug molecule from a matrix system is described based on Fickian diffusion. The assumption of this model is that the drug has an initial concentration within the matrix that is higher than its solubility in the surrounding medium.

b) Peppas Model [92]

$$C_t = k_P t^n \tag{11}$$

where k_P is the Peppas release constant, which incorporates the geometric characteristics of the drug dosage form, and n is the diffusion or release exponent, whose value describes the release mechanism involved. Peppas model is also known as “power law” model and describes drug release from a polymeric system considering simultaneous release mechanisms, such as diffusion, swelling, and dissolution. To apply this equation, the ratio of the system's width/thickness or length/thickness should be at least 10. This model is typically used to study the release of pharmaceutical polymeric dosage forms when the release mechanism is unclear or when multiple release phenomena may occur.

c) Makoid-Banakar Model [92]

$$C_t = k_{MB} t^n e^{-ct} \tag{12}$$

where k_{MB}, n and c are empirical parameters.

3.1.10 Bioreactor tests

A bioreactor is a device that replicates the physiological environment and allows for the control of individual variables, thus enabling the creation, conditioning, and testing of cells, tissues, organs, and supports *in vitro*. In the context of this thesis work, a bioreactor for tissue engineering was addressed, capable of providing appropriate stimuli to prepare the graft for *in vivo* biological conditions.

The set objective was to analyze the release profile from the coated scaffold under dynamic conditions. First, a study was conducted using the same sampling times as in the static case to allow for comparison, followed by a study with longer sampling times to simulate real behavior in the case of implantation in the body.

The fabricated scaffolds have been tested in a high-performance bioreactor (APTUS Bioreactors) to simulate the behavior of the prostheses within the cardiovascular system.

The system consists of several key components:

- a vascular chamber that accommodates up to three prostheses at once per test;
- three chambers known as the compliance chamber, pulse dampener, and reservoir, where the solution to be circulated within the circuit and prosthesis is placed;
- a peristaltic pump to flow the solution through the circuit;
- a pinch valve to mimic heartbeats;
- two transducers that measure the pressure at the vascular chamber's inlet and outlet;
- a flow meter for monitoring system flow;
- three clamps for adjusting and controlling the system's pressure and flow.

The bioreactor is connected to a control box that interfaces with software, allowing real-time monitoring of flow rates and inlet and outlet pressures over time. A schematic representation of the various components of the bioreactor is shown in Figure 34.

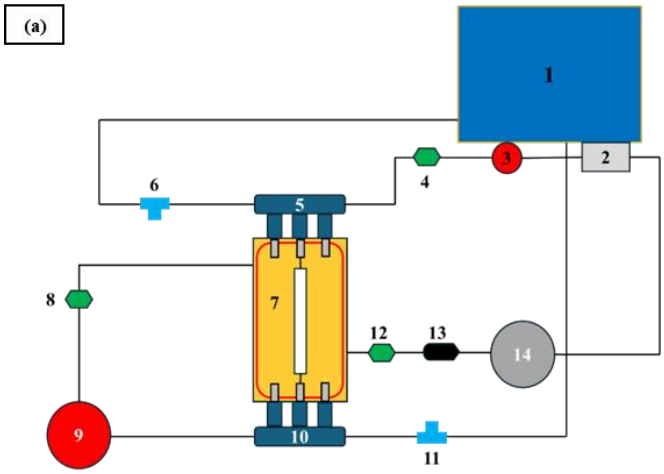

Number	Bioreactor component
1	Control box
2	Peristaltic pump
3	Dampener
4, 8 and 12	Clamps
5	Inlet manifold
6 and 11	Pressure transducers
7	Vascular chamber
9	Compliance chamber
10	Outlet manifold
13	Flow meter
14	Reservoir

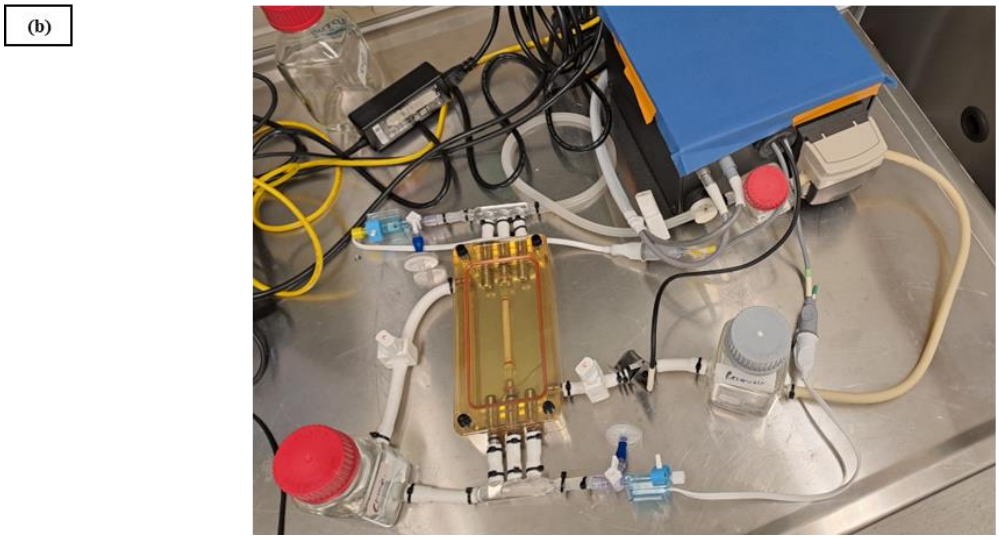

Figure 34. (a) Schematic representation of the bioreactor; (b) APTUS bioreactor.

The prosthesis is positioned inside the vascular chamber using specific adapters designed to accommodate scaffolds of various diameters and lengths. Following this, the bioreactor is filled with approximately 700 ml of phosphate buffer saline solution (PBS), initially introduced into the reservoir. It was decided to use PBS in the bioreactor instead of deionized water because it simulates more precisely the human physiological environment, being a buffer solution capable of maintaining a neutral pH, the same as blood and bodily fluids.

Any air bubbles present within the circuit are manually expelled with the assistance of the pressure transducers. By adjusting the peristaltic pump, the pinch valve, and the clamps, it is possible to control the flow rate circulating in the circuit.

Two dynamic release experiments were conducted. The first test lasted a total of 24 hours, with sampling times matching those of the static case (i.e., at 30 minutes, 1 hour, 2 hours, 3 hours, 4 hours, 6 hours, 8 hours, and 24 hours). The second test spanned 15 days, with samples collected at 12 hours, 1 day, 5 days, 6 days, 7 days, and 15 days. In both cases, the tests were carried out by placing a

prosthesis with 3 layers of coating with a gelatin concentration of 5.2 mg/ml in the bioreactor. The flow was set to a value of 0.135 l/min, and periodic samples of 70 ml were taken, each time replaced with fresh PBS to maintain the working volume. Analogous to the static case, the release media were analyzed using an analytical technique that considers the cumulative contribution of gelatin, tannic acid, and quercetin.

3.2 Results and discussion

3.2.1 Coating process

The layer-by-layer (LbL) coating technique was evaluated using gelatin concentrations of 5.2 mg/ml, 10.4 mg/ml, and 41.6 mg/ml to investigate the influence of gelatin concentration on coating deposition. A stepwise analysis was performed on individual coating layers to identify trends related to the concentration of gelatin. The scaffolds were weighed before the coating process and again after each individual layer application. To ensure complete drying between layers, mass measurements were taken 24 hours apart. All scaffolds had comparable geometric characteristics, such as length and diameter, although initial mass varied slightly among samples.

The LbL coating results, shown as mean measurements ± standard deviation and presented in Figure 35, are expressed as the mass difference between the scaffold's initial weight and its weight after each layer was applied. For the second and third layers, the previous layer's mass was subtracted to isolate each individual layer's weight. The cumulative mass difference reflects the total coating mass and was calculated by subtracting the initial uncoated scaffold weight from the final weight post-coating. The results demonstrate that, for a given gelatin concentration, the mass added with each additional layer remained consistent across scaffolds. Furthermore, as the gelatin concentration increased, the mass of each deposited layer also increased proportionally, indicating a scalable, controllable trend. These findings suggest that the implemented method allows for precise control over the gelatin quantity deposited on the scaffold by adjusting a single process parameter, thus supporting the standardization of the LbL coating technique.

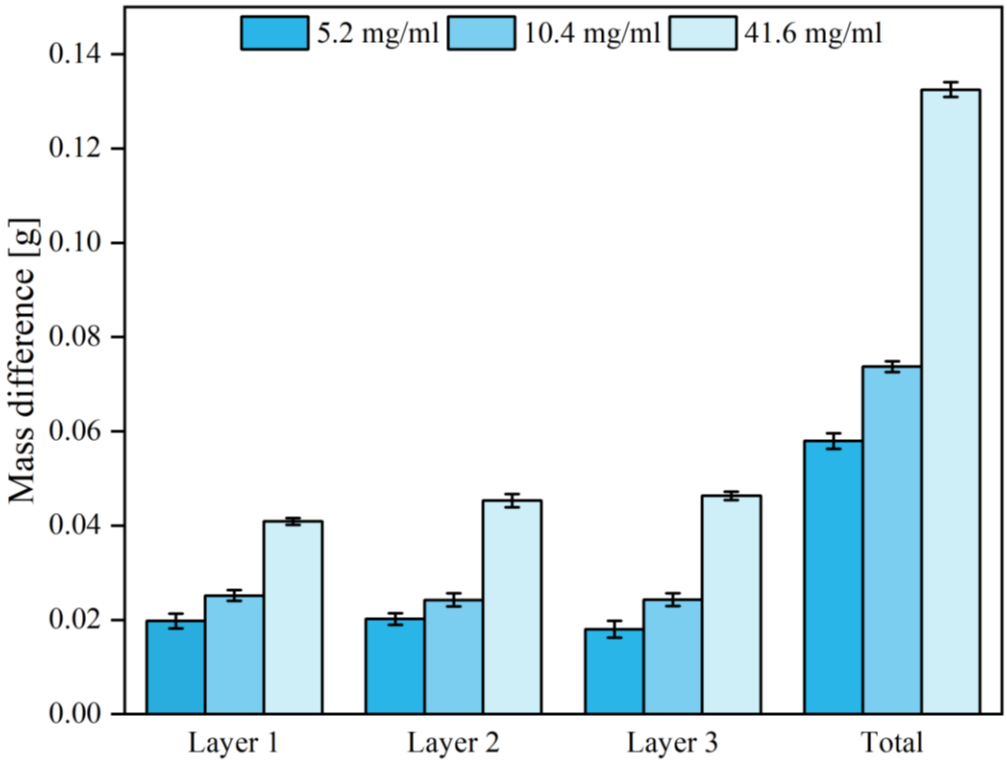

Figure 35. Results of the layer-by-layer coating method expressed in terms of mass deposited after the application of each individual layer.

3.2.2 Morphological analysis

Scanning Electron Microscopy (SEM) imaging was performed to evaluate the morphological characteristics of the electrospun scaffolds after the application of gelatin and tannic acid coating using layer-by-layer (LbL) assembly technique with varying gelatin concentrations.

Scaffolds coated with the lowest and highest tested gelatin concentrations, specifically 5.2 mg/ml and 41.6 mg/ml, were analyzed. The SEM images, shown in Figure 36, reveal that the application of the coating layers was successful. The gelatin appears as a thin film deposited over the polymer fibers. Additionally, as the gelatin concentration increases, there is a noticeable thickening of the coating layer, leading to a reduction in the scaffold's porosity. The overall fibrous architecture of the scaffold was preserved, demonstrating that the coating process did not disrupt the structural integrity of the electrospun fibers.

However, it was not possible to determine the fiber diameter distribution, as the gelatin coating obscures the visualization of individual fibers in the SEM images. Nevertheless, it can be hypothesized that the average fiber diameter increases with higher gelatin concentrations and follows a similar trend with an increasing number of coating layers.

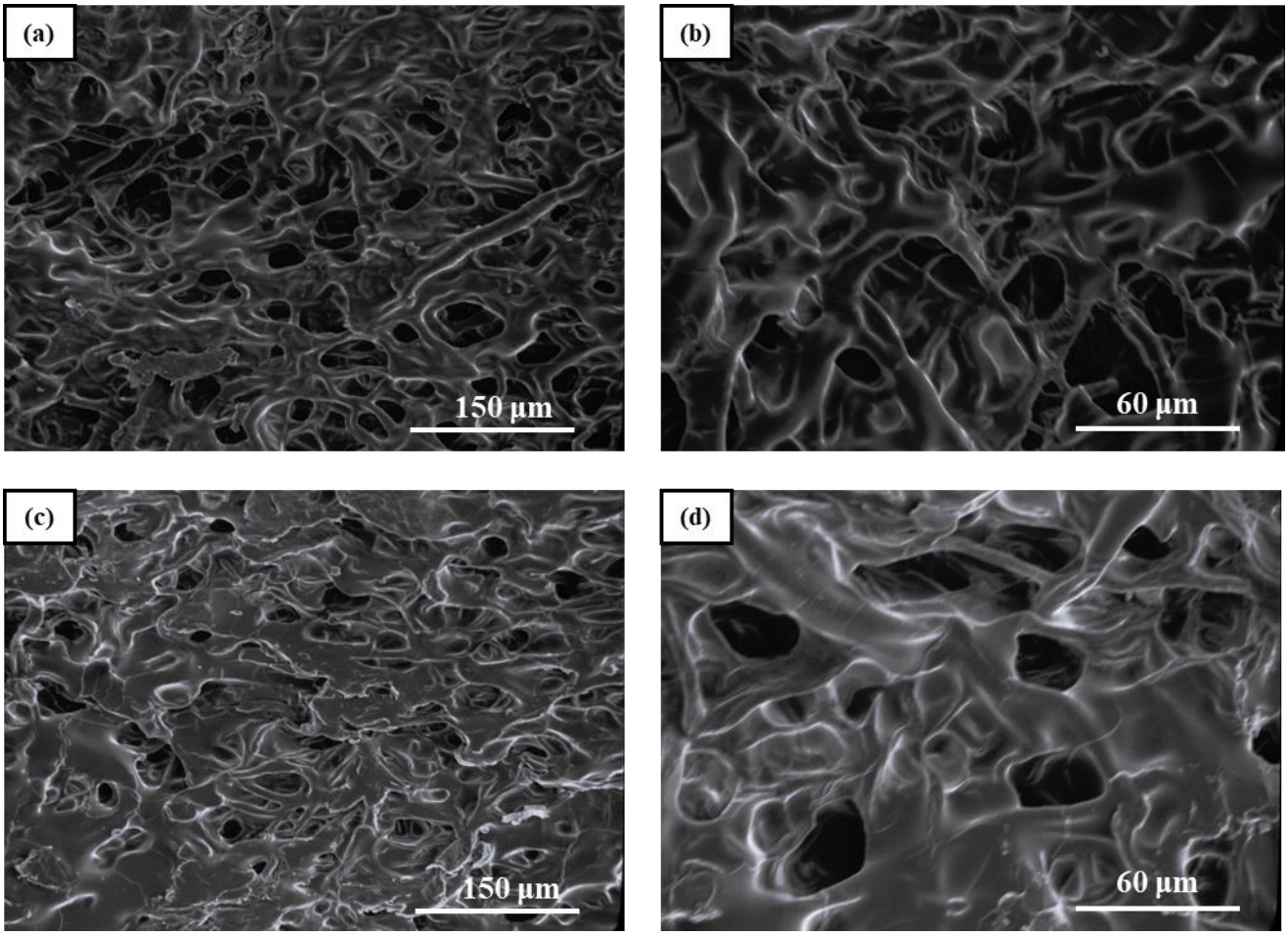

Figure 36. SEM images for LbL coated scaffolds with gelatin concentration of: (a) 5.2 mg/ml at lower magnification; (b) 5.2 mg/ml at higher magnification; (c) 41.6 mg/ml at lower magnification; (d) 41.6 mg/ml at higher magnification.

3.2.3 FTIR analysis

From the FTIR analysis of the scaffolds coated with the layer-by-layer technique, the characteristic absorption peaks of gelatin can be identified. Since gelatin is a protein, it is important to remember that amide bonds, which exist between various amino acids, present different absorption bands due to the various vibrational modes of the peptide bond.

From Figure 37, the characteristic peaks of the scaffolds related to the amide bands can be observed. In the range of 1580-1750 cm^{-1}, the Amide-I band is observed, corresponding to the stretching of the C=O group. In the range of 1490-1580 cm^{-1} the Amide-II band can be identified, related to the bending vibration of the N-H groups and the stretching of the C-N group. Between 1120 and 1270 cm^{-1}, the Amide-III band, also correlated to the in-plane vibrations of the C-N and N-H groups, is found. The main difference between the two bands lies in the fact that the Amide-II band is more influenced by

the N-H bond, while the Amide-III band is more related to the C-N vibrations. The peaks identifiable between 1270 and 1490 cm^{-1} can be attributed to the symmetric and asymmetric stretching of the methyl group.

Regarding tannic acid, the broad band present between 3100 and 3700 cm^{-1} is assigned to the stretching of the hydroxyl groups OH, widely present in TA's structure. The peaks observed at 2854 and 2921 cm^{-1} are linked to the symmetric and asymmetric stretching vibrations of the C-H bonds in CH_2 and CH_3 groups, respectively.

Comparing the FTIR analyses of scaffolds produced with varying gelatin concentrations in the layer-by-layer coating, an increase in the intensity of characteristic peaks is observed as the concentration rises. The amide bands are more pronounced at higher concentrations due to the greater number of molecules in solution, leading to the detection of more molecular vibrations.

The position of the characteristic bands remains nearly unchanged, as it depends on the nature of the chemical bonds rather than the concentration. These results confirm that the layer-by-layer coating process was successfully completed for all tested concentrations, demonstrating a proportional relationship between peak intensity and the chosen gelatin concentration.

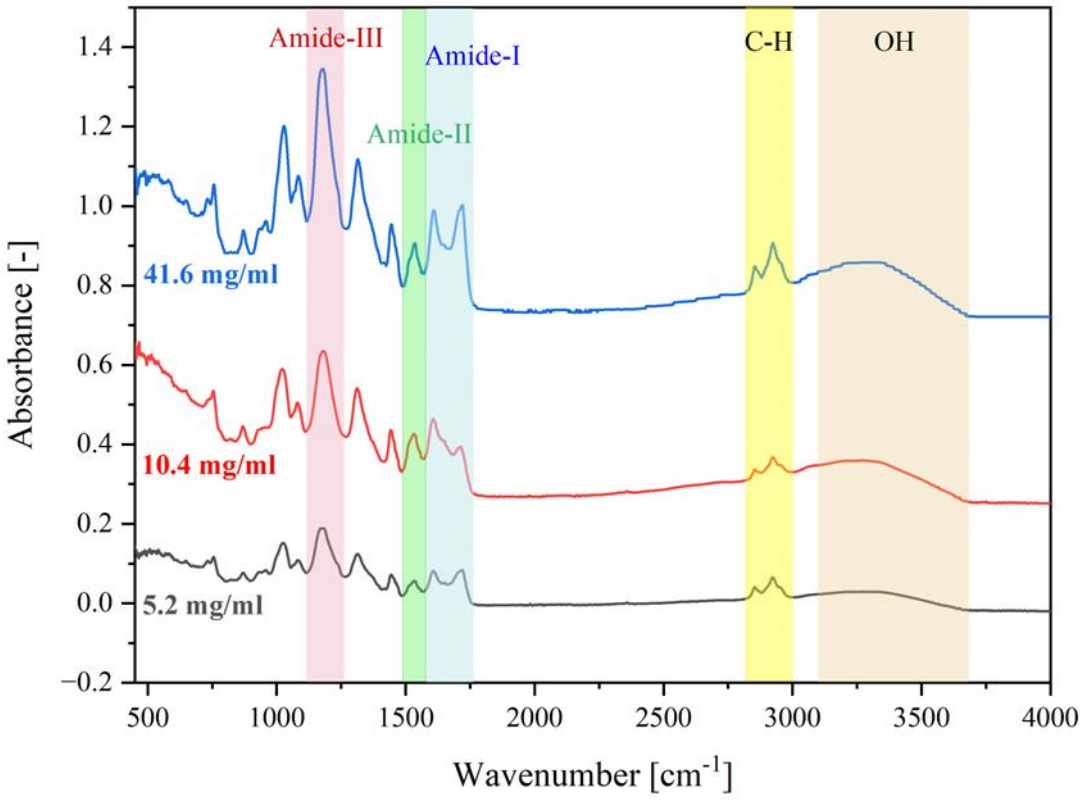

Figure 37. FTIR spectra for LbL-coated scaffolds with different concentrations of gelatin.

3.2.4 TGA analysis

Thermogravimetric analysis was conducted on the layer-by-layer (LbL) coated scaffolds to quantify the amount of single components effectively incorporated in the synthesized polymer matrix. To assess the specific quantities of each component in the coated scaffold, TGA was also performed on 5.2 mg/ml aqueous gelatin solutions, 0.125 g/ml tannic acid solutions, and the gelatin/tannic acid complex. The thermal parameters from these analyses are listed in Table 7, while the respective thermogravimetric curves are shown in Figure 38. For comparison, TGA results for the base PCL/PGS/quercetin scaffold are also provided.

Gelatin displays two primary thermal decomposition steps. The initial decomposition step begins at 31.5 °C and occurs up to approximately 213 °C with a weight loss of 12.5%, primarily due to water content in the solution. Specifically, surface water is removed up to 100 °C, while internal water within the structure is lost by the end of this first decomposition stage. Gelatin, being an hygroscopic material, have the tendency to absorb moisture from the air. The second decomposition step occurs within the 213-555 °C range, involving a 66.4% weight loss attributed to the breakdown of side and main protein chains.

Similarly, tannic acid exhibits two decomposition steps. The first, attributed to moisture loss due to numerous hydroxyl (OH) groups, takes place between 31 °C and 156 °C with an 8.8% weight loss. The second, that occurs between 178 °C and 389 °C, is attributed to its step-by-step decomposition, initiated by decarboxylation reaction. This step has shown a 56.7% weight loss, related to the degradation of phenolic rings.

The gelatin/tannic acid complex follows a similar pattern of the single components of TA and gelatin. It can be observed that in the Gel/TA sample the residual weight at 750 °C was higher than the free gelatin and tannic acid. This behavior is due to the hydrogen bonding between gelatin and tannic acid, which has reduced chain mobility and increased consequently thermal stability.

For the LbL-coated scaffold, the presence of gelatin is evident in the upper part of the thermogravimetric curve, mirroring the thermal behavior of the gelatin solution. A first decomposition step is observed between 165 °C and 327 °C, followed by the decomposition of the polymeric chains in a second step occurring between 327 °C and 508 °C with a 76.1% weight loss. By comparing the thermogravimetric curve of the uncoated scaffold with that of the coated scaffold and analyzing the data at approximately 500°C, where decomposition is complete for both samples, the weight loss attributed solely to the coating was determined to be 5.88%. Considering that the coated sample used

in the TGA measurement had a total mass of 9.431 mg, the calculated mass of the coating is 0.555 mg.

Table 7. TGA thermal parameters.

Sample		**T_{onset} [°C]**	**T_{offset} [°C]**	**Weight Loss in the range $T_{onset} < T < T_{offset}$ [%]**
Gelatin	First step	31.5	213.5	12.5
	Second step	213.5	554.9	66.4
Tannic acid	First step	31.5	156.3	8.8
	Second step	178.9	389.1	56.7
Gel/TA	First step	31.5	164.2	11.6
	Second step	164.2	502.8	58.9
PCL/PGS/querc	First step	30	65.4	0.39
	Second step	182.8	483.1	98.5
3 layers LbL 5.2 mg/ml gel	First step	165.6	327.2	14.6
	Second step	327.2	508.3	76.1

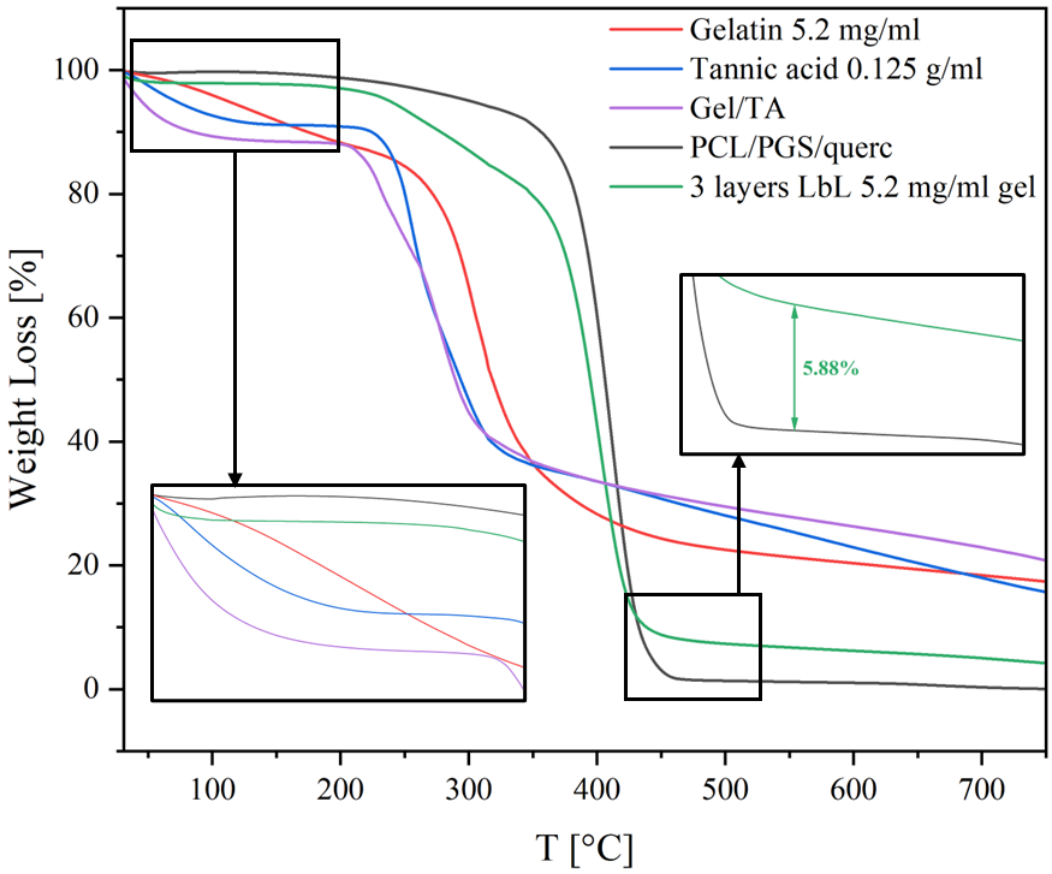

Figure 38. Weight loss curves for analyzed samples.

3.2.5 Contact angle

The contact angle test was performed to assess the surface wettability and hydrophilicity of the produced polymeric scaffolds, including PCL, PCL/PGS, PCL/PGS/Quercetin, and scaffolds coated using the Layer-by-Layer (LbL) technique with gelatin and tannic acid. These measurements provide insights into the modifications imparted by blending or coating processes and their impact on scaffold surface properties. The obtained results are shown in Figure 39.

The PCL scaffold exhibited an initial contact angle of 116.18°, which increased slightly to 118.52° after 30 seconds. This behavior highlights the hydrophobic nature of the PCL surface and the minimal change over time observed indicates limited water absorption and interaction.

The incorporation of PGS into the PCL matrix significantly reduced the initial contact angle to 95.38°, which further decreased to 34.65° within 3 seconds. This sharp decline suggests an increase in the scaffold's hydrophilicity, attributable to the polar functional groups introduced by PGS, enhancing scaffold's wettability.

The inclusion of quercetin within the PCL/PGS blend led to an initial contact angle of 99.21°, slightly higher than that of PCL/PGS but still considerably lower than pure PCL. The angle decreased to

44.98° after 5 seconds, suggesting a moderate water absorption rate. This behavior indicates a balanced effect, where the hydrophobic characteristics of quercetin are counteracted by the hydrophilic properties of PGS. Quercetin's integration maintains a favorable surface for cellular adhesion.

The LbL coated scaffold exhibited an initial contact angle of 85.76°, which decreased to 53.24° after 15 seconds. This outcome confirms the significant improvement in hydrophilicity imparted by the gelatin and tannic acid coating, improving surface wettability and scaffold's biocompatibility, as the coating may enhance cellular adhesion.

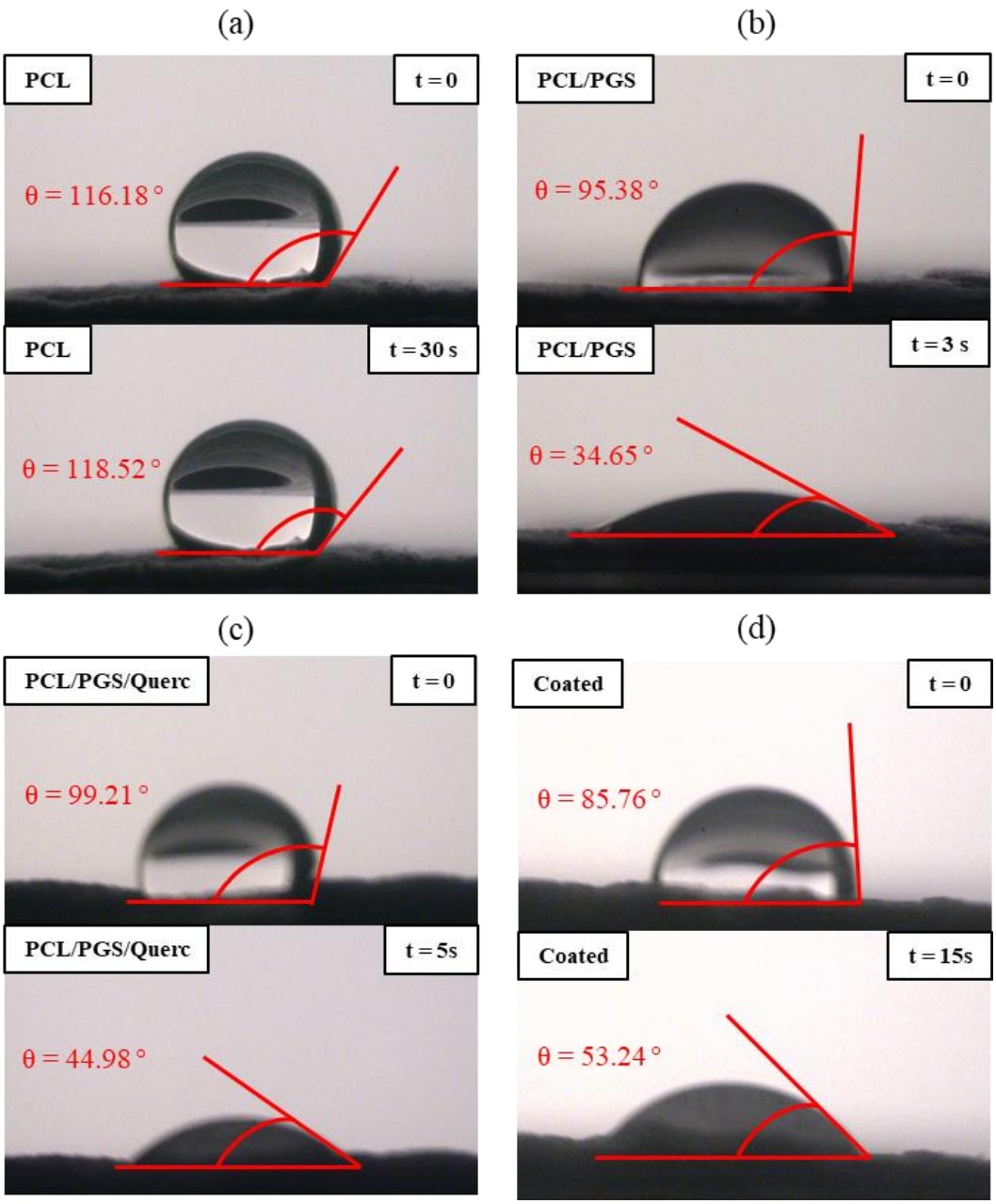

Figure 39. Hydrophilicity tests with contact angle performed on: (a) PCL; (b) PCL/PGS; (c) PCL/PGS/Querc; (d) Coated scaffold with layer-by-layer method.

3.2.6 Antioxidant activity of TA-coated prosthesis

The antioxidant activity of the prostheses coated with the gelatin and tannic acid layer-by-layer (LbL) coating method was assessed using both the DPPH and ABTS assays.

3.2.6.1 DPPH assay

In this protocol, DPPH reagent served as a source of radicals for the analysis. Antioxidant substances are capable of transferring a hydrogen atom to the radical compound, resulting in a decolorization of the solution.

Tannic acid is known for its strong antioxidant activity, a characteristic further investigated and confirmed in this thesis. A series of aqueous tannic acid solutions at varying concentrations were prepared and analyzed using the DPPH protocol. The findings, presented below, showcase both the gradual discoloration of the solutions and the corresponding UV spectroscopy results. As shown in Figure 40(a), an increase in tannic acid concentration results in progressively more transparent samples, with a loss of color intensity. This trend is corroborated in Figure 40(b), where the UV spectra display a decrease in the characteristic absorbance peak at 517 nm as the tannic acid concentration increases.

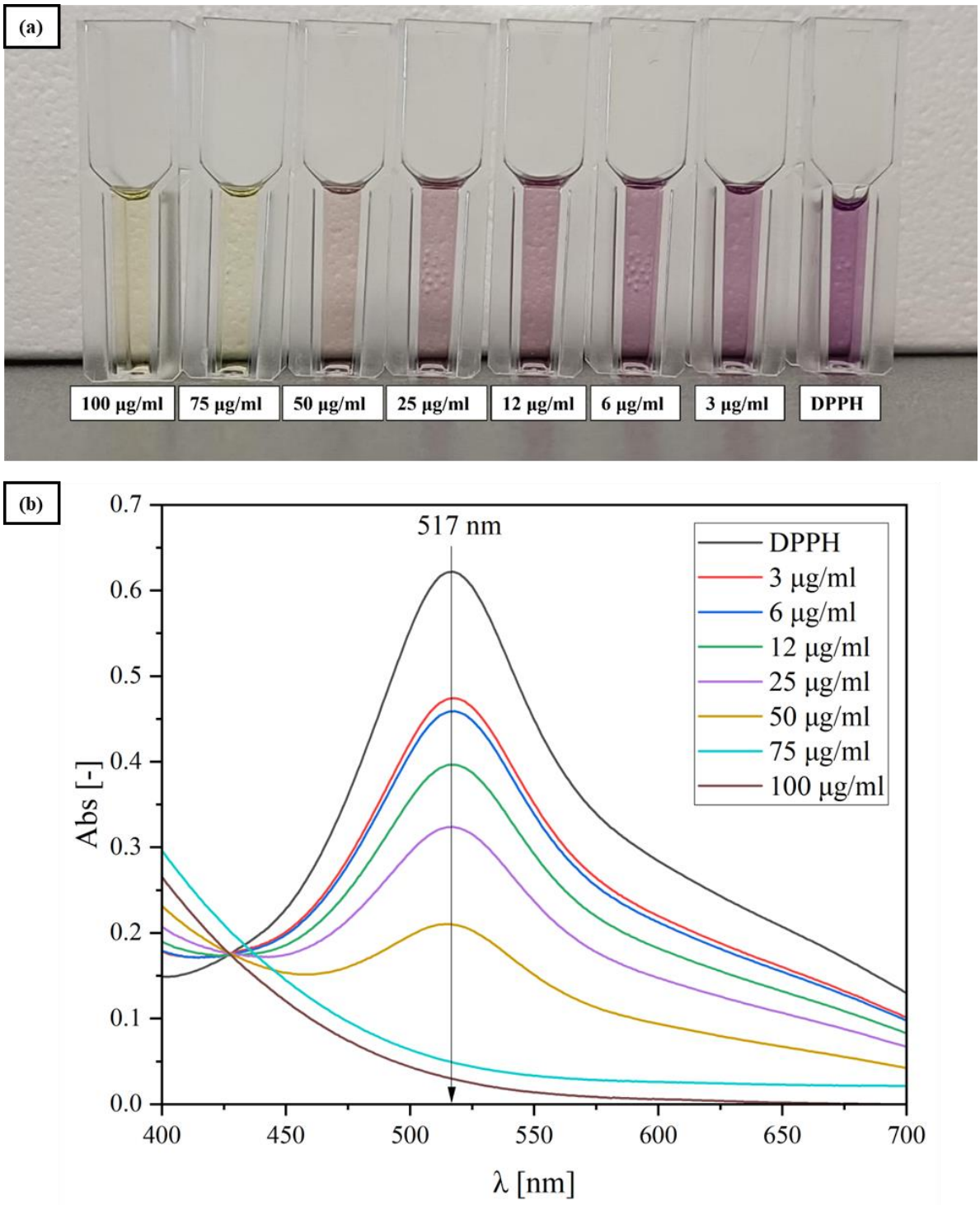

Figure 40. (a) Color change in DPPH solution depending on the concentration of TA's solutions; (b) UV/vis spectra of TA's solutions in DPPH assay.

After confirming the antioxidant properties of tannic acid, the absorbance of the analyzed material samples was measured at 517 nm. For each sample, the antioxidant activity was calculated using equation (7) provided in Chapter 3.1.8.1. The PCL/PGS control scaffold shows minimal antioxidant activity, reaching a value of about 1.4%. The aqueous gelatin solution, at a

concentration of 5.2 mg/ml, demonstrates moderate antioxidant activity, approximately 46%. The PCL/PGS scaffold containing quercetin displays a high antioxidant capacity of around 89.5%, directly attributed to the presence of the polyphenolic compound within the prosthesis. Tannic acid in water (0.125 g/ml) and quercetin in ethanol (5.5 mg/ml) solutions exhibit even greater antioxidant activity, with values of 94.6% and 95.2%, respectively. The scaffold coated using the layer-by-layer technique achieves the highest AA%, at 96.6%, thanks to the combined presence of quercetin and tannic acid in the structure. The data are expressed as the mean ± standard deviation of the triplicate analyses, as displayed in the histogram in Figure 41.

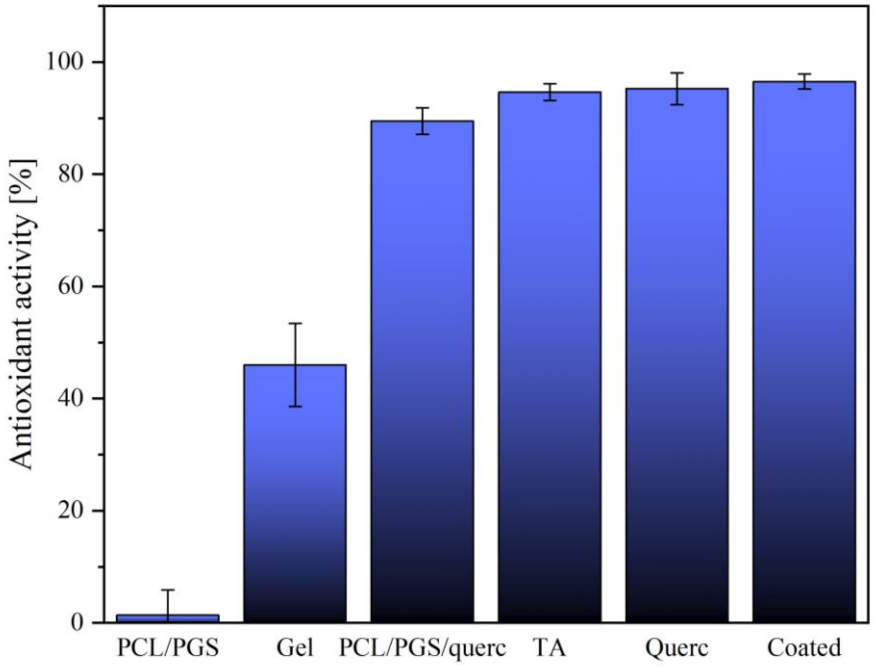

Figure 41. Results in terms of AA% from the DPPH protocol.

The results obtained in terms of AA% were validated by the degree of discoloration in samples with higher antioxidant properties, along with the corresponding decrease in the characteristic absorbance peak at 517 nm. As shown in Figure 42(a), the PCL/PGS sample maintained a purple hue similar to the pure DPPH solution, while the gelatin exhibited slight discoloration. In contrast, all other samples showed nearly complete discoloration. Figure 42(b) presents the UV spectra of the analyzed samples. Pure ethanol, which displayed no absorbance, was included in the analysis to confirm that the solvent used did not influence the measurements.

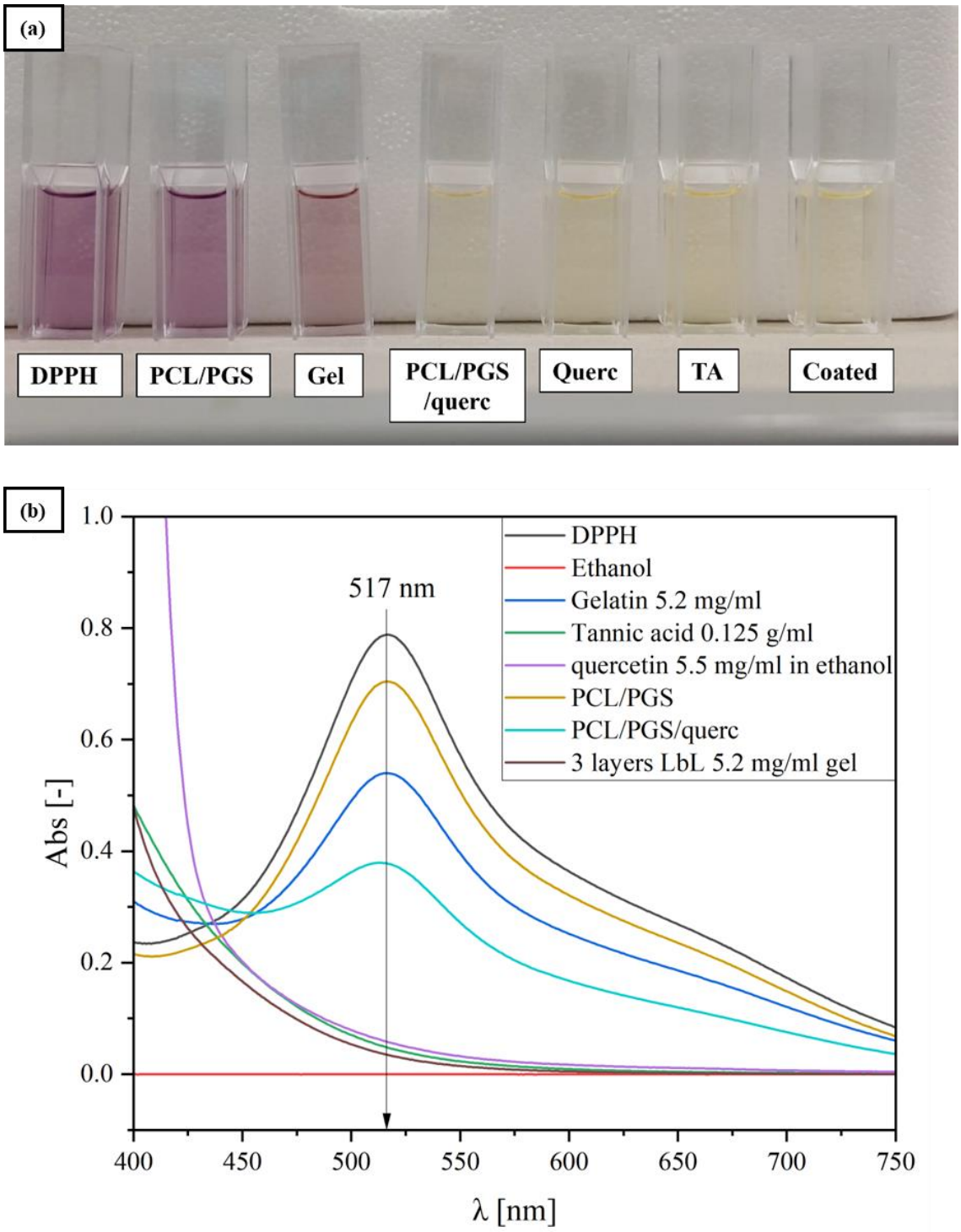

Figure 42. (a) Color change in DPPH solution depending on sample analyzed; (b) UV/vis spectra of samples analyzed in DPPH assay.

3.2.6.2 ABTS assay

To further investigate the antioxidant capacity of the produced prostheses, their scavenging activity against the ABTS* radical cation, 2,2'-azino-bis (3-ethylbenzothiazoline-6-sulfonic acid),

was assessed. This protocol relies on detecting the reduction of the ABTS* radical through spectrophotometric analysis in the presence of antioxidant molecules.

The absorbance at 734 nm was measured for each sample under investigation. For all samples under examination, the radical scavenging activity (RSA) was calculated using equation (8) provided in Chapter 3.1.8.2. Overall, the ABTS radical scavenging activity of the samples showed similarities to the DPPH protocol results. The PCL/PGS control scaffold exhibited low antioxidant activity, with an RSA value of 9.7%. In the case of the scaffold with quercetin, antioxidant properties improved slightly, with an RSA value of 19%, which can be attributed to the presence of quercetin. Samples containing aqueous solutions of gelatin and tannic acid, with concentrations of 5.2 mg/ml and 0.125 g/ml respectively, demonstrated high radical scavenging activity, showing values of approximately 97.3% and 99.7%. The scaffold coated using the layer-by-layer technique achieved nearly complete radical scavenging activity, around 99.4%, due to the synergistic action of gelatin and tannic acid. Data are presented as the mean value ± standard deviation based on triplicate measurements, shown in the histogram in Figure 43.

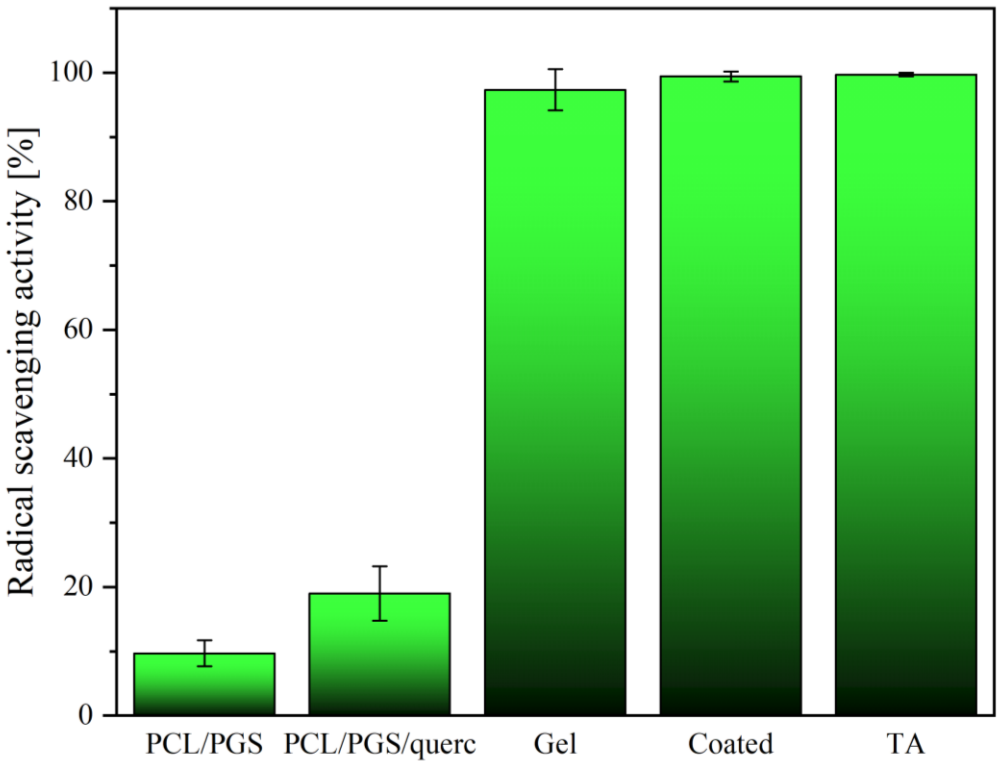

Figure 43. Results in terms of RSA% from the ABTS protocol.

The discoloration of the ABTS solutions containing the samples, along with the corresponding UV spectra, confirmed the results in terms of RSA%. The color change of the ABTS solution

corresponds to the varying antioxidant activity of each material. The more the solution becomes decolorized, the greater the antioxidant capacity of the sample, indicating that the ABTS* radical has been largely reduced.

In Figure 44(a), it can be observed that the PCL/PGS sample maintains a color similar to the pure ABTS solution, while the scaffold with quercetin shows a slight discoloration. All other samples, which achieved near-maximum RSA% values, displayed complete discoloration. This trend is similarly reflected in Figure 44(b), which shows the UV spectra of the various samples. A decrease in the characteristic absorbance peak at 734 nm is observed as the radical scavenging activity of the sample increases. Deionized water, which shows no absorbance spectrum, was also included in this analysis to demonstrate that the solvent used does not influence the test results.

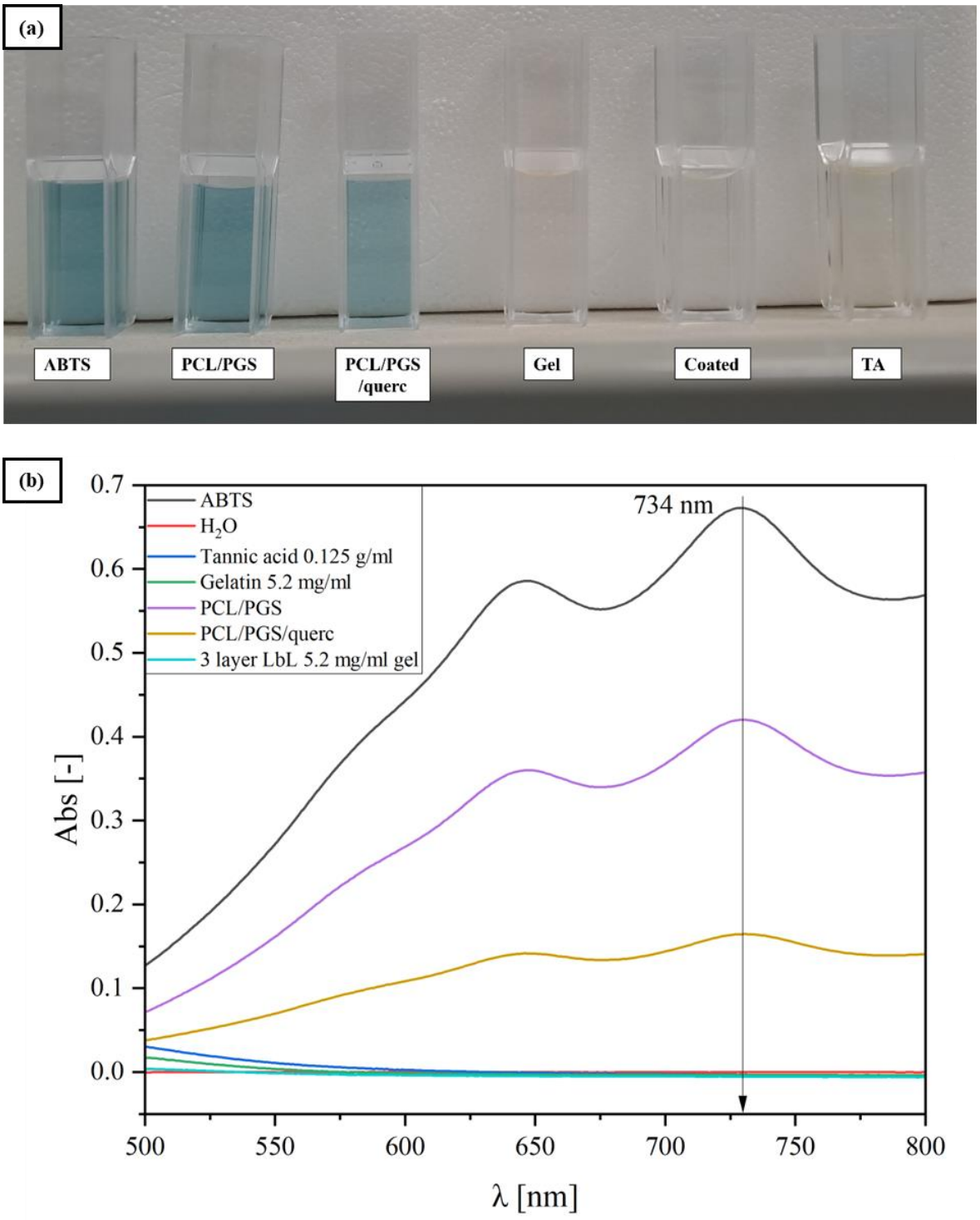

Figure 44. (a) Color change in ABTS solution depending on sample analyzed; (b) UV/vis spectra of samples analyzed in ABTS assay.

3.2.7 Static release test

The absorption spectrum of tannic acid in PBS is shown in Figure 45. The tannic acid samples in PBS were diluted until a smooth absorption curve was achieved, free of noise and with absorbance values

close to or less than 1. A smooth spectrum was obtained at a concentration of 0.01 mg/ml of TA in PBS.

The UV/vis spectrum of TA presents two maximum absorption bands at 212 and 279 nm. The 10 galloyl residues of TA structure act as a strong UV absorbing chromophore and show intense absorption bands in the range 190-230 nm, so the peak at 212 nm is assigned for π→π* transitions given by aromatic units and C=O groups. The transitions associated with aromatic groups can extend to longer wavelengths, in the range of around 260-280 nm, where n-π* transitions occur, originating from groups with non-bonding electron pairs. The peak observed at 279 nm can therefore be attributed to these n-π* transitions, caused by the non-bonding electrons of the oxygen atoms present in the hydroxyl (-OH) groups attached to the aromatic rings of the tannic acid structure [92].

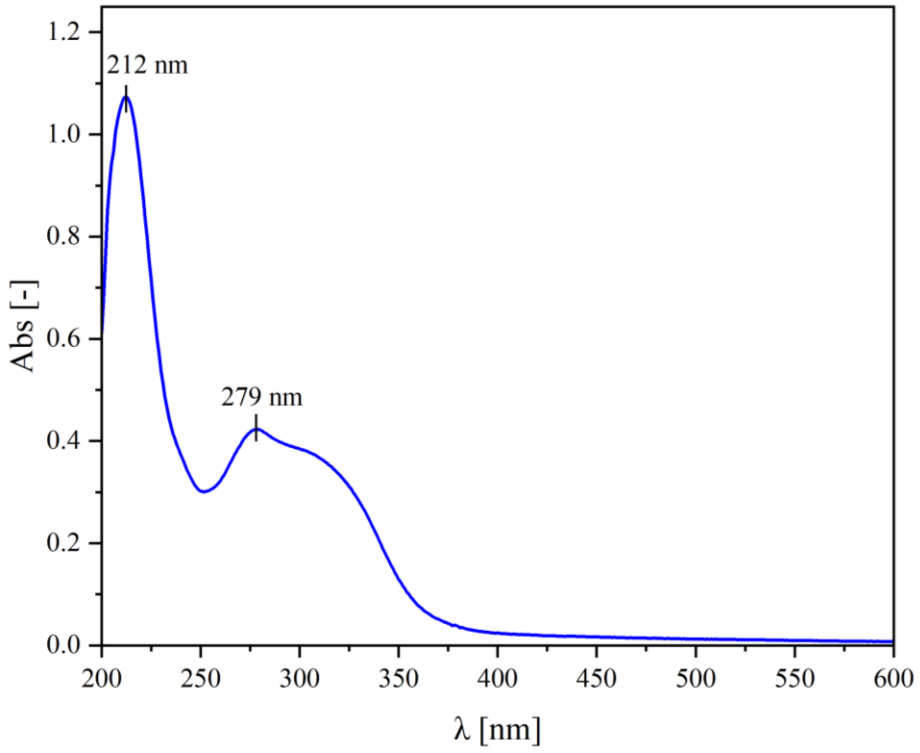

Figure 45. UV-vis spectrum of tannic acid (0.01 mg/ml) in PBS.

The static release study was conducted at the main peak of 212 nm of TA in PBS.

Figure 46(a) shows the cumulative release profile of TA, quercetin and gelatin from coated LbL prosthesis with a gelatin concentration of 5.2 mg/ml. Release tests were conducted in triplicate, and the average values obtained are reported along with the corresponding standard deviation. Concentration in the release media was determined using the calibration curve generated using known concentrations of TA in PBS (shown in Figure 46(b)) and performing regression analysis based on the corresponding absorbance readings at 212 nm.

The obtained static release profile does not show a burst release behavior. The release is sustained during the first 8 hours of the analysis, then reaches a plateau after 24 hours. The percentage of components released after 24 hours corresponds to 5.47% of the initial mass of the coated scaffold. Specifically, starting with a coated scaffold weighing 44.066 mg, a total of 2.412 $mg_{TA\ equivalent}$ was released, given by the cumulative contribution of tannic acid, gelatin, and quercetin.

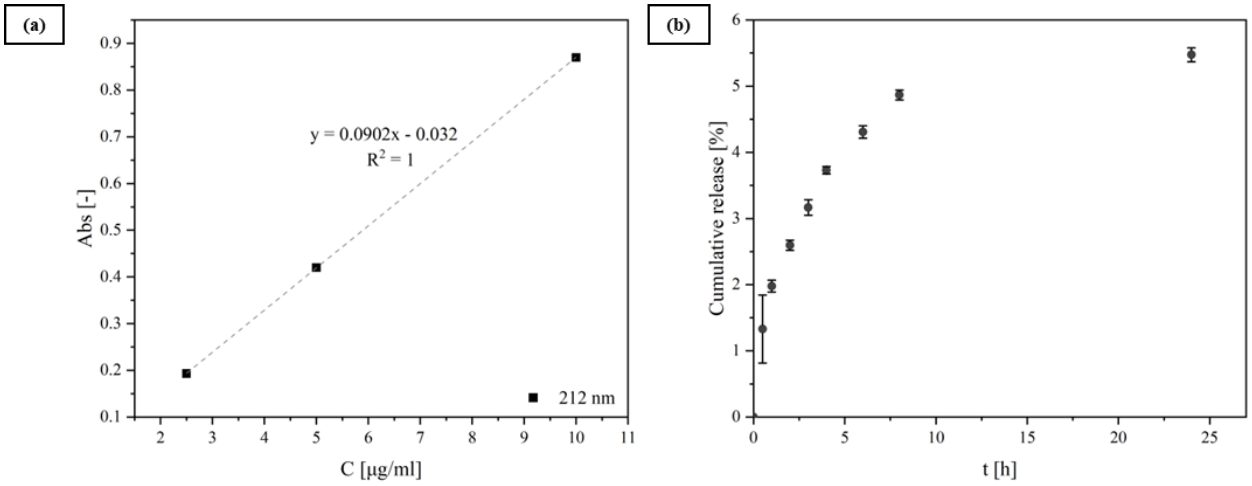

Figure 46. (a) Standard curve of TA in PBS at 212 nm; (b) Cumulative release in PBS at 212 nm.

The results of the mathematical modeling of static release profile are shown in Figure 47. Among the various kinetic models tested, the best fit, i.e., the one with the R^2 value closest to 1, was obtained using the Makoid-Banakar model. However, the parameters of this model are entirely empirical and not based on fundamental principles or real kinetic laws that could help us understand the actual release mechanism followed by tannic acid, gelatin and quercetin. It can be observed that the parameter c of the Makoid-Banakar model approaches zero; consequently, considering it negligible, the model simplifies to the Peppas equation. This latter model has provided a satisfactory fit of the release, with an R^2 value of 0.944. Furthermore, it should be emphasized that the Peppas model is applicable in our specific case, as the ratio of length to thickness of the scaffolds is greater than 10. The value of n equal to 0.307 for a cylindrical geometry suggests a predominantly diffusion-controlled release mechanism, in accordance with Fick's law.

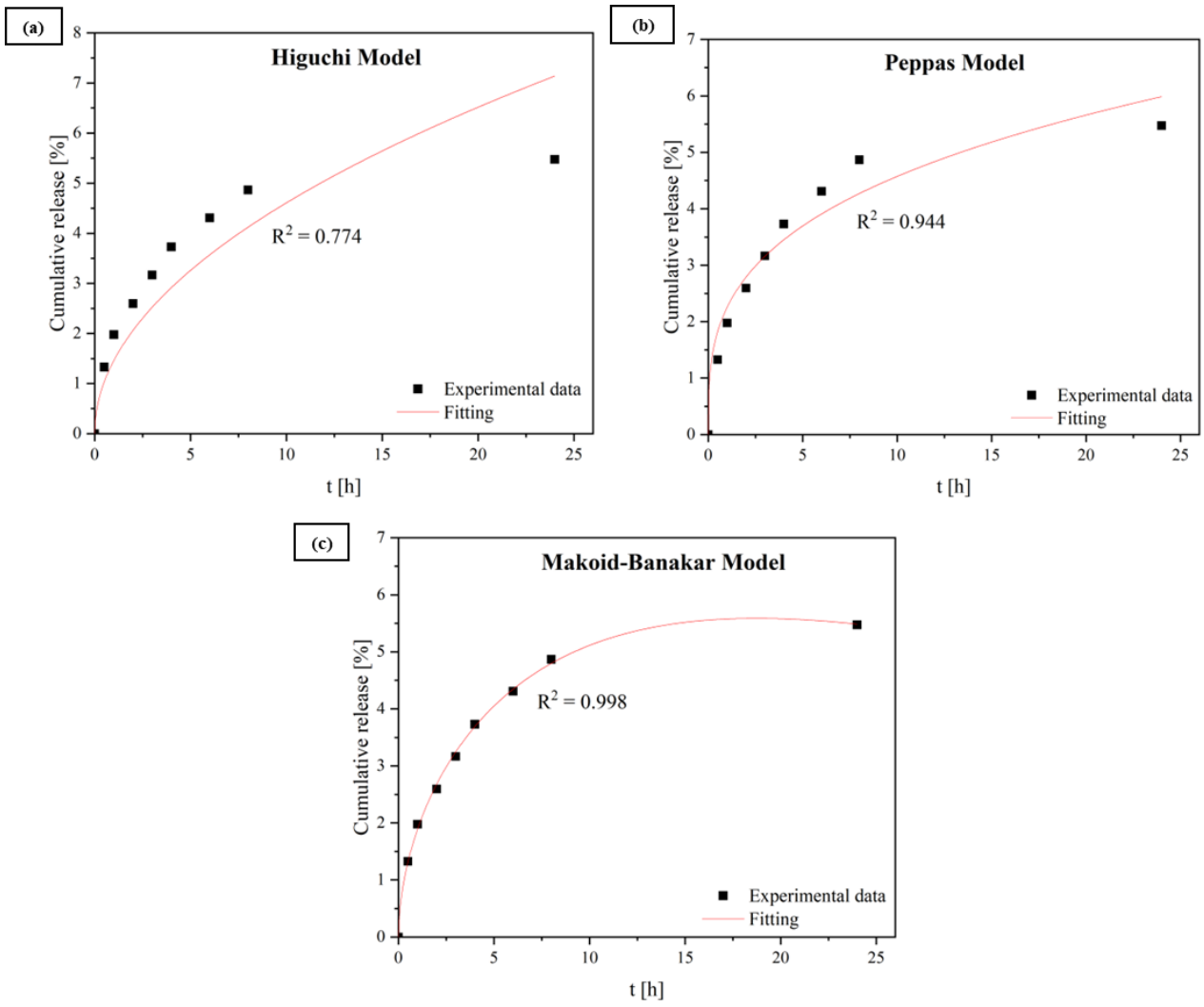

Figure 47. Fitting of static release profile at 212 nm with: (a) Higuchi model; (b) Peppas model; (c) Makoid-Banakar model.

Table 8. Kinetic parameters of the mathematical models tested for the fitting of static release.

Mathematical model	**Characteristic parameters**		**R^2**
Higuchi	k_H $[h]^{-0.5}$	1.457	0.774
Peppas	k_P $[h]^{-n}$	2.253	0.944
	n [-]	0.307	
Makoid-Banakar	k_{MB} $[h]^{-n}$	1.941	0.998
	n [-]	0.547	
	c $[h]^{-1}$	0.029	

3.2.8 Dynamic release in bioreactor

Figure 48 presents the cumulative release profile over a 24-hour duration obtained under dynamic conditions, using the same sampling times as in the static case. The profile exhibits a sustained release during the first 8 hours of analysis, stabilizing to a plateau after 24 hours. The percentage of components released at the end of the 24-hour period is 6.47% relative to the initial mass of the coated scaffold, slightly higher than the value observed under static conditions. Specifically, starting with a coated scaffold weighing 237.5 mg, a total of 15.32 $mg_{TA\ equivalent}$ was released over the 24-hour period analyzed.

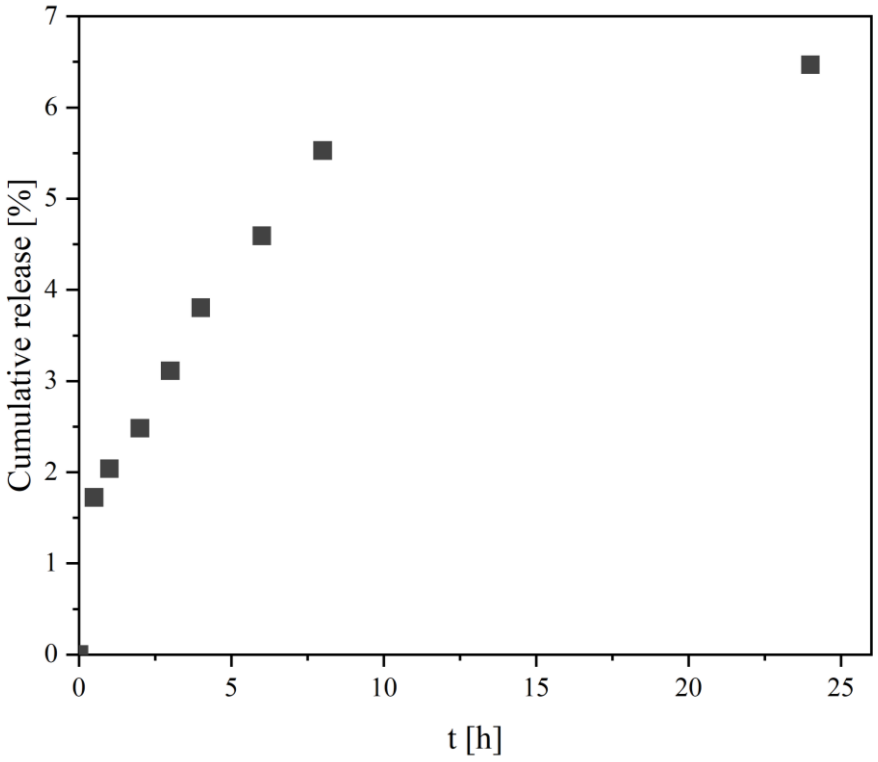

Figure 48. Cumulative 24-hour release curve under dynamic conditions in bioreactor using an LbL coated scaffold with a gelatin concentration of 5.2 mg/ml.

To determine if the differences between the static and dynamic cases at the same sampling times are statistically significant, an appropriate statistical test was conducted (ANOVA, Tukey's post-hoc test). Static and dynamic analyses revealed different quantities of bioactive molecules released. Statistical analysis showed that the amount of bioactive substances released in the bioreactor study was greater

than that obtained for the same times in static conditions ($p < 0.005$). This increase in released bioactive components is due to the flow to which the prosthesis is subjected in the bioreactor.

The cumulative release profile over a total duration of 15 days is shown in Figure 49. Apparently, the obtained profile seems to exhibit burst release behavior, but this is due to the lack of focus on the very first hours of release, as the first sampling was done after 12 hours. The percentage of components released after 15 days is 12.85% relative to the initial mass of the coated scaffold. Considering that the initial mass of the coated prosthesis was 251.11 mg, a total of 32.27 $mg_{TA\ equivalent}$ was released over the analyzed period.

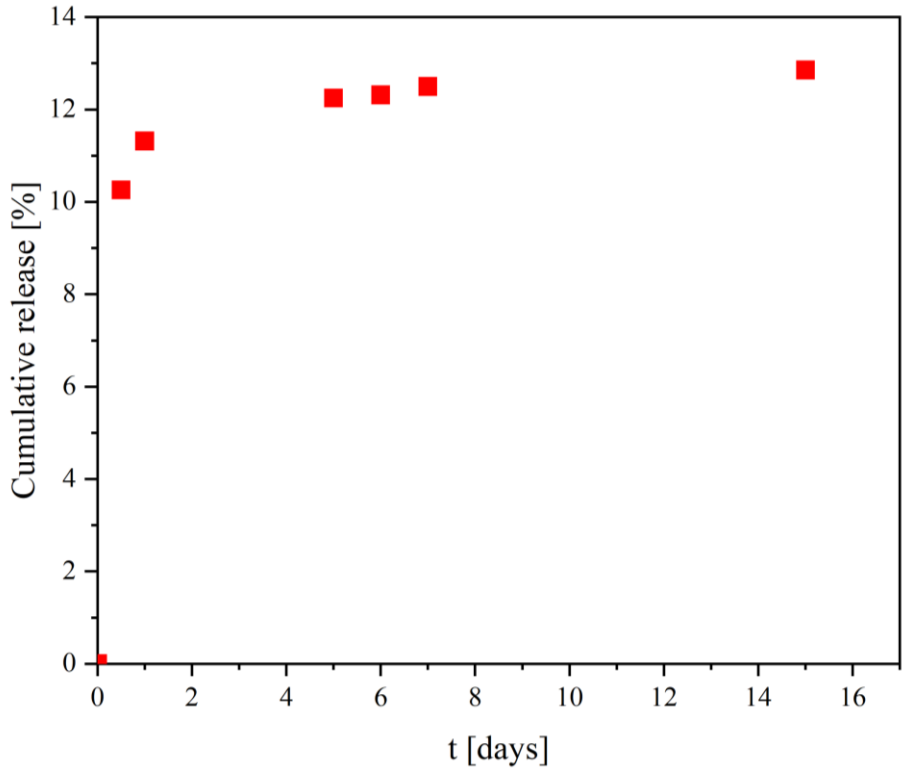

Figure 49. Cumulative 15-days release curve under dynamic conditions in bioreactor using an LbL coated scaffold with a gelatin concentration of 5.2 mg/ml.

The dynamic release samples over 15 days were also analyzed using the ferric chloride protocol, which resulted in the cumulative release curve shown in Figure 50(b). It can be observed that the released percentages are three times higher compared to the measurements obtained through spectrophotometric reading. A probable explanation for this behavior may lie in the fact that part of the polymer component of the scaffold partially degrades, interfering with the assay. Therefore, the measurement is falsed by the overlap of the biologically active components (tannic acid and quercetin) with the degraded polymer material, although gelatin is not detected with this protocol.

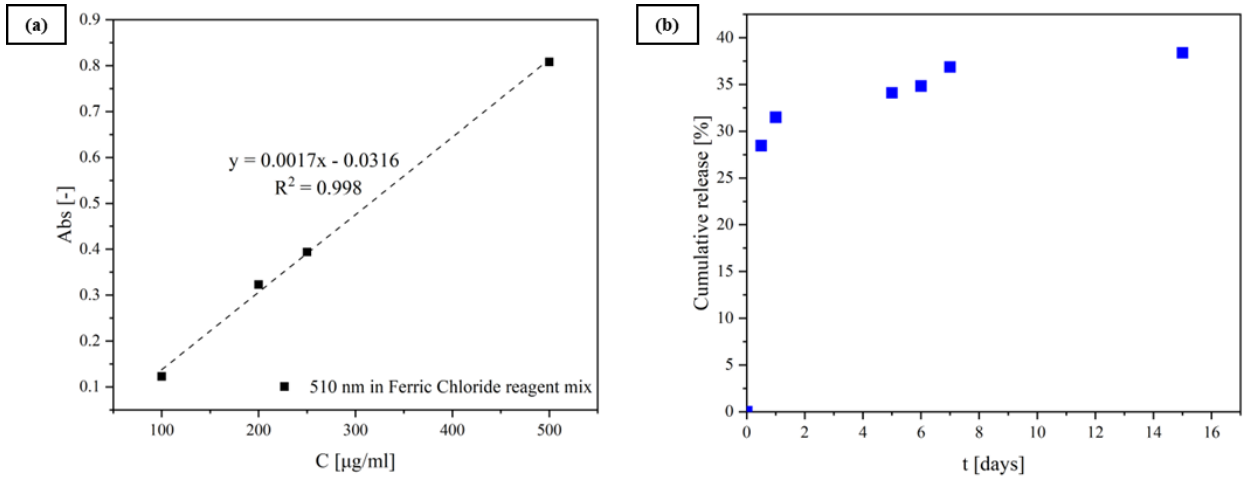

Figure 50. (a) Standard curve of TA in Ferric Chloride protocol reagent mix; (b) Cumulative 15-days release curve under dynamic conditions in bioreactor.

To get a clearer overview of the various protocols tested for the analysis of release samples, refer to Table 9 below. Although the Ferric Chloride protocol is suitable for detecting polyphenols as widely demonstrated in literature, in our specific case, the assay is not adequate as it is likely influenced by the degradation of the polymeric scaffold.

Table 9. Schematic representation of the various protocols tested to individually detect the components present in the release media.

	COMPONENTS		
	Gelatin solution with C=5.2 mg/ml	**Tannic acid solution with C=0.125 g/ml**	**Quercetin solution in ethanol with C=5.5 mg/ml**
UV Spectroscopic reading at 212 nm	Positive	Positive	Partially positive
Folin Ciocalteu	Positive	Positive	Positive
Ferric Chloride	Negative	Positive	Partially positive
BCA	Positive	Positive	Negative

4 Bioengineering of scaffolds for diagnostics

In the field of cardiovascular medicine, the development of vascular grafts has seen significant advancements, particularly with the incorporation of nanotechnology to enhance both diagnostic and therapeutic outcomes. Although progress has been made in improving the biocompatibility and mechanical performance of these biomaterial-based grafts, their clinical translation remains slow due to the extensive validation required. For any new vascular graft to be approved for clinical use, it must demonstrate efficacy and safety through rigorous *in vitro* and *in vivo* testing, followed by clinical trials.

Nanoparticles (NPs), particularly iron oxide nanoparticles (IONPs), have emerged as a promising tool in this context. Their unique properties make them ideal candidates for use in multifunctional molecular imaging techniques, such as magnetic resonance imaging (MRI), as well as for applications in drug delivery and tissue engineering. The magnetic properties of IONPs allow them to serve not only as contrast agents in MRI but also as carriers for targeted drug delivery, either by attaching bioactive molecules or by responding to external magnetic fields. For example, in a study conducted in 2012 ([93]), iron oxide nanoparticles were successfully incorporated into electrospun polystyrene fibers with the ultimate goal of developing an innovative mediator for magnetic hyperthermia as an anti-tumor therapy. In the study, the magnetic fibers exhibited excellent heating capacity when exposed to alternating magnetic fields. Furthermore, the magnetic field-induced hyperthermia proved to be much more efficient and faster than heating in a hot water bath in killing cancer cells.

Additionally, the inclusion of IONPs within the polymeric scaffold offers more than just imaging benefits. These nanoparticles have been shown to support regenerative processes by directing stem cells to specific sites within the body. When incorporated into tissue-engineered vascular grafts (TEVGs), IONPs can not only help to visualize the graft's location but also enhance tissue regeneration by magnetically guiding therapeutic cells to the injury site. This dual functionality, combining regenerative support with non-invasive monitoring, significantly boosts the clinical potential of these advanced prostheses [94].

In this thesis work, vascular prostheses embedded with iron oxide nanoparticles were developed, following the confirmation of the biocompatibility of the bare polymeric scaffold, which had not undergone any prior engineering modifications. This preliminary validation ensured that the base material was safe and compatible with biological tissues. After this step, IONPs were integrated into the scaffold to enable the precise localization of the prostheses post-implantation using MRI. In fact, IONPs can serve as T2 contrast agents because they have the ability to create hypointense areas in

MRI images. This capability offers a valuable tool for clinicians, as it allows for real-time visualization of the prosthesis within the vascular system and continuous monitoring of its functionality. Furthermore, tracking the position of IONP-labeled grafts helps in the early detection of potential issues such as graft migration or failure, thereby supporting prompt medical interventions when necessary.

4.1 Materials and methods

4.1.1 Production of Iron Oxide Nanoparticles

The Iron Oxide Nanoparticles were prepared using co-precipitation technique, following the method reported in Maboudi et al., 2017 [77]. Initially a solution of $FeCl_3 \cdot 6H_20$ (540 mg) and $FeSO_4 \cdot 7H_2O$ (278.05 mg) was prepared by dissolving these salts in 60 ml of deionized water. The dissolution of the salts was facilitated by using an ultrasonic bath (FALC, Treviglio) for 1 minute and stirring on a magnetic plate at 1500 rpm under a nitrogen gas atmosphere. Subsequently, 0.1 ml of oleic acid and 7.5 ml of ammonia were added to the stirring solution under chemical wood, and the temperature was raised to approximately 100 °C for about 25 minutes. Additional oleic acid with a volume of 0.1 ml was introduced into the solution every 5 minutes, repeating this process four times. The same stirring and temperature conditions, 1500 rpm and 100 °C respectively, were then maintained for 30 minutes, after which the temperature was lowered to 25 °C for 5 minutes. To separate the produced nanoparticles, three centrifugations (Centrifuge MF 20-R, Alliance Bio Expertise, Guipry) were performed at 10000 rpm for 10 minutes each. After each centrifugation, the supernatant was removed, and the pellet was rinsed with deionized water before the next centrifugation. Finally, to remove all residual aqueous components from the supernatant after the last centrifugation, the samples were placed in an oven (ISCO laboratory thermostatic oven) and weighed at the end of the drying process.

4.1.2 Preparation of polymeric solution with NPs and electrospinning process

For the preparation of scaffolds with magnetic nanoparticles, the goal is to achieve a final polymer mix of PCL:PGS in a 1:1 ratio at a concentration of 20% w/v, using a solvent mixture of chloroform and ethanol (with quercetin in ethanol at a concentration of 5.5 mg/ml) in a 9:1 ratio. To achieve this, it is essential to consider that the nanoparticles must be dissolved in chloroform, and this volume must be accounted for in the final polymer solution.

First of all, iron oxide nanoparticles were dissolved in chloroform to reach a concentration of 0.0616 g/ml for subsequent incorporation into cardiovascular prostheses. Consequently, knowing that 1 ml

of the chloroform solution containing NPs will be added, the PCL and PGS solutions were dissolved in the chloroform/ethanol solvent mixture using a volume of chloroform suitable for achieving the final desired 9:1 ratio.

The chloroform solution containing the magnetic nanoparticles was ultrasonicated to ensure complete dissolution. Afterward, 1 ml of this solution was incorporated into the polymer mixture and placed on a stirrer at high speed. Prior to the electrospinning process, the nanoparticle-infused polymer solution underwent a further 10 minutes of ultrasonication. Following this, the same electrospinning process described in Chapter 2.1.2 was carried out.

All operational conditions used for the production of scaffolds with incorporated magnetic nanoparticles are summarized in Table 10 below for clarity.

Table 10. Parameters adopted for the production of NPs-loaded scaffolds through electrospinning.

	Parameters	**Set-up values**
Before Electrospinning	Ultrasonication [min]	10
Electrospinning	Volume to be electrospun [ml]	2
	Flow rate [ml/h]	1.1
	Voltage applied to the electrodes [kV]	17
	Rotation speed of the collector [rpm]	500
	Translation speed of the collector [mm/min]	600
	Vertical distance needle-collector [cm]	18

4.1.3 Characterization of NPs-loaded scaffolds

To thoroughly evaluate the morphology and chemical composition of the vascular scaffolds embedded with iron oxide magnetic nanoparticles Scanning Electron Microscopy (SEM) and Fourier-transform Infrared Spectroscopy (FTIR) were conducted. The goal of these analyses was to confirm the incorporation of the nanoparticles within the polymer matrix, as well as to assess the structural and chemical integrity of the scaffold.

SEM analysis was employed to examine the surface morphology of the NPs-loaded scaffolds, in order to obtain detailed information on fiber arrangement. Furthermore, using ImageJ software, size distribution curves were generated from the SEM images to analyze fiber diameters quantitatively. A minimum of 100 fibers were measured for each sample to ensure statistically significant results. These distribution curves allow for a detailed comparison between the scaffolds with and without nanoparticles, revealing any morphological changes resulting from the incorporation of the nanoparticles.

FTIR spectroscopy was used to investigate the chemical composition of the NPs-loaded scaffolds, particularly focusing on characteristic functional groups associated with the scaffold materials and the iron oxide nanoparticles. This method has allowed us to detect any chemical modifications within the polymer matrix due to the presence of iron oxide nanoparticles, providing insights into the scaffold's compatibility with the incorporated nanoparticles. By comparing the FTIR spectra of pure polymer scaffolds with the NPs-loaded versions, the influence of the nanoparticles on the scaffold's chemical structure was assessed, ensuring that the embedding process did not compromise the integrity of the polymer components.

4.1.4 Magnetic Resonance Imaging (MRI)

Although the PCL/PGS/querc scaffold demonstrates excellent biocompatibility, its inability to be detected through non-invasive imaging renders it an untraceable element when utilized as a vascular prosthesis scaffold. To overcome this problem, scaffolds fibers have been labeled with iron oxide nanoparticles, with the aim to permit prosthesis visualization with MRI.

Iron oxide nanoparticles possess superparamagnetic properties that make them suitable for use as T2 contrast agents in magnetic resonance imaging (MRI). T2-weight images are based on the T2 relaxation time, which measures how quickly protons excited by the magnetic field lose the energy they previously acquired. T2 contrast agents can alter the magnetic environment surrounding the protons, causing an acceleration of energy loss. This results in a decrease in the T2 relaxation time, leading to sharper and clearer contrast in the resulting images. In the case of iron oxide nanoparticles, they produce a local magnetic field in the presence of an external magnetic field (thanks to their high magnetic moment), which disrupts the behavior of the surrounding protons.

In this thesis work, MRI was utilized to evaluate the functionality of iron oxide nanoparticles incorporated into the vascular scaffolds as T2 contrast agents.

The goal of this analysis was to evaluate the localization and distribution of the prostheses and to confirm the successful incorporation of IONPs into the scaffold structure.

The protheses, containing IONPs synthesized as described in Chapter 4.1.2, were scanned using a high-resolution MRI system. Imaging was performed using T2-weighted sequences to exploit the superparamagnetic properties of the IONPs, which generate local magnetic field inhomogeneities, resulting in hypointense (dark) regions on the images.
The measurements were conducted using a Bruker BioSpec 70/20 USR 7T MRI scanner (Bruker BioSpin GmbH, Germany). The system was equipped with a ^{1}H transmit-receive volume coil with active detuning with an inner diameter of 82 mm and a bore length of 112 mm. For comparison, a PCL/PGS/quercetin scaffold without incorporated NPs was also analyzed.

4.2 Results and discussion

In order to visualize the electrospun prosthesis in the Magnetic Resonance Imaging (MRI), Iron Oxide nanoparticles were added as a contrast agent, enabling the precise identification of the scaffold's correct positioning after implantation.
The production phase for the iron oxide nanoparticles resulted in a final mass of 0.308 g. To achieve the desired concentration of 0.0616 g/ml, the nanoparticles were dissolved in 5 ml of chloroform. Despite the addition of magnetic nanoparticles, the electrospinning process proceeded smoothly without complications. The scaffolds were successfully produced and are distinguished by a dark coloration due to the presence of the nanoparticles, as shown in Figure 51 where they have been compared with the conventional scaffold.

Figure 51. Visual differences of scaffolds: (a) PCL/PGS/querc; (b) Iron-Oxide loaded scaffold.

4.2.1 Morphological analysis

The morphological characterization of the scaffolds aims to verify any structural changes in the fibers caused by the presence of magnetic nanoparticles. SEM images of the produced samples were

collected, while to analyze the dimensional distribution of the fibers, ImageJ software was employed to measure fiber diameters, with a minimum of 100 fibers sampled to ensure reliable statistical data. In order to make a comparison with the starting scaffold, Figure 52(a) shows the SEM image and the size distribution curve of the PCL/PGS scaffold with quercetin.

As seen in Figure 52(b), the incorporation of magnetic nanoparticles into the scaffold did not result in any structural changes to the fibers, which still show a random arrangement and orientation, similar to the pure scaffold. However, from the analysis of the size distribution curve, it can be observed that the average fiber diameters are larger, with a value around 5.4 μm (see Table 11 for reference). This increase can be attributed to the fact that the nanoparticles are dispersed within the polymer solution rather than fully dissolved, as is the case with quercetin. Furthermore, SEM analysis of the scaffolds with incorporated NPs reveals smooth fibers, confirming the nanoscale dimensions of the produced particles. If the particles had been micrometer-sized, the fibers would have appeared rougher.

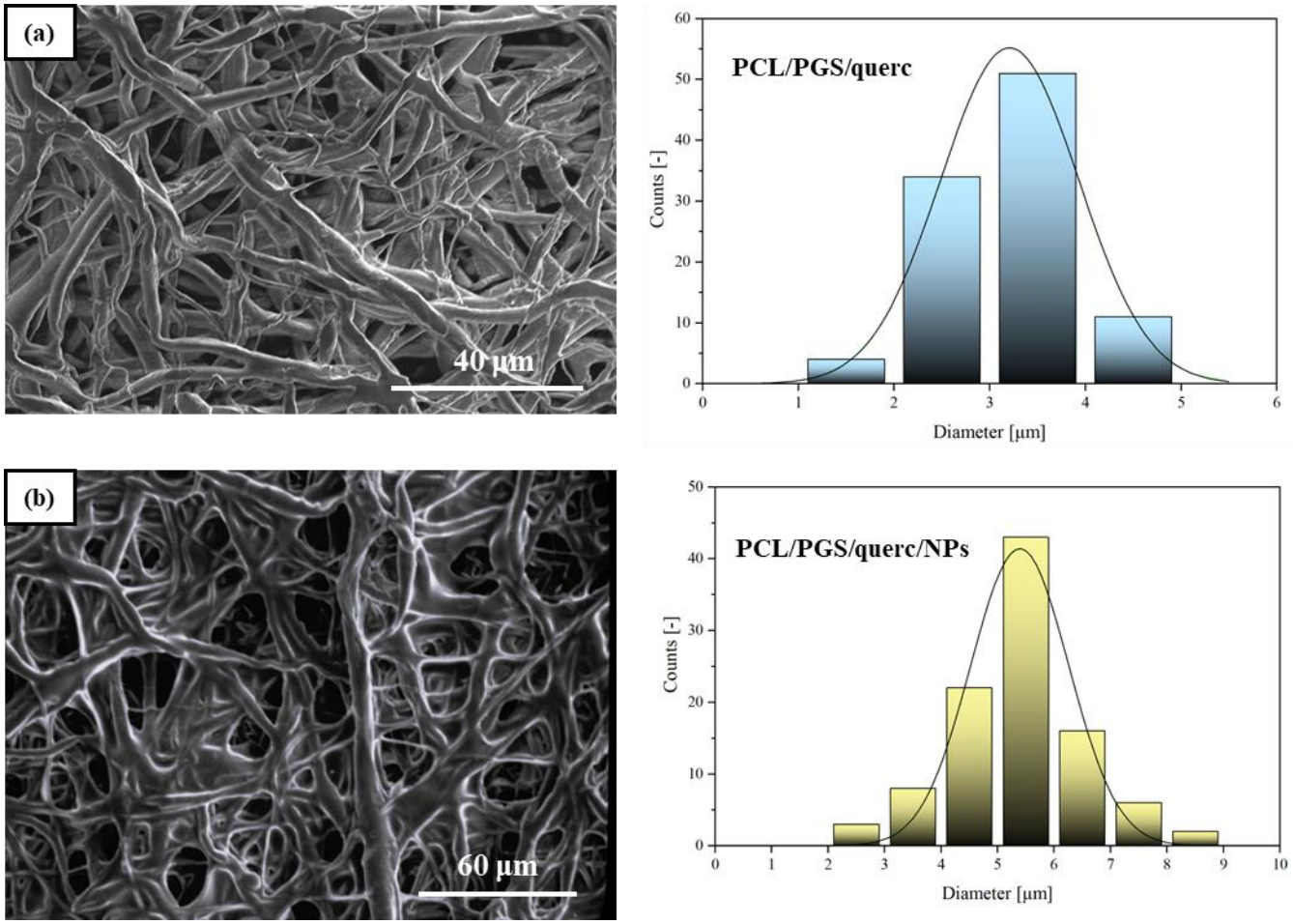

Figure 52. SEM images and dimensional distribution curves for: (a) PCL/PGS/querc; (b) NPs-loaded scaffolds.

Table 11. Fiber diameter of polymeric scaffolds. Results are reported as mean of 100 measurements ± standard deviation.

Sample	Mean Fiber Diameter [µm]
PCL/PGS/querc	3.247 ± 0.758
NPs-loaded scaffold	5.384 ± 1.162

4.2.2 FTIR analysis

The FTIR analysis conducted on the iron oxide nanoparticles and the scaffolds containing these magnetic nanoparticles aimed to confirm the actual presence of the NPs within the structure and to verify that their incorporation did not alter the chemical composition of the prosthesis. The results are shown in Figure 53, where, for clarity, the FTIR spectrum of the PCL/PGS/querc scaffold, previously analyzed in Chapter 2.2.3, is also included.

In the FTIR spectrum of the synthesized nanoparticles, shown in Figure 53(a), a broad peak can be observed in the range 550-650 cm^{-1}, attributed to the Fe–O bond vibrations associated with magnetite. In the range 1400-1650 cm^{-1}, small peaks of weak intensity are visible, corresponding to the vibrations of the carboxylate ion COO^-. These peaks confirm the functionalization of the magnetic nanoparticles by oleic acid. The peaks visible in the range 2800-2950 cm^{-1} are due to the stretching of the C-H bond, while the broad absorption band observable in the range 3200-3600 cm^{-1} is attributed to the vibrations of the hydroxyl group OH.

By comparing the FTIR spectra of the PCL/PGS/querc scaffolds with and without the incorporation of magnetic nanoparticles, broad peaks can be observed in both samples at around 3450 cm^{-1}, corresponding to OH group stretching. The peaks observed in the 2800–2950 cm^{-1} range are attributed to C–H stretching. The high-intensity peak visible at 1720 cm^{-1} is attributed to the vibration of the C=O bond of the ester group, characteristic of both PCL and PGS. In the range of 1150-1250 cm^{-1}, medium-intensity peaks associated with the stretching of C-O-C groups present in both PCL and PGS are identified. These absorption bands are characteristic of the polymeric structure and the intrinsic components of the scaffolds, namely quercetin, PCL, and PGS. Since these peaks are present in both samples, it can be concluded that the inclusion of iron oxide nanoparticles did not impact or alter the chemical structure of the prosthesis.

The presence of iron oxide nanoparticles (NPs) within the scaffolds could not be detected via FTIR analysis due to the overlap between the characteristic absorption peaks of iron oxide NPs, located in the 550–650 cm^{-1} range, and the absorption bands of the polymeric structure's individual components (PCL, PGS, and quercetin). Additionally, the low concentration of NPs added to the electrospinning solution further limits their detectability in this analysis.

However, the effective incorporation of the nanoparticles within the scaffold is confirmed through their characteristic dark coloration and SEM analysis, which provides clear evidence of their successful embedding in the scaffold matrix.

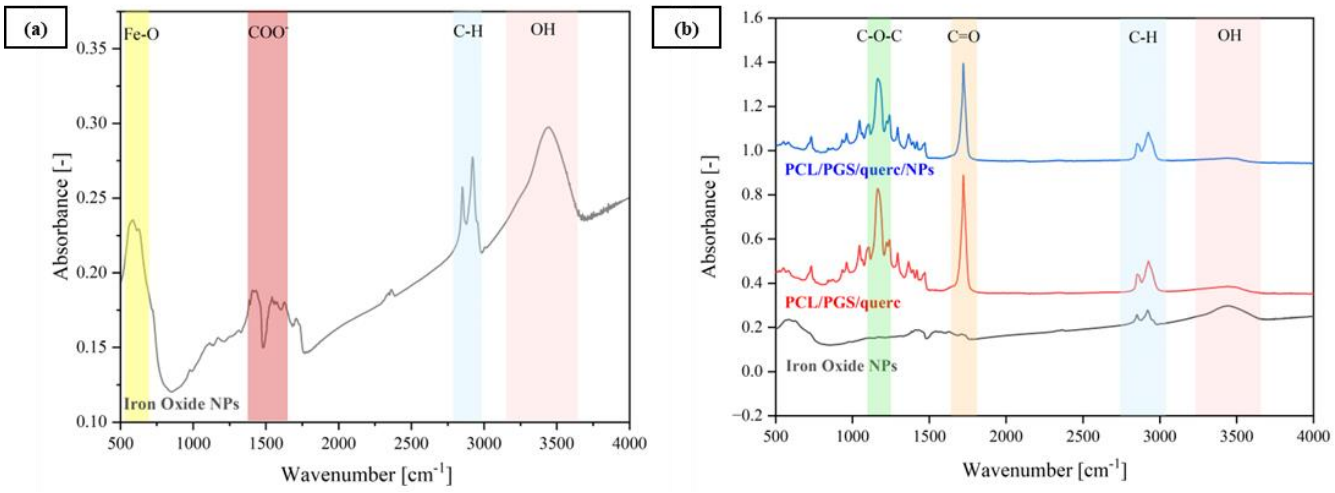

Figure 53. FTIR spectra for: (a) Iron Oxide NPs; (b) PCL/PGS/querc scaffold with and without incorporation of NPs.

4.2.3 Visualization of NPs-loaded scaffold through MRI

The incorporation of iron oxide nanoparticles into vascular scaffolds enabled the detectability of the polymer constructs through magnetic resonance imaging, as shown in Figure 54, where the magnetic nanoparticles generated hypointense regions.

The displayed images were acquired from different regions of the samples, showing cross-sections of the scaffolds. It is evident that, in the case of scaffolds with incorporated NPs, the resulting signal is highly intense, enabling a clear and distinct visualization of the structure. In contrast, for the control PCL/PGS/quercetin scaffold, only a weak, negligible signal was detected, likely attributed to contamination from other molecules or residual iron traces.

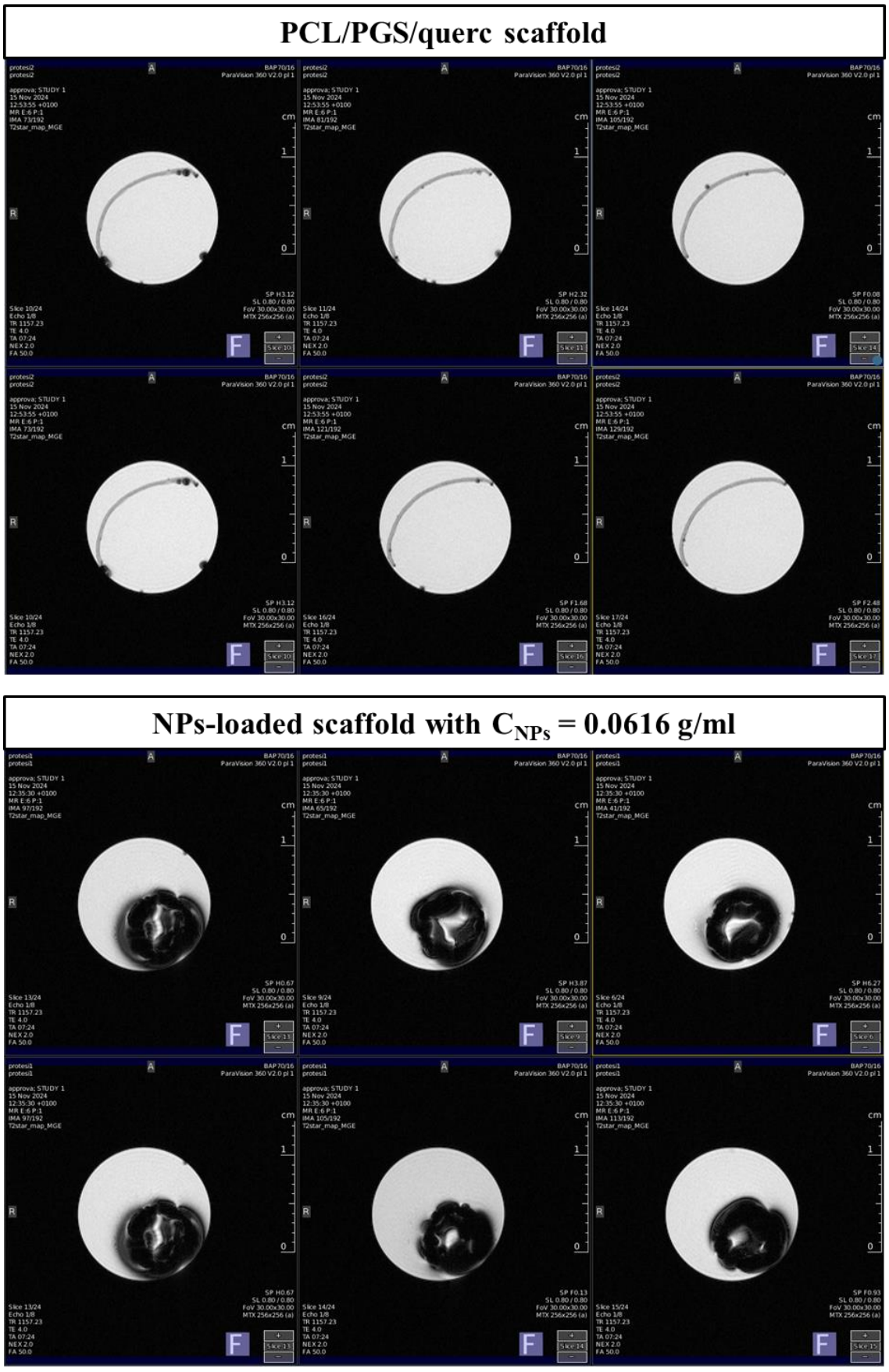

Figure 54. T2 weighted MRI images of PCL/PGS/querc scaffold and NPs-loaded scaffold with C_{NPs} = 0.616 g/ml.

5 Conclusions and future perspectives

In recent years, the demand for prostheses as substitutes for small-caliber vessels to treat atherosclerosis and other obstructive cardiovascular diseases has significantly increased. Scientific research has focused on creating biocompatible and biodegradable vascular scaffolds for small-caliber applications. Electrospinning has emerged as the most widely used technique in Vascular Tissue Engineering for the production of biomaterials, as it enables the fabrication of fibrous structures that closely mimic the extracellular matrix.

In this thesis work, small-caliber vascular scaffolds were fabricated via electrospinning using a 1:1 v/v blend of PCL and PGS with incorporated quercetin, aimed at modulating the inflammatory response during implantation. In the initial phase of the study, the scaffolds were coated with a conventional gelatin layer to reduce prosthesis permeability and prevent potential blood leakage. The method involved immersing the scaffold in a gelatin solution for a predetermined time, followed by a drying phase. However, the limitations of this approach became evident, as precise control over the deposited coating mass was not possible, making the method difficult to reproduce and standardize. Despite these limitations, the biocompatibility and hemocompatibility of the gelatin-coated scaffolds were demonstrated, representing a promising foundation for subsequent phases of the study.

To overcome the issues of the traditional coating method, an innovative layer-by-layer coating process was implemented using gelatin and tannic acid simultaneously. These biologically active compounds interact with each other, forming hydrogen bonds that stabilize the coating and preserve its integrity. Furthermore, the presence of tannic acid provides antioxidant properties to the coated scaffolds. It has been demonstrated that the layer-by-layer coating methodology allows precise control over the deposited layers by varying individual process parameters, enabling the method to be standardized. An *in vitro* release analysis of the bioactive components from the coated scaffold was conducted to identify the predominant release mechanism. It was found that gelatin, tannic acid, and quercetin are primarily released through Fickian diffusion, following the Peppas kinetic model. Additionally, the vascular scaffolds with LbL coating were tested in a bioreactor to simulate the stimuli the graft is subjected to under biological conditions. Dynamic release analyses were conducted to verify the correct behavior of the scaffolds under appropriate flow and pressure stimuli.

In the final phase of this study, vascular scaffolds incorporating iron oxide nanoparticles (IONPs) were fabricated for diagnostic applications. IONPs have demonstrated their potential as T2 contrast agents in Magnetic Resonance Imaging (MRI), enabling scaffold visualization using this technique.

This result is promising for verifying the correct positioning of the scaffold following *in vivo* implantation.

Future perspectives include performing mechanical tests on the vascular scaffolds to ensure that the LbL coating or the incorporation of NPs does not compromise their mechanical properties. Additionally, developing a methodology to detect individually the bioactive compounds released from the scaffold could provide more detailed insights into their respective release mechanisms. Finally, investigating scaffold behavior under varying flow conditions in bioreactor would be a significant step forward.

6 Bibliography

[1] D. J. Beetler *et al.*, “The evolving regulatory landscape in regenerative medicine,” Jun. 01, 2023, *Elsevier Ltd*. doi: 10.1016/j.mam.2022.101138.

[2] A. S. Mao and D. J. Mooney, “Regenerative medicine: Current therapies and future directions,” *Proc Natl Acad Sci U S A*, vol. 112, no. 47, pp. 14452–14459, Nov. 2015, doi: 10.1073/pnas.1508520112.

[3] K. Grens, “The Next Frontier of CAR T-Cell Therapy: Solid Tumors,” The Scientist. Accessed: Nov. 20, 2024. [Online]. Available: https://www.the-scientist.com/the-next-frontier-of-car-t-cell-therapy--solid-tumors-65612

[4] M. Vuga, “Le terapie cellulari,” AIRC. Accessed: Nov. 20, 2024. [Online]. Available: https://www.airc.it/cancro/affronta-la-malattia/guida-alle-terapie/terapie-cellulari-car-t

[5] “TERAPIA GENICA,” Fondazione Telethon ETS. Accessed: Nov. 20, 2024. [Online]. Available: https://www.telethon.it/cosa-facciamo/terapie-e-diagnosi/terapie-avanzate/terapia-genica/

[6] “Building a gene therapy engine for a range of rare diseases,” Sarepta Therapeutics. Accessed: Nov. 20, 2024. [Online]. Available: https://www.sarepta.com/science/gene-therapy-engine

[7] “Trattare le malattie mirando alle basi genetiche,” Osservatorio Terapie Avanzate. Accessed: Nov. 20, 2024. [Online]. Available: https://www.osservatorioterapieavanzate.it/terapie-avanzate/terapia-genica

[8] “Spotlight on Cell and Gene Therapy,” Lonza. Accessed: Nov. 20, 2024. [Online]. Available: https://www.lonzabioscience.com.au/cell-and-gene-therapy/

[9] V. J. P. Langer Robert, “Tissue Engineering,” *Science (1979)*, vol. 260, no. 5110, pp. 920–926, May 1993.

[10] S. Sohn, M. Van Buskirk, M. J. Buckenmeyer, R. Londono, and D. Faulk, “Whole Organ Engineering: Approaches, Challenges, and Future Directions,” Jun. 01, 2020, *MDPI AG*. doi: 10.3390/app10124277.

[11] A. Elizalde-Cárdenas, R. M. Ribas-Aparicio, A. Rodríguez-Martínez, G. Leyva-Gómez, C. Ríos-Castañeda, and M. González-Torres, “Advances in chitosan and chitosan derivatives for

biomedical applications in tissue engineering: An updated review," Mar. 01, 2024, *Elsevier B.V.* doi: 10.1016/j.ijbiomac.2024.129999.

[12] S. Tajvar, A. Hadjizadeh, and S. S. Samandari, "Scaffold degradation in bone tissue engineering: An overview," May 01, 2023, *Elsevier Ltd*. doi: 10.1016/j.ibiod.2023.105599.

[13] R. S. Hsu *et al.*, "Adaptable Microporous Hydrogels of Propagating NGF-Gradient by Injectable Building Blocks for Accelerated Axonal Outgrowth," *Advanced Science*, vol. 6, no. 16, Aug. 2019, doi: 10.1002/advs.201900520.

[14] V. D'Anna, "Le malattie cardiovascolari: prima causa di morte al mondo," Federazione Nazionale Degli Ordini dei Biologi. Accessed: Nov. 20, 2024. [Online]. Available: https://www.fnob.it/2023/12/18/le-malattie-cardiovascolari-prima-causa-di-morte-al-mondo/

[15] B. Zhou *et al.*, "Worldwide trends in hypertension prevalence and progress in treatment and control from 1990 to 2019: a pooled analysis of 1201 population-representative studies with 104 million participants," *The Lancet*, vol. 398, no. 10304, pp. 957–980, Sep. 2021, doi: 10.1016/S0140-6736(21)01330-1.

[16] "Malattie cardiovascolari," Ministero della Salute. Accessed: Nov. 20, 2024. [Online]. Available: https://www.salute.gov.it/imgs/C_17_navigazioneSecondariaRelazione_1_listaCapitoli_capitoliItemName_1_scarica.pdf

[17] C. S. Fox *et al.*, "Trends in cardiovascular complications of diabetes," *JAMA*, vol. 292, Nov. 2004.

[18] A. Battistoni *et al.*, "Persistent increase of cardiovascular and cerebrovascular events in COVID-19 patients: a 3-year population-based analysis," *Cardiovasc Res*, vol. 120, no. 6, pp. 623–629, Mar. 2024.

[19] E. O. Lopez, B. D. Ballard, and A. Jan, "Cardiovascular Disease," *StatPearls Publishing LLC*, Aug. 2023.

[20] Y. Nie *et al.*, "The role of the immunoproteasome in cardiovascular disease," Jun. 01, 2024, *Academic Press*. doi: 10.1016/j.phrs.2024.107215.

[21] "MALATTIE CARDIOVASCOLARI," Biotechmed. Accessed: Nov. 20, 2024. [Online]. Available: https://www.biotechmed.it/patologie/malattie-cardiovascolari/

[22] D. Das, G. Jothimani, A. Banerjee, A. Dey, A. K. Duttaroy, and S. Pathak, “A brief review on recent advances in diagnostic and therapeutic applications of extracellular vesicles in cardiovascular disease,” Aug. 01, 2024, *Elsevier Ltd*. doi: 10.1016/j.biocel.2024.106616.

[23] I. Njølstad, E. Arnesen, and P. G. Lund-Larsen, “Smoking, serum lipids, blood pressure, and sex differences in myocardial infarction.,” *Circulation*, vol. 93, pp. 450–456, Feb. 1996.

[24] J. S. Currier *et al.*, “Coronary heart disease in HIV-infected individuals.,” *Acquired Immune Deficiency Syndromes*, vol. 33, pp. 506–512, 2003.

[25] R. Rabinelli, M. Dettin, S. Imran, and G. Gerosa, “Endotelizzazione di pericardio bovino decellularizzato e funzionalizzato covalentemente con RedV per applicazioni cardiovascolari,” Bioingegneria, Università degli Studi di Padova, Padova, 2022.

[26] “Endotelio,” Mypersonaltrainer. Accessed: Sep. 02, 2024. [Online]. Available: https://www.my-personaltrainer.it/fisiologia/endotelio.html

[27] “Tessuto muscolare liscio,” chimica-online.it. Accessed: Sep. 03, 2024. [Online]. Available: https://www.chimica-online.it/biologia/tessuto-muscolare-liscio.htm

[28] “Comprensione dell’anatomia vascolare: come distinguere tra vene e arterie.” Accessed: Aug. 16, 2024. [Online]. Available: https://www.nysora.com/it/notizie/comprendere-l%27anatomia-vascolare-come-distinguere-tra-vene-e-arterie/

[29] “Le vene.” Accessed: Aug. 16, 2024. [Online]. Available: https://www.medi-italia.it/salute/corpo/vene/

[30] R. N. Mitchell and M. K. Halushka, *Robbins & Cotran Pathologic Basis of Disease*, Elsevier, Inc. Philadelphia, PA, 2021.

[31] L. P. Gartner and J. L. Hiatt, *Color Textbook of Histology*, Grune & Stratton Inc. 2006.

[32] S. Castelnuovo, “ANATOMIA DELLA PARETE ARTERIOSA.” Accessed: Aug. 16, 2024. [Online]. Available: http://www.centrogrossipaoletti.org/2017/09/25/anatomia-della-parete-arteriosa/

[33] A. Incandela, “I vasi sanguigni e la circolazione del sangue.” Accessed: Aug. 16, 2024. [Online]. Available: https://liceoalighieri.edu.it/wp-content/uploads/2024/01/14%5E-e-15%5E-Lezione-I-vasi-sanguigni-e-la-circolazione-del-sanguei.pdf

[34] E. A. Loiacono, “Qual è la differenza tra arteria e vena?” Accessed: Aug. 17, 2024. [Online]. Available: https://medicinaonline.co/2016/11/23/qual-e-la-differenza-tra-arteria-e-vena/?utm_content=cmp-true

[35] S. Saraceni and G. Strumia, *Osservare e capire la vita*, Edizione Azzurra. Bologna: Zanichelli, 2012.

[36] C. Franceschi and R. Domenico, “LE MALFORMAZIONI VASCOLARI CONGENITE.” Accessed: Aug. 18, 2024. [Online]. Available: http://www.domenicoricci.it/images/lavori_scientifici/ANGIODISPLASIA_UNIVERSO27.pdf

[37] C. De Stefano, “Le anomalie vascolari.” Accessed: Aug. 18, 2024. [Online]. Available: https://admin.policlinicocampusbiomedico.it/wp-content/uploads/2023/04/VADEMECUM-ANOMALIE-VASCOLARI.pdf

[38] “Il processo emostatico.” Accessed: Sep. 02, 2024. [Online]. Available: https://www.unmedicopertutti.it/amp-version-emostasi.html

[39] K. S. Saladin and R. (Curatore) De Caro, *Anatomia umana*. Piccin-Nuova Libraria, 2021.

[40] K. L. McCance, S. E. Huether, V. L. Brashers, and N. S. Rote, *Fisiopatologia ed elementi di patologia generale*, 2016th ed. 2016.

[41] A. V. Chobanian *et al.*, “Seventh report of the Joint National Committee on Prevention, Detection, Evaluation, and Treatment of High Blood Pressure,” Dec. 2003. doi: 10.1161/01.HYP.0000107251.49515.c2.

[42] Y. Ostchega, C. D. Fryar, T. Nwankwo, and D. T. Nguyen, “Hypertension Prevalence Among Adults Aged 18 and Over: United States, 2017-2018 Key findings Data from the National Health and Nutrition Examination Survey,” 2017. [Online]. Available: https://www.cdc.gov/nchs/products/index.htm.

[43] A. Belfiore and V. O. Palmieri, “IPERTENSIONE ARTERIOSA,” *G Ital Arterioscler*, vol. 12, no. 1, pp. 35–45, 2021.

[44] F. Collini *et al.*, “Le endoprotesi vascolari nel trattamento della patologia aneurismatica aortica addominale in Toscana.” Accessed: Nov. 22, 2024. [Online]. Available: https://www.ars.toscana.it/rapporti-relazioni-e-sintesi/2015/3326-le-endoprotesi-vascolari-

nel-trattamento-della-patologia-aneurismatica-aortica-addominale-in-toscana-luglio-2015.html

[45] “Coronary Artery Stenting Baytown.” Accessed: Aug. 31, 2024. [Online]. Available: https://www.houstoncardiovascularinstitute.com/cardiology-heart-services-baytown/coronary-artery-stenting/

[46] “Angioplastica Coronarica.” Accessed: Aug. 27, 2024. [Online]. Available: https://www.auxologico.it/angioplastica-coronarica

[47] M. Bracale, “Biomateriali per Protesi e Organi Artificiali,” Napoli, Mar. 2002.

[48] M. Vaccaretti, “Bypass aorto-coronarico: cos’è e quando è indicato.” Accessed: Aug. 27, 2024. [Online]. Available: https://www.nurse24.it/specializzazioni/cardiologia/bypass-aorto-coronarico-cos-e-e-quando-e-indicato.html#:~:text=Il%20bypass%20aorto%2Dcoronarico%20(Coronary,mediante%20inserimento%20di%20uno%20stent.

[49] R. Dimonte, “Endoarterectomia carotidea: procedura, indicazioni, rischi,” The Wom Healthy. Accessed: Aug. 27, 2024. [Online]. Available: https://healthy.thewom.it/terapie/endoarterectomia-carotidea/

[50] U. Baccaglini, “SCLEROTERAPIA ECOGUIDATA CON MOUSSE.” Accessed: Aug. 28, 2024. [Online]. Available: https://www.ugobaccaglini.it/images/libretti/8_SCLEROTERAPIA_ECOGUIDATA_sitoWEB.pdf

[51] “Capillari e vene varicose: curali con la scleroterapia.” Accessed: Aug. 28, 2024. [Online]. Available: https://www.grupposandonato.it/news/2021/aprile/scleroterapia-mini-vasiva-capillari-gambe-vene-varicose

[52] G. Sinagra and F. Brun, “LA TERAPIA ANTICOAGULANTE ORALE: GUIDA PRATICA PER IL PAZIENTE ED I FAMILIARI,” Trieste, Apr. 2024.

[53] L. M. Taylor, J. M. Edwards, and J. M. Porter, “Present status of reversed vein bypass grafting: Five-year results of a modern series,” *J Vasc Surg*, vol. 11, no. 2, pp. 193–206, Feb. 1990, doi: 10.1067/mva.1990.17235.

[54] F. Bolner and A. Bagno, “Innesti vascolari di piccolo calibro,” Università degli Studi di Padova, Padova, 2010.

[55] G. Cappellato and A. Bagno, “Realizzazione e caratterizzazione meccanica di condotti tubulari per applicazioni in ambito vascolare,” Ingegneria Biomedica, Università Degli Studi di Padova, Padova, 2023.

[56] L. Pandis and V. Vindigni, “Sostituti biologici vascolari a base di acido ialuronico,” Biologia e Medicina della Rigenerazione, Università degli Studi di Padova, Padova.

[57] E. Minio, A. Bagno, and P. Aguiari, “Valutazione biomeccanica del pericardio bovino e porcino per la produzione di protesi valvolari cardiache,” Università degli Studi di Padova, Padova, 2012.

[58] Z. Zhang, Z. Wang, S. Liu, and M. Kodama, “Pore size, tissue ingrowth, and endothelialization of small-diameter microporous polyurethane vascular prostheses,” *Biomaterials*, vol. 25, no. 1, pp. 177–187, 2004, doi: 10.1016/S0142-9612(03)00478-2.

[59] P. Losi, S. Lombardi, E. Briganti, and G. Soldani, “Luminal surface microgeometry affects platelet adhesion in small-diameter synthetic grafts,” *Biomaterials*, vol. 25, no. 18, pp. 4447–4455, Aug. 2004, doi: 10.1016/j.biomaterials.2003.11.025.

[60] N. Rosenberg, A. Martinez, P. N. Sawyer, S. A. Wesolowski, R. W. Postlethwait, and M. L. Dillon, “Tanned collagen arterial prosthesis of bovine carotid origin in man. Preliminary studies of enzyme-treated heterografts.,” *Ann Surg*, vol. 164, pp. 247–256, Aug. 1966.

[61] T. Huynh, G. Abraham, J. Murray, K. Brockbank, P.-O. Hagen, and S. Sullivan, “Remodeling of an acellular collagen graft into a physiologically responsive neovessel,” *Nat Biotechnol*, vol. 17, pp. 1083–1086, Nov. 1999.

[62] D. R. Clarke, R. M. Lust, Y. S. Sun, K. S. Black, and J. D. Ollerenshaw, “Transformation of Nonvascular Acellular Tissue Matrices Into Durable Vascular Conduits,” 2001.

[63] C. A. Bustos, C. M. García-Herrera, and D. J. Celentano, “Mechanical characterisation of Dacron graft: Experiments and numerical simulation,” *J Biomech*, vol. 49, no. 1, pp. 13–18, Jan. 2016, doi: 10.1016/j.jbiomech.2015.11.014.

[64] D. M. Scharn, M. Dirven, W. B. Barendregt, A. P. M. Boll, D. Roelofs, and J. A. van der Vliet, “Human Umbilical Vein versus Heparin-bonded Polyester for Femoro-popliteal Bypass: 5-year Results of a Prospective Randomized Multicentre Trial,” *European Journal of Vascular and Endovascular Surgery*, vol. 35, no. 1, pp. 61–67, Jan. 2008, doi: 10.1016/j.ejvs.2007.08.004.

[65] A. Tiwari, H. Salacinski, A. M. Seifalian, and G. Hamilton, “New prostheses for use in bypass grafts with special emphasis on polyurethanes,” 2002. [Online]. Available: www.elsevier.com/locate/cardiosur

[66] R. J. Zdrahala, “Small caliber vascular grafts. Part II: Polyurethanes revisited,” *J Biomater Appl*, vol. 11, no. 1, pp. 37–61, Jul. 1996.

[67] P. Losi, S. Lombardi, E. Briganti, and G. Soldani, “Luminal surface microgeometry affects platelet adhesion in small-diameter synthetic grafts,” *Biomaterials*, vol. 25, no. 18, pp. 4447–4455, Aug. 2004, doi: 10.1016/j.biomaterials.2003.11.025.

[68] N. Beshchasna *et al.*, “Recent advances in manufacturing innovative stents,” Apr. 01, 2020, *MDPI AG*. doi: 10.3390/pharmaceutics12040349.

[69] A. Ershad-Langroudi, N. Babazadeh, F. Alizadegan, S. Mehdi Mousaei, and G. Moradi, “Polymers for implantable devices,” Sep. 25, 2024, *Korean Society of Industrial Engineering Chemistry*. doi: 10.1016/j.jiec.2024.03.030.

[70] X. W. Wen *et al.*, “Study on an antifouling and blood compatible poly(ethylene-vinyl acetate) material with fluorinated surface structure,” *J Mater Sci*, vol. 45, no. 10, pp. 2788–2797, May 2010, doi: 10.1007/s10853-010-4268-z.

[71] “International A. ASTM ISO/ASTM52900-15 standard terminology for additive manufacturing - general principles - terminology,” 2015, *West Conshohocken,PA*.

[72] W. Wu, A. Deconinck, and J. A. Lewis, “Omnidirectional printing of 3D microvascular networks,” *Advanced Materials*, vol. 23, no. 24, Jun. 2011, doi: 10.1002/adma.201004625.

[73] T. J. Hinton *et al.*, “Three-dimensional printing of complex biological structures by freeform reversible embedding of suspended hydrogels,” *Sci Adv*, vol. 1, no. 9, Oct. 2015, doi: 10.1126/sciadv.1500758.

[74] C. Xu, K. Christensen, Z. Zhang, Y. Huang, J. Fu, and R. R. Markwald, “Predictive compensation-enabled horizontal inkjet printing of alginate tubular constructs,” *Manuf Lett*, vol. 1, no. 1, pp. 28–32, 2013, doi: 10.1016/j.mfglet.2013.09.003.

[75] B. Huber *et al.*, “Blood-Vessel Mimicking Structures by Stereolithographic Fabrication of Small Porous Tubes Using Cytocompatible Polyacrylate Elastomers, Biofunctionalization and Endothelialization,” *J Funct Biomater*, vol. 7, no. 2, p. 11, Apr. 2016, doi: 10.3390/jfb7020011.

[76] X. Kuang, K. Chen, C. K. Dunn, J. Wu, V. C. F. Li, and H. J. Qi, “3D Printing of Highly Stretchable, Shape-Memory, and Self-Healing Elastomer toward Novel 4D Printing,” *ACS Appl Mater Interfaces*, vol. 10, no. 8, pp. 7381–7388, Feb. 2018, doi: 10.1021/acsami.7b18265.

[77] P. Calabrò and E. Moscarella, “Angiografia coronarica,” *G Ital Arterioscler*, vol. 12, no. 1, pp. 206–212, 2021.

[78] D. Di Marco, “La TAC Coronarica.” Accessed: Nov. 21, 2024. [Online]. Available: https://www.degasperis.it/tac-coronarica.html

[79] M. A. Mafraji, “Imaging a risonanza magnetica,” Rush University Medical Center. Accessed: Nov. 21, 2024. [Online]. Available: https://www.msdmanuals.com/it/professionale/argomenti-speciali/principi-di-imaging-radiologico/imaging-a-risonanza-magnetica

[80] D. Kawahara and Y. Nagata, “T1-weighted and T2-weighted MRI image synthesis with convolutional generative adversarial networks,” *Reports of Practical Oncology and Radiotherapy*, vol. 26, no. 1, pp. 35–42, 2021, doi: 10.5603/RPOR.a2021.0005.

[81] A. Buecker, E. Spuentrup, A. Ruebben, and R. W. Günther, “Artifact-free in-stent lumen visualization by standard magnetic resonance angiography using a new metallic magnetic resonance imaging stent,” *Circulation*, vol. 105, no. 15, pp. 1772–1775, Apr. 2002, doi: 10.1161/01.CIR.0000015852.60212.DB.

[82] Y. Guo and X. Jiang, “Simulations of the stent artifacts in magnetic resonance imaging,” *IEEE Trans Magn*, vol. 48, no. 2, pp. 659–662, 2012, doi: 10.1109/TMAG.2011.2176473.

[83] C. Mariotti, “Ecografia intravascolare - IVUS,” Nurse24+it. Accessed: Nov. 22, 2024. [Online]. Available: https://www.nurse24.it/specializzazioni/cardiologia/ecografia-intravascolare-ivus.html

[84] “ OCT (optical coherence tomography/tomografia a coerenza ottica).” Accessed: Nov. 22, 2024. [Online]. Available: https://www.degasperis.it/notizie/214/oct_optical_coherence_tomography-tomografia_a_coerenza_ottica.html

[85] “Microscopia Elettronica A Scansione (SEM),” AlfaTest. Accessed: Nov. 22, 2024. [Online]. Available: https://www.alfatest.it/tecniche/sem-microscopia-elettronica-scansione/

[86] L. Miraglia, “Caratteristiche del sistema analitico SEM-EDS: valutazione dell’accuratezza e della precisione delle analisi eseguite su standards internazionali di minerali e vetri,” *Rapporti Tecnici ISSN*, vol. 233, pp. 5–17, 2012.

[87] S. Pierucci *et al.*, “Small Diameter Vascular Grafts Coated with Gelatin,” in *CHEMICAL ENGINEERING TRANSACTIONS*, 2017. [Online]. Available: www.aidic.it/cet

[88] C. Werner, M. F. Maitz, and C. Sperling, “Current strategies towards hemocompatible coatings,” *J Mater Chem*, vol. 17, no. 32, pp. 3376–3384, 2007, doi: 10.1039/b703416b.

[89] P. T. Hammond and D. H. Koch Chair, “Building biomedical materials layer-by-layer,” *Materials Today*, vol. 5, pp. 196–206, May 2012.

[90] J. Zhao *et al.*, “Fabrication of ultrathin membrane via layer-by-layer self-assembly driven by hydrophobic interaction towards high separation performance,” *ACS Appl Mater Interfaces*, vol. 5, no. 24, pp. 13275–13283, Dec. 2013, doi: 10.1021/am404268z.

[91] K. Park, H. Jeong, J. Tanum, J. chan Yoo, and J. Hong, “Developing regulatory property of gelatin-tannic acid multilayer films for coating-based nitric oxide gas delivery system,” *Sci Rep*, vol. 9, no. 1, Dec. 2019, doi: 10.1038/s41598-019-44678-2.

[92] A. Gopalakrishnan, J. Mathew, J. M. Thomas, G. Thankachan, C. T. Aravindakumar, and U. K. Aravind, “Spectro-kinetic investigations on the release mechanism of lysozyme from layer-by-layer reservoirs,” *Colloids Surf B Biointerfaces*, vol. 222, Feb. 2023, doi: 10.1016/j.colsurfb.2023.113135.

[93] C. Huang *et al.*, “Magnetic Electrospun Fibers for Cancer Therapy,” *Adv Funct Mater*, vol. 22, pp. 2479–2486, 2012.

[94] R. P. Friedrich, I. Cicha, and C. Alexiou, “Iron oxide nanoparticles in regenerative medicine and tissue engineering,” Sep. 01, 2021, *MDPI*. doi: 10.3390/nano11092337.